ERASMUS MUNDUS MSC PROGRAMME

COASTAL AND MARINE ENGINEERING AND MANAGEMENT

CoMEM

IMPACT OF BEACH STATES ON NET LONGSHORE SEDIMENT TRANSPORT

Delft University of Technology
24 June 2015

Astrid Vargas Solis
4342704

The Erasmus Mundus MSc Coastal and Marine Engineering and Management is an integrated programme organized by five European partner institutions, coordinated by Norwegian University of Science and Technology (NTNU).

The joint study programme of 120 ECTS credits (two years full-time) has been obtained at three of the five CoMEM partner institutions:

- Norges Teknisk- Naturvitenskapelige Universitet (NTNU) Trondheim, Norway
- Technische Universiteit (TU) Delft, The Netherlands
- City University London, Great Britain
- Universitat Politècnica de Catalunya (UPC), Barcelona, Spain
- University of Southampton, Southampton, Great Britain

The first year consists of the first and second semesters of 30 ECTS each, spent at NTNU, Trondheim and Delft University of Technology respectively.
The second year allows for specialization in three subjects and during the third semester courses are taken with a focus on advanced topics in the selected area of specialization:

- Engineering
- Management
- Environment

In the fourth and final semester, an MSc project and thesis have to be completed.
The two year CoMEM programme leads to three officially recognized MSc diploma certificates. These will be issued by the three universities which have been attended by the student. The transcripts issued with the MSc Diploma Certificate of each university include grades/marks for each subject. A complete overview of subjects and ECTS credits is included in the Diploma Supplement, as received from the CoMEM partner university, Delft University of Technology (TU Delft).

Information regarding the CoMEM programme can be obtained from the programme coordinator and director:

Dr. Ir. Øivind A. Arntsen
Associate Professor in Marine Civil Engineering
Deputy Head, Department of Civil and Transport Engineering
NTNU Norway
Telephone: +4773594625 Cell: +4792650455 Fax: + 4773597021
Email: oivind.arntsen@ntnu.no

IMPACT OF BEACH STATES ON NET LONGSHORE SEDIMENT TRANSPORT

MSc Candidate

Astrid Vargas Solis

Thesis Committee

Prof. dr. ir. M.J.F. Stive	(Chairman, TU Delft)
Ir. B.J.A Huisman	(TU Delft and Deltares)
Dr.ir. M. de Schipper	(TU Delft)
Prof.dr.ir. A.J.H.M Reniers	(TU Delft)

Deltares
Enabling Delta Life

NTNU – Trondheim
Norwegian University of Science and Technology

TU Delft Delft University of Technology

UNIVERSITY OF Southampton

CoMEM Thesis

This thesis was completed by:
Astrid Vargas Solis

Under the supervision of:

Prof. dr. ir. M.J.F. Stive	*(Chairman, TU Delft)*
Ir. B.J.A Huisman	*(TU Delft and Deltares)*
Dr.ir. M. de Schipper	*(TU Delft)*
Prof.dr.ir. A.J.H.M Reniers	*(TU Delft)*

As a requirement to attain the degree of
Erasmus Mundus Master of Science in Coastal and Marine Engineering and Management (CoMEM)

Taught at the following educational institutions:

Norwegian University of Science and Technology (NTNU)
Trondheim, Norway

Delft University of Technology (TUD)
Delft, The Netherlands

University of Southampton
Southampton, Great Britain

At which the student has studied from August 2013 to June 2015.

Acknowledgements

I would like to thank the Erasmus Mundus and CoMEM board to allow me with the opportunity to be part of this MSc program. The experiences and knowledge I have gained in the past two years are invaluable. To professor César Mösso in Barcelona for introducing the program to me and provide me with the motivation to accept this wonderful challenge.

To my thesis committee Matthieu, Marcel Ad and especially Bas, thank you for your time, your guidance and your thoughts, vital for the realization and shaping up of this study. Many thanks to Deltares for providing me with the facilities and allowing me to be part of this project.

To all my family and friends, nearby or across the ocean, thank you for your enthusiasm and support. To my mother and father, Alex and Jacinto, whom I dedicate this work to, thank you very much for unconditionally being there for me, for listening, for your motivation and for all your love.

Summary

The response of longshore sediment transport to the morphodynamic state of the beach was assessed with the use of the process based numerical model, Delft3D. For this purpose, idealized simulation bathymetries that reflect morphological characteristics of two different beach states (namely longshore bar and trough and transverse bar and rip) were created on the basis of observations of the subaqueous topography at the Sand Motor, a mega-nourishment located in the coast of South Holland.

Sediment transport simulations were performed for a range of hydrodynamic conditions that reflect typical sea conditions at the Dutch coast. It was found that two dominant morphological aspects determine the response in net longshore transport: 1) the alongshore variability of morphology and 2) the slope and general configuration of the beach profile; and the relative importance of these two are dependent on the hydrodynamic forcing exerted on the system. Relevance of the profile shape on determining sediment transport behaviours increases as the angle of wave approach increases: Steeper slopes in the swash zone promote higher transport rates for medium and especially for high wave angles. Generation of topographically controlled rip currents that increase or decrease net longshore transport rates depends on the angle of the incoming waves with respect to the coast. Situations with nearly normal wave incidence result in larger potential for rip current development than situations with obliquely incident waves.

Contents

1 Introduction

1.1 Problem description

Wave driven longshore sediment transport is a dominant morphological process in many sandy coasts and its understanding is of paramount importance in the coastal science and engineering field, given that shoreline change and the consequent long term coastal evolution are primarily dictated by spatial gradients of this process. Basic principles in coastal morphodynamics state that these gradients can occur due to changes in transport capacity (i.e. the hydrodynamic forcing) along the coast or due to the presence of features that will interfere with the transport rates: either natural such as inlets, underwater canyons and cliffs acting as sources and sinks of sediments; or human interventions that input and remove sediment into the system or obstruct its natural flux.
On the medium time scales (i.e. years to decades) and spatial scales (i.e. kilometers and larger) coastal evolution is fairly well understood and can be reproduced accurately with the use of numerical models that simulate longshore transport and the aforementioned mechanisms. However accuracy drops in the estimation of coastal evolution for shorter scales. Much attention remains to be paid to the understanding of longshore transport in response to highly dynamic shorter scale morphological features, as is the case of different bathymetrical configurations of sandy beaches.

As a result of a feedback between hydrodynamics and existing morphological elements, sandy coasts exhibit a wide range of shapes on their underwater topographies that are known to constantly fluctuate in space and time. From featureless profiles with high alongshore uniformity to complex 3D patterns of bars and rips and significantly alongshore variability , these features are referred to as beach states and their generation, development and potential impact to larger scale longshore and cross-shore sediment redistribution remains under extensive research.
This study therefore aims at obtaining understanding of how the existence of different beach states can impact the net alongshore sediment transport.

1.2 Objective research and research questions

This thesis focuses on investigating the impact of existing beach states on net longshore sediment transport. The analyses carried out are aimed to represent a range of scenarios consisting of morphological elements and hydrodynamic conditions occurring at the Dutch coast, and particularly along the coast of a mega scale nourishment referred to as the Sand Motor. The main questions for this research, along with their relevant sub questions, are therefore:

I. What are realistic combinations of beach states and environmental conditions for the San Motor?
    a. What are typical beach states occurring at the coast of the Sand Motor?
    b. To what hydrodynamic conditions (i.e. waves) can they be related to?
    c. How can the different beach states be defined based on the morphological characteristics, such as bar height, trough depth, and rip channel spacing?

II. How is net longshore sediment transport impacted by the existence of different beach states?

a. Do net longshore transport rates vary significantly amongst different beach states?
b. What is the sensibility in the variation of transport rates to different hydrodynamic forcings?

III. How to differentiate between the impacts of the beach profile slope and the 3D morphological features?

a. To what extent is longshore transport affected by morphological variability?
b. Under which circumstances is the profile slope dominant for the outcome of net longshore transport?

1.3 Methodology

In order to investigate the impact of beach states on alongshore sediment transport, this study consists mainly of two steps:
1) Identification of beach states
2) Model investigation of the impact of beach states

1.3.1 Identification of beach states

The initial part of the study is focused on identification of beach states along the coast of the Sand Motor from survey bathymetry data. The characteristic features in the nearshore morphology, such as: bar height, bar width and cross-shore distance; trough depth, rip channel spacing and beach gradients are measured in order to acquire a more solid definition of the beach states occurring at the study site.
Simulation bathymetries are constructed on the basis of the observed predominant beach states. These include four alongshore variable bathymetries that represent closely the measured bathymetric features and their respective alongshore uniform versions that reflect only characteristics of their mean profile.

1.3.2 Model investigation of the impact of beach states.

A process based model (Delft3D), is used to simulate initial sediment transport trough the various beach states. A first analysis is made for a reference wave condition and a sensibility analysis is later performed by varying parameters in the wave climate.
Finally, the estimated net longshore sediment transport rates for the alongshore variable and their respective alongshore uniform bathymetries are compared in order to assess what the relative importance of the mean profile slope versus an alongshore variable morphology is for the determination of longshore sediment transport.

1.4 Study outline

Chapter 2 in this thesis provides a summary of the literature review that served as the theoretical background in the study. The identification of beach states and construction of the simulation bathymetries is described in chapter 3. Chapter 4 includes description of the model set up, sensitivity analysis and quantitative approaches undertaken to assess the importance of alongshore morphological variability in the response of longshore sediment transport. Conclusions and further research questions are provided in chapter 5.

2 Literature review

2.1 Beach states: Wright and Short's descriptive classification.

Sandy beaches are subject to highly dynamic variations of the upper shoreface profile and landscape on time scales as short as wave events. This is due to the continuous feedback between hydrodynamic forcing (i.e. waves, currents and water levels) and morphology, where one influences and modifies the other towards reaching an equilibrium state. However, hydrodynamic forgings are rarely, if not never, constant in time resulting in an ever fluctuating upper shoreface morphology (Bosboom & Stive , 2013).

Wright and Short (1984) carried out extensive morphological research around the coast of Australia, and introduced the concept of "Beach states" to describe a range of depositional forms and their coupled hydrodynamics process signatures occurring in beach and surf zones of wave dominated micro-tidal coasts. Additionally, they relate the above to a dimensionless fall velocity parameter (Ω), discriminating between energy dissipative, reflective and intermediate domains. The dimensionless fall velocity $\Omega = \frac{H_b}{\omega_s T}$, where H_b is breaker height, ω_s is the fall velocity of the beach sand, and T is peak breaker period; was able to predict well occurrence of the different morphodynamics states for the 1984 study, as it includes both sediment and wave characteristics.

The two extremes in Wright and Short's (1984) qualitative descriptive model describe highly dissipative or fully energy reflective environments (Figure 2.1). The former, correlated to a Ω value> 6, is considered as "the highest state" and it corresponds to flat shallow beaches with relatively large subaqueous sand storage. It is analogous to "storm" or "winter" profiles, with very low gradients (e.g.$\tan\beta = 0.01 - 0.02$) and wide multi-barred surf zones. Wave energy is progressively dissipated trough spilling breakers, and is relatively small at the beach face. The dominant modes of fluid motion are the oscillatory flows related to incident waves and oscillatory (or quasi-oscillatory) flows corresponding to lower frequency infragravity waves: The later increases its relative contribution (with respect to the incident wave frequency signals) as it approaches the coastline, where it even exceeds the former.
The fully reflective domain (the lowest state), associated with a threshold of $\Omega < 1$ is characterized by steep ($\tan\beta = 0.01 - 0.02$) and narrow surf zones where incoming waves partially dissipate only until they have reached the zone of high run-up on the beach face and they break in surging or collapsing mode. This profile resembles a "summer" or "swell" type of profile, where besides incident wave energy, there is a significant contribution of first subharmonic (i.e. standing waves) frequencies, especially close to the coast. While for dissipative beaches some rhythmicity may be present in the form of beach cusps, both the dissipative and the reflective morphodynamics state are characterized by high alongshore uniformity in their subaqueous topographies (Wright & Short, 1984).

Four intermediate beach states are described, which possess both dissipative and reflective characteristics determined by $1 < \Omega < 6$. These states exhibit the most complex bathymetries, including three-dimensional features such as rip channels, crescentic and transverse bars, and intertidal ridge and runnel patterns which in general favour plunging breakers.

Even though particular systems may exhibit a modal beach state, cycling through various beach states occurs depending on the amount (and frequency signal) of energy approaching

the coast: Wave conditions which move a beach toward a higher state are generally found to cause erosion and wave conditions which move a beach downstate generally cause accretion (Ranasinghe, et al., 2004). The two extreme states (dissipative and reflective) are found to be the most morphodynamically stable, despite of large variations of Ω (i.e. bellow 1 or above 6 respectively) no corresponding variations in state occur. While for $1 < \Omega < 6$ large variation of state may arise.

Figure 2.1 Plan and profile configuration of the dissipative and reflective morphodynamics states of wave dominated beaches. From Short (2006).

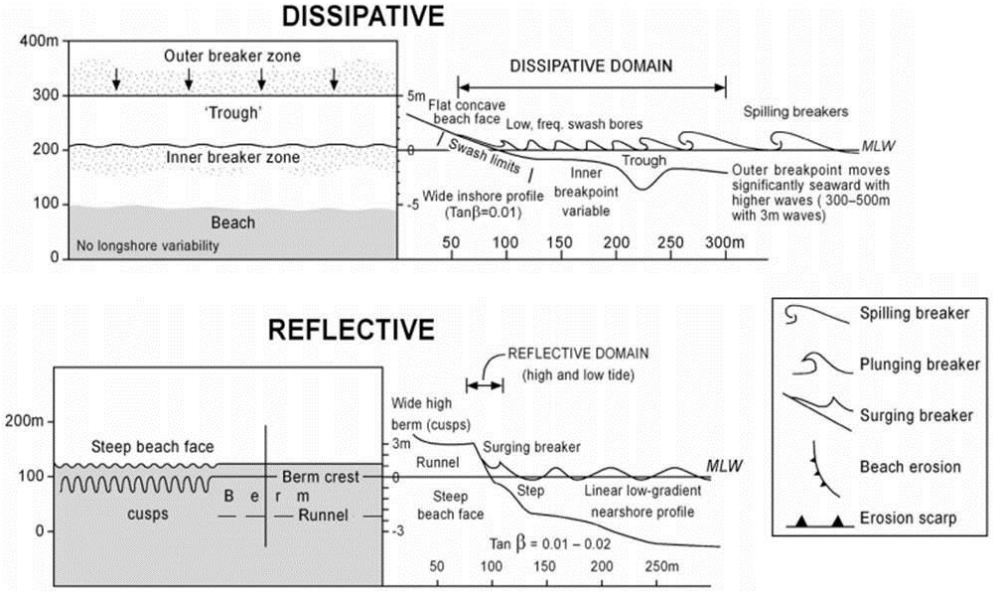

The Longshore Bar and Trough (LBT) and Rhythmic Bar and Beach (RBB) states (figure 2.2a and b) can develop from dissipative morphologies that are subject to accretionary (downstate) processes. Morphologically they are described by offshore bar(s) continuous in the alongshore direction, immediately followed landwards by a trough(s). In contrast to the dissipative extreme, beach faces are generally steeper and the bar and trough relief is much more profound which results in a cease in decay of energy of the broken waves as they pass through the deep troughs. LBT and TBR morphologies differ mainly in the crescentic patterns of the bars and troughs and longshore undulations of the sub aerial beach for the later state. Interruption of the bars, with spacing in the order of 100-300m might occur with weak to moderate rip circulation. Hydrodynamic signature processes are dominated by incident wave frequencies; nevertheless the contribution of incident wave generated currents, as well as currents at subharmonic and infragravity frequencies increase in proximity to bar tips (if present) (Wright & Short, 1984).

Transverse Bar and Rip states (figure 2.2c) are also most commonly developed during downstate sequences, when the antecedent offshore bars attach to the shore in rhythmic patterns. This results in bathymetrical configurations with the highest degree of alongshore variability amongst all beach states (Wright, et al., 1985): Wave energy dissipative transverse bars alternate with deep reflective embayments; this promotes the strongest rip circulation (for any given wave height), with offshore directed currents occupying the deep channels.

Consequently, wave generated currents are the dominant mode of fluid motion inside and in proximity of the rip channels (i.e. rip feeder currents); currents at infragavity frequencies, also follow this pattern however their contribution is lower in relation to motion attributed to incident waves. Finally, intertidal ridge and runnel patterns (figure 2.2d) are characteristic of the last and lowest intermediate state (LTT). In which the degree of reflection and dissipation of wave energy depends highly on the tidal phase: where beaches are typically reflective at high tide and dissipative at low tide. Additionally weak and irregularly spaced rips, associated with pre-existing rips might be present.

Figure 2.2 Intermediate beach states. In descending order: Longshore bar and trough(a), rhythmic bar and beach(b), transverse bar and rip(c) and ridge-runnel/low tide terrace(d).From Short (2006).

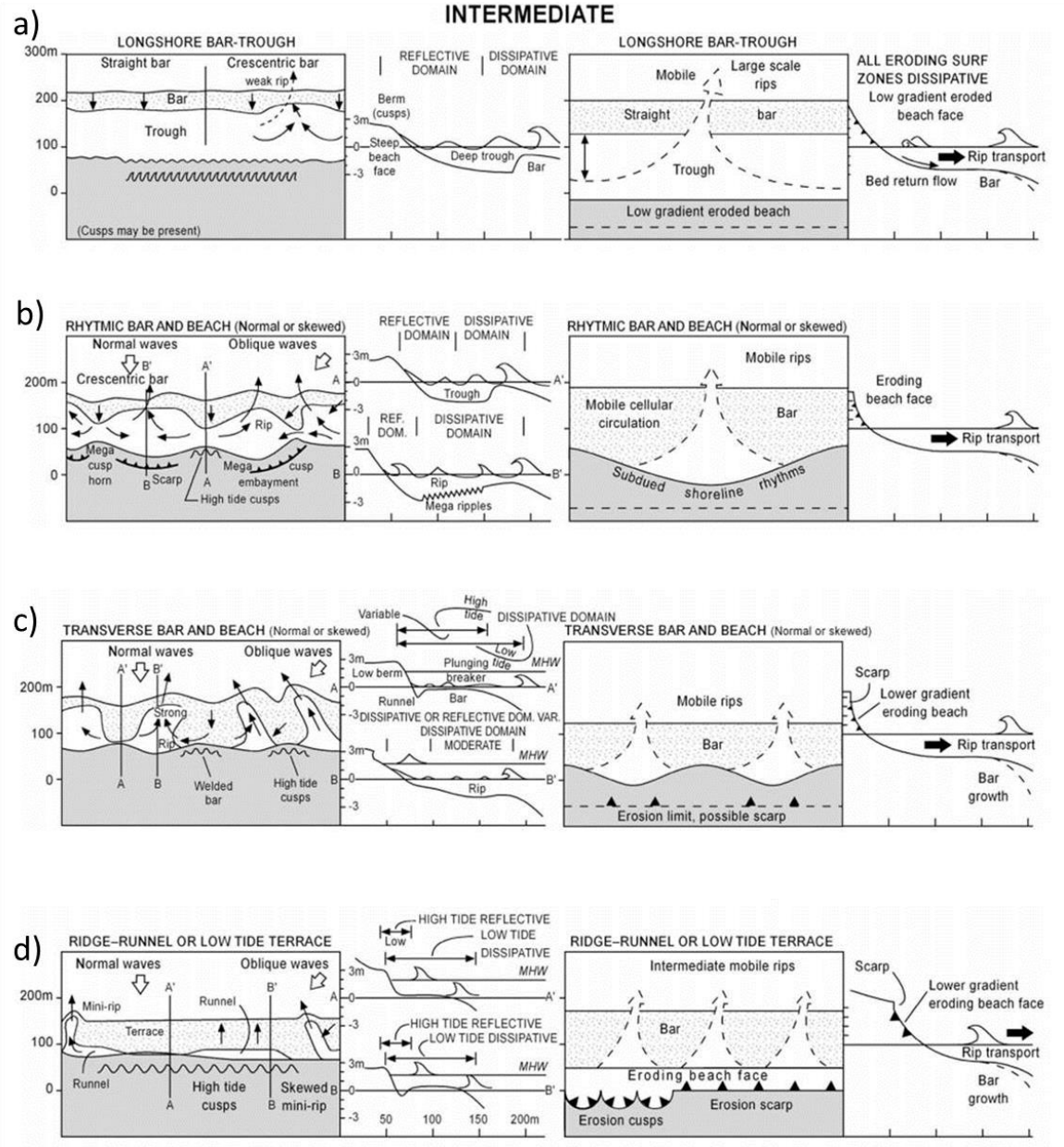

Extensive research has been carried out to determine the hydrodynamic and morphodynamic processes governing intermediate beach states and their transition into other intermediate states. Additional from the downstate transitions described above, upstate transitions can occur. However, in contrast to accretionary sequences, where in general the transitions are single step transitions (e.g. from LBT to RBB, RBB to TBR, etc), upstate sequences are mainly driven by high energy events that wipe out three dimensional features and reset the morphology from a low state into the more alongshore uniform higher state (i.e. LBT morphology) (Lippman & Holman, 1995; Ranasinghe, *et al*., 2004).

2.2 Wave induced nearshore circulation patterns: Longshore and cross-shore currents.

Sediment transport in sandy beaches is closely dependent on the nearshore (i.e. upper shoreface) circulation patterns. For low mesotidal or microtidal systems far from inlets or fresh water inputs, wave generated currents are attributed as responsible for transporting the sediments (either along or across the coast) that have already been stirred up, mainly by the action of wave breaking. As many sediment transport formulations can be roughly generalized into the product of a stirring term (determining the amount of sediment load or sediment concentration) and a transporting term (i.e. the current velocity) at some point in space (Bayram, et al., 2001), it is important to describe the main mechanisms for wave related current generation.

For the most simplified scenario, waves approaching normally towards a straight and alongshore uniform coast will generate offshore directed velocities in the lower and middle part of the water column. The momentum that waves carry between their crests and troughs while they propagate must be balanced by a counteracting mass flux as they reach a solid boundary (e.g. a coastline), as otherwise water will increasingly pile up against it (Bosboom & Stive , 2013). This gives rise to a return current, that under breaking waves, exhibits larger velocities (given the higher mass transport between their crests and troughs) and is referred to as undertow (figure 2.3).

Figure 2.3 Circulation in the vertical plane generated by waves approaching normally a straight uniform coast. From Svendsen (1984)

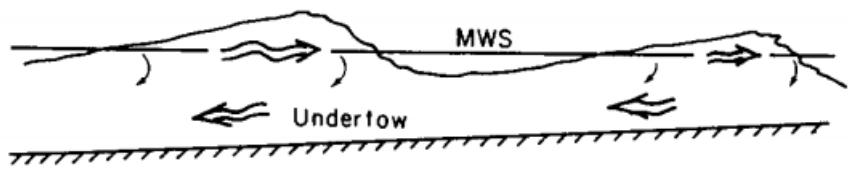

An important concept used to explain wave generated circulation in coastal engineering applications is the so called radiation stress. It can be defined as the depth integrated and wave-averaged horizontal flux of momentum through a vertical plane, given by propagating waves. Spatial changes in the radiation stress give rise to wave forces acting on the fluid in a particular direction (e.g. *x* or *y* direction)that will impact mean water motion and levels (Bosboom & Stive , 2013).From derivation of an expression according to linear wave theory, radiation stress is a function of *n*, the ratio of wave group velocity and phase velocity; *E*, wave energy in the water column which is proportional to the square of the wave height; and φ, angle between the incoming wave crest and the normal to the coastline. Horizontal gradients

in radiation stress are generated since the former fluctuate as a part of wave transformation from deep to shallow waters.

The magnitude of the radiation stress in the direction of wave propagation, as described by Longuet-Higgins and Stewart (1964) is particularly dependent on the water depth and wave length (determining phase ang group velocity) and the wave height (determining the amount of wave energy). When traveling through deep waters, the wave propagation speed is constant, and it is a function only of wave frequency, neither the wave length or heigh is affected by depth; for intermediate waters however, both the wave height and *n* increase as waves shoal. An increase in radiation stress in the landward dierction (a possitive cross-shore gradient) results in a seaward force exherted in the water column. Equilibrium of forces is then restored by a slight reduction in the water level towards the coast (and the consequent hydraulic pressure gradient) up to the point of initiation of wave breaking, referred to as wave set-down(figure 2.4). When waves begin to break in the surf zone, dissipation of energy leads to a decrease in radiation stress, which eventually becomes zero close to the coastline. The landward directed force is counteracted by the seaward pressure force originated after wave set-up: a slight increase in the water levels from the begginig of the surf zone towards the water line (Bosboom & Stive , 2013).

Figure 2.4 Wave set-up and set-down in the shoaling and breaker zone respectively (top) ,and the associated pressure forces(bottom). From Bosboom & Stive (2013).

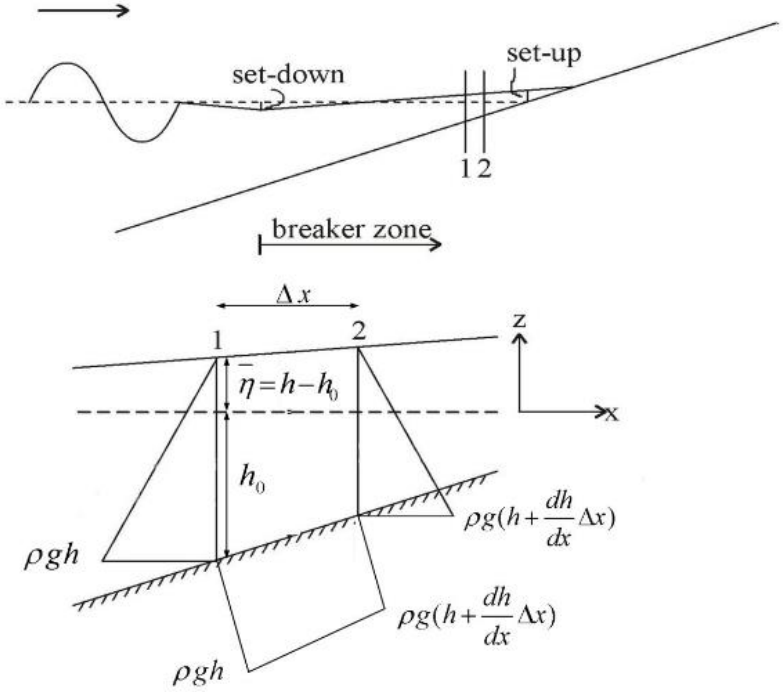

On the other hand, cross shore gradients in radiation stress perpendicular to wave propagation direction (also called radiation shear stress) give rise to the forces that generate a current parallel to the coast, in the case where waves approach obliquely to it. This force (acting perpendicular to the wave propagation, i.e. the *y* direction) depends of *n,* φ and the wave energy dissipation rate D_w. The first two remain constant in *y* as given by Snell's Law *sin* φ/*c*=*constant*; and it is therefore only D_w that determines the magnitude of the force: outside the surf zone in the absence of wave breaking, no force in *y* is exerted on the fluid,

while inside the surf zone the largest forces, will take place under the location of higher wave dissipation, i.e. the breaker line (Bosboom & Stive , 2013).
Mass flux under the wave trough, which is purely offshore directed under normal wave incidence, begins to exhibit a longshore component driven by the above described forces as the angle of wave incidence increases. This current flowing parallel to the coast is referred to as the longshore current.
The magnitude of the depth averaged longshore current velocity varies inside the surf zone as a function of dissipation, height and water depth. The relation between wave height and water depth, commonly represented by the breaker index $\gamma = H/h$, determines the position of wave energy dissipation through breaking and the location of highest velocities. Excluding turbulence effects, an idealized constant beach slope would result in current velocities varying proportionally with the water depth with a maximum at the breaker line. For the very common barred type of beach profile velocity maxima can occur over the shallow bar(s) (in the case that wave breaking occurs) and close to the shoreline where the remaining wave energy is dissipated also trough breaking (figure 2.5).
The deep water wave climate will also determine the magnitude of the longshore currents: the higher the waves are when breaking, the larger the maximum velocities will be; additionally, for small angles of incidence (i.e. 20-30°) the magnitude of the longshore will increase almost linearly with φ, while the highest velocities will occur in the case of waves approaching approximately at 45° to the coastline (Bosboom & Stive , 2013).

Figure 2.5 Computed cross-shore distribution of the longshore current for a multi-barred beach. Bottom plot represents the bed elevation. Depending on the local wave height, wave breaking can occur over all bars (top plot) or only the inner bars closer to shore (middle plot). From Deigaard, et al. (1986).

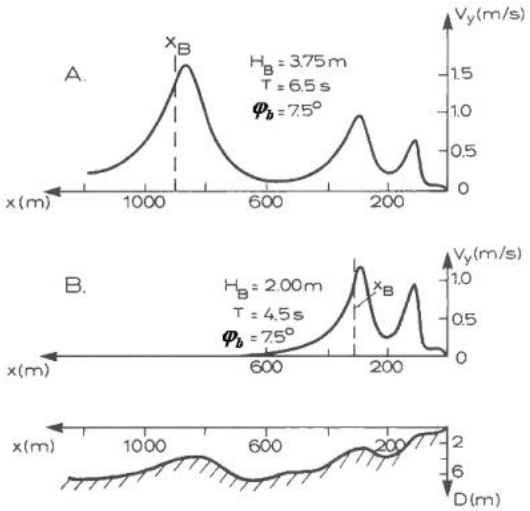

More complex circulation patterns arise when waves approach an irregular coastline, i.e. when the coastline and depth contours are not uniform in the longshore direction. Due to refraction processes convergence or divergence of energy can occur around concave and convex depth contours respectively (figure 2.6). Consequently, a higher wave set-up will take place in locations where energy is focused than in locations where energy is spread. This results in longshore directed currents that flow from the position with higher set-up towards

the position of lowest set-up and are later deviated seaward to form a rip current. Rhythmic patterns of rip currents were classically argued to be more likely to develop under normal and near normal wave incidence, given that the longshore currents resulting from high obliquely wave incidence are commonly strong enough to overshadow the effects of set-up differences (Bosboom & Stive , 2013). Nevertheless, recent observations have shown that cell-like circulation can exist even under large wave angles. This is briefly addressed in the following section.

Figure 2.6 Refraction by a submarine ridge (a) and submarine canyon (b). Orthogonals indicate convergence or divergence of wave energy. From US Army Corps of Engineers (1984).

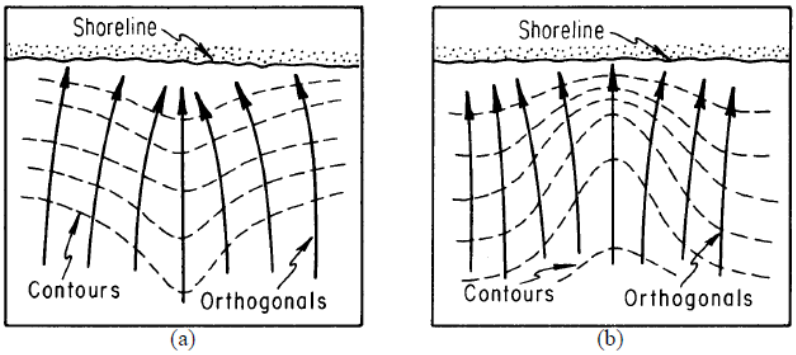

2.3 Nearshore circulation over intermediate beach states

Circulation patterns in the particularly complex morphologies that characterize intermediate beach states have been studied continuously in recent years through field experiments and numerical modelling. Great attention has been paid to the topographically controlled rip circulation that generates over interrupted shore-parallel bars, transverse bar and rip, and low tide-terrace morphologies. Offshore velocities ranging from 0.2 to 1m/s and even as high as 2m/s (MacMahan, et al., 2005) have been observed in the field and attributed to be a function of the forcings exerted by specific combinations of the different hydrodynamic processes. Given the spatial non-homogeneity in wave breaking patterns, increasing energy dissipation over the bars, driving stronger alongshore gradients in set-up, has consistently been reported to enhance rip circulation. The above appears to be modulated to a great extent by the tidal cycle (in the case of meso-macro tidal environments) and the consequent variations in water levels. For low energy waves, rips have been observed to be active only during low tides (Castelle, et al., 2009) as only then depth induced wave breaking will occur over the bars.

Higher offshore velocities for decreasing water levels and increasing wave energy have not only been reported for systems with normal or near normal wave incidence (Bruneau, et al., 2009; MacMahan, et al., 2005), but also under oblique wave incidence (Castelle, et al., 2009; Houser, et al., 2013 ; Winter, et al., 2014). Circullation patterns have been observed to transition between longshore currents that meander over the alongshore variable morphology, offshore currents over rip channels that eventually deviate and flow parallel to the coast outside the surf zone and closed rip circulation cells, as a function of the amount of wave energy dissipation over the bars, in the same way as was mentioned above, for angles between offshore wave crests and shore normals as high as 50°.

To investigate the discrepancies between these observations and previous study conclussions where longshore currents under high oblique wave incidence would suppress

the offshore flow in rip channels, Winter et al. (2014) carried out schematised simulations of the flow over interruppted offshore bars considering both a narrow (50m) and a wide (110m) rip channel widht and wave height angles increasing from 0° to 50°. It was found that in the absence of wave breaking within the wide rip channel, longshore currents would loose its momentum and its velocities would reduce to zero over it, thus maintining rip circulation even fot the highest wave angles. While for the narrow channel, the longshore current would not loose its momentum completely for angles higher than 20° and the flow would bypass the rip channel and continue flowing parallel to the shore. Thus additional from hydrodyanmic processes, the inherent morphollogy and length scales in bathymetrical feautures are also an important factor determining the balance between the cross-shore and alongshore forcings that dictate specific circulation patterns.

2.4 The Sand motor

The Sand Motor (figure 2.7) is a first of its kind mega scale sand nourishment intended to restore and protect the coastline in the province of South Holland in the Netherlands. The project was designed and executed with the aim to find a more efficient and sustainable method to maintain the coastline at a desired position. The “dynamic preservation of the coastline” policy was adopted as a national policy for coastal defense in the Netherlands in 1990 (Ministry of Transport, Public Works & Water Management, 1995). Ever since, beach nourishments have been executed every 3 to 5 years in order to avoid structural retreat of the entire Dutch coastline.

The 21.5 million cubic meters of sand originally placed in a 128 hectares surface are expected to spread due to natural processes (i.e. wind, waves and currents) along the Delfland coast, between Hook of Holland and Scheveningen (highlighted in green in figure 2.8) in a period of 20 years. If successful, not only the lifetime of replenishments carried out in the area will be extended 15 years, but also better flood protection for the province of South Holland and extra room for nature and recreation will result from the 35 hectares of new beaches and dunes that are expected to be created (Province of Zuid-Holland, 2014).

Extensive monitoring campaigns in the Sand Motor have taken place and will continue to be carried out, providing valuable information for many areas of research. The morphological development of the Sand Motor from its construction in August 2011 has been reported by De Schipper, et al (2014). Originally built as a hook-shaped peninsula, the nourished sediment is reworked into a nearly symmetrical bell curve-live shape in less than 1.5 years. Kaji (2013) associated the above to the hydrodynamic forcing by computing sediment transport rates around the nourishment and concluded that the overall evolution of the Sand Motor is event-driven, with high energetic conditions (i.e. waves, winds, and surges) leading to high sediment transport rates and therefore intense erosion.

Occurrences of three-dimensional bathymetry features have been observed at the Sand Motor and seem to be persistent in location between consecutive topographic surveys (Kaji, 2013). Attempts have also been carried out to relate these to the hydrodynamics. However some discrepancies have been found when evaluating the dimensionless fall velocity parameter proposed by Wright and Short (1984) at the Sand Motor: Ω values persistently suggest a highly dissipative state in the nearshore morphology, contrary to the observations from bathymetric surveys (Kaji, 2013). Possible explanations for the above include the

derivation of the Ω parameter as a discriminator of different beach states under hydrodynamic and morphological characteristics that differ from that of the Sand Motor (i.e. storm versus swell conditions, and straight versus curved coastline), as well as the fact that a distinctly developed antecedent bathymetry will hardly adjust to changes in hydrodynamic conditions (Smit, et al., 2012).

Figure 2.7 The Sand Motor October, 2013. Approximately 2 years after its construction was finalized. From Rijkswaterstaat (2013).

Figure 2.8 Location of the Sand Motor in the Delfland coast. The area between Hook of Holland and Scheveningen is highlighted in green. From (Kustvisie Zuid-Holland, 2015)

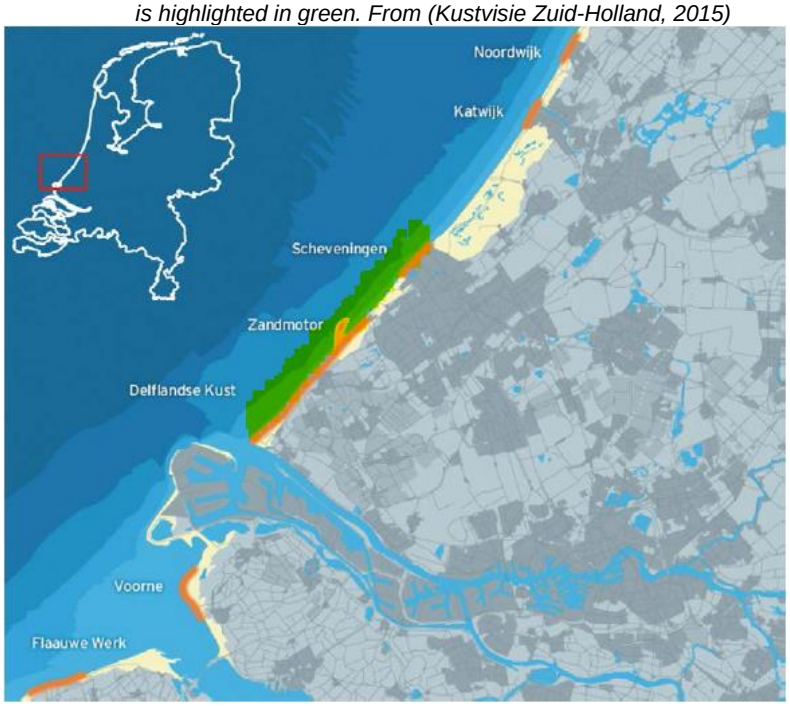

3 Beach state analysis

3.1 Introduction

This chapter discusses the analysis performed on a number of bathymetrical survey data sets of the Sand Motor which lead to identification of particular beach states that were eventually used to construct the bathymetries for which sediment transport simulations would be carried out. Section 3.2 describes briefly the main morphological features observed at the coast of the mega-nourishment throughout consecutive surveys as well as a more detailed description of 4 particular beach states. Assembling of the simulation bathymetries is treated in section 3.3 while section 3.4 concerns association of hydrodynamics occurring at the Delfland Coast.

3.2 Beach state identification

3.2.1 General

Sand bar systems at the Sand Motor have been observed since the very first bathymetric survey, carried out soon after its construction in August 2011, while widening of the bars and appearance of three-dimensional features such as crescentic and oblique sand bars and rip channels were recorded during following surveys (September to November 2011) (Kaji, 2013). Beach states at the Sand Motor reached a developed phase in the period from October 2012 to August 2013 (Tan, 2014). Compared to earlier periods, this stage was characterized by the occurrence of well-defined beach states along its entire length. Based on these findings, bathymetry data analysis started from surveys performed in October 2012 but also included surveys up to November 2014. Visual inspection of the existent morphology in these data sets was made in order to identify underwater topographies that fit into the description of beach states by Wright and Short (1984).

Three regions are distinguished at the Sand Motor according to orientation of the coastline: the southern coast, oriented SSW-NNE; the northern coast, with orientation WSW-ENE; and the head, with approximately the same orientation as the original coastline (SW-NE) (Kaji, 2013). Consistently throughout all analysed surveys, a bar and trough system parallel to the coast occurred at the southern coast of the Sand Motor (figure 3.1a, b, c and d). Position of the bar, relative to the coast varied to a small extent between consecutive surveys; however a distinction can be made for the bathymetries surveyed during 2014 (figure 3.1d), where the bars are notoriously positioned farther from the coast and consequently deeper crests are followed landwards by wider and deeper troughs.

The northern coast of the Sand Motor exhibited the widest range of morphological features both in time and space. An offshore bar, with crescentic patterns but no profound trough relief, was observed to occupy most part of this region during surveys executed from December 2012 to March 2013 (figure 3.1a). After this, the bathymetry becomes more irregular and is characterized by complex patterns of shore normal sand bars alternating with deeper channels from April to December 2013 (figure 3.1b and c); eventually a crescentic offshore bar reforms and is present throughout the surveys in 2014.

The head of the Sand Motor was characterized by a set of transverse bars connected to the shore from December 2012 to December 2013(figure 3.1a, b and c). For the following surveys, the bars are wiped out and replaced by mixed patterns of shore-connected and unconnected shoals (figure 3.1d).

Figure 3.1 Bathymetric surveys dated 2012-12 (a) 2013-04 (b), 2013-12 (c) and 2014-09 (d).Bed elevations lower than -5m and higher than 0m (with respect to NAP) are not depicted in order to highlight variability in the nearshore morphology.

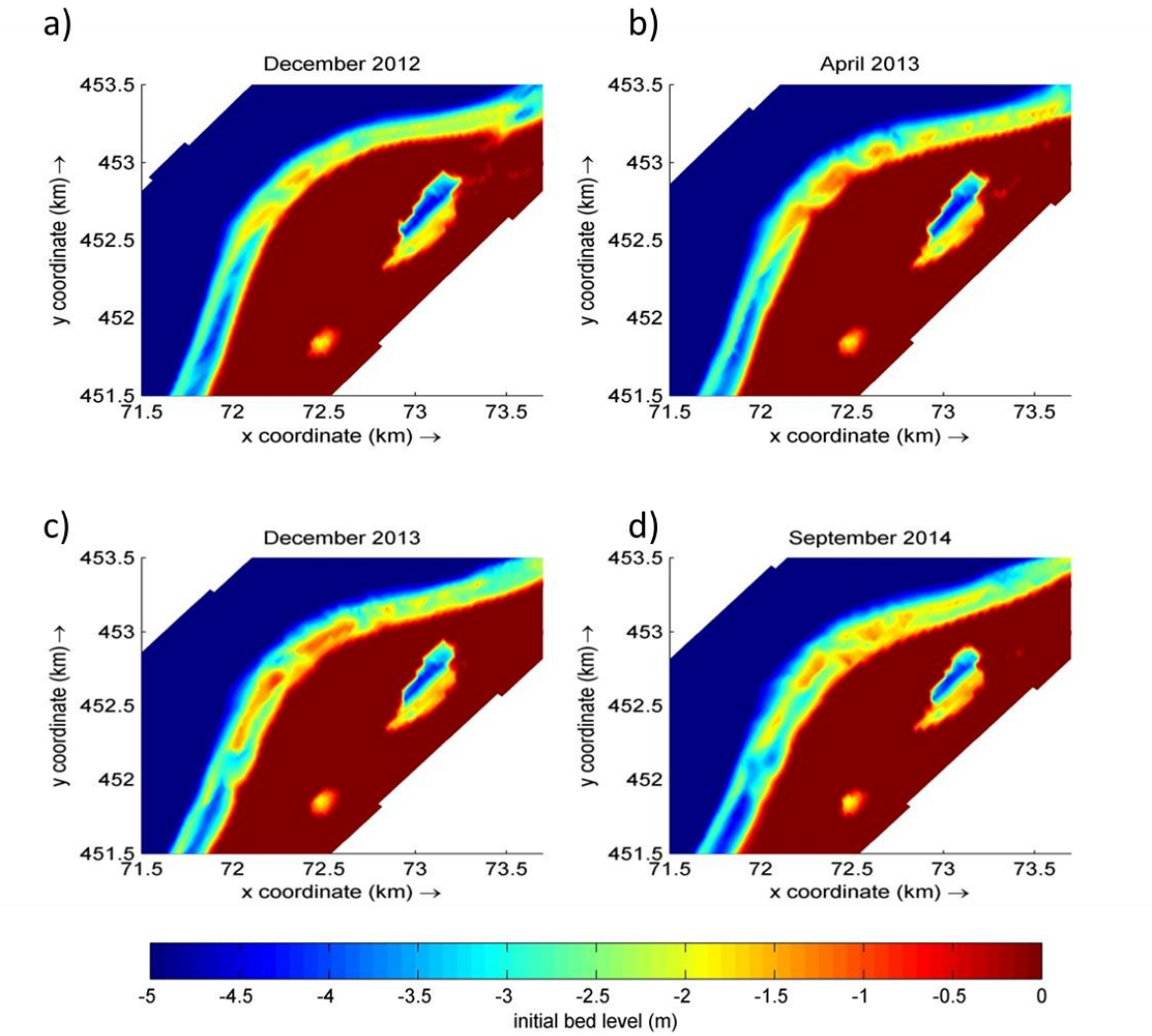

Bathymetry surveyed on 23-Aug-2013 (figure 3.2) was selected for this study, since well-defined morphological features could be identified along its three main regions. The following characteristic beach states were found:

- South coast: A longshore bar and trough system with few rhythmicity that stretched over the whole region.
- Head of Sand Motor: Well developed transverse bar and rip morphology.
- North coast: A series of smaller transverse bars, some of which are detached to the shoreline, separated by deeper rip channels.

Additionally the longshore bar and trough morphology from the last analysed bathymetrical survey (dated 1-Nov-14) was considered given that it displayed different characteristics that that of the August 2013 survey: The bar is located farther from the coast and is followed by a much wider trough.

Figure 3.2 Bathymetry surveyed 2013-08-26. Bed elevation with respect to NAP

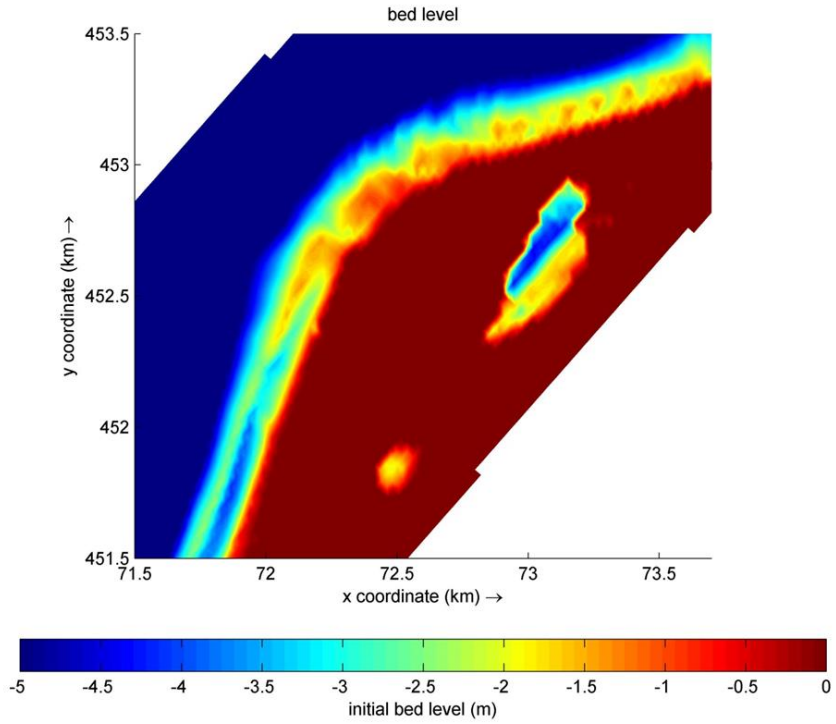

3.2.2 Measuring characteristic parameters

In order to gain a more solid definition of the different beach states observed, several parameters in the bathymetry were measured.

Measurements were performed with the bathymetry-visualizing and manipulating module, QUICKIN, of the Delft3D software suite. The relevant bathymetric features of the selected beach states were quantified based on their depth and cross shore distance. For the transverse bars connected to the shore, additional dimensions had to be recorded. To avoid significant errors that could occur when measuring cross-shore distances with respect to a rhythmic coastline, a straight (non-rhythmic) transect behind the 0m contour (the "longshore axis"), was defined as the initial cross-shore position in each of the areas of interest.

Longshore Bar and Trough morphologies (narrow and wide trough)

The offshore sand bar in the south coast of the Sand Motor exhibits landwards and seaward migration (in the order of 10m) among successive surveys. Its most landward position is recorded in the surveys performed between April and August 2013. More energetic conditions in the month of December (both 2012 and 2013) result in a seaward migration of the bar. It is however during the surveys of 2014, where the bar is observed to be positioned farther from the coast. For the survey of November 2014 the bar shows its most seaward position, and it is consequently followed by a rather wide and deep trough. Additionally, different rhythmic patterns are developed in its crest.

Given the relative smoothness of LBT morphology in comparison to the other intermediate beach states, very few parameters need to be recorded in order to describe it. Four transects approximately 20m apart and perpendicular to the longshore axis were defined to measure the following parameters in the August 2013 and November 2014 (figure 3.3) LBT morphologies:

- Bar crest and trough depth and cross-shore distance

The crest was defined as the shallowest point in the bar intersecting each of the transects. Its position was measured as its distance to the longshore axis. In the same way, the position and depth of the deepest point in the trough were determined (Table 3.1).

- Bar and trough width in cross-shore direction
  Given that shore parallel bars and troughs can be adequately described in 2D, width of these features was determined by measuring the distance between specific depth contours (Table 3.1). The 3.5m and 3.9m depth contours were found to delimit well the bar and trough areas for the August 2013, and November 2014 bathymetries respectively (figure 3.4)
- Slope sea ward of bar and swash zone
  The depth gradient was determined from the seaward limit of the bars(Slope seaward of bar, table 3.1), to approximately the 6m isobath located offshore; and from the landward limits of the troughs to the 0m contour (slope swash zone, table 3.1) .

Figure 3.3 Bed elevation (with respect to NAP) and measuring transects (T1,T2,T3, and T4 from south to north) for the LBT morphologies observed in the August 2013 (a) and November 2014 (b) surveys.

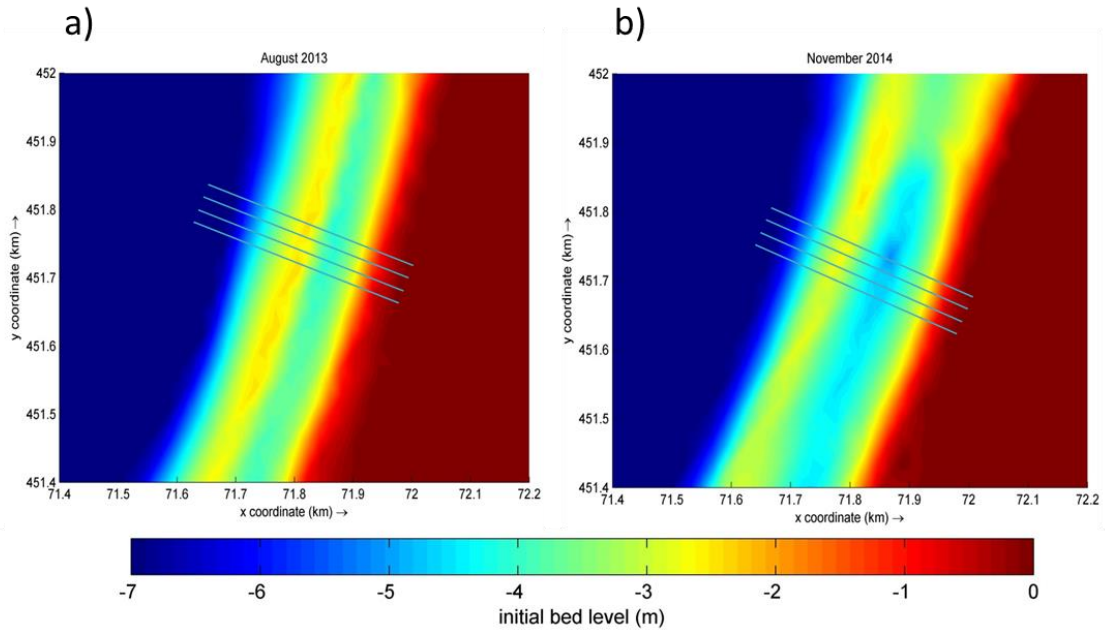

Table 3.1 Measured parameters for the LBT bathymetries observed in August 2013 and November 2014. Depths are expressed as positive values.

Parameter	LBT 2013				LBT 2014			
	T1	T2	T3	T4	T1	T2	T3	T4
Bar crest depth (m)	2.5	2.5	2.6	2.4	2.7	2.7	2.7	2.7
Cross-shore distance to crest (m)	221	220	218	217	264	255	247	236
Bar width cross-shore direction (m)	78	76	74	72	78	80	79	78
Trough depth (m)	3.9	4	4	3.9	4.5	4.5	4.5	4.5
Cross-shore distance to trough (m)	160	165	161	169	161	159	155	151
Trough width cross-shore direction (m)	46	48	47	46	81	80	82	81
Slope sea ward of bar	0.043	0.041	0.04	0.037	0.05	0.048	0.046	0.046
Slope swash zone	0.035	0.035	0.036	0.037	0.031	0.031	0.03	0.029

Figure 3.4 Representation of the measured bar and trough widths for the LBT morphologies in the August 2013 (a), and November 2014 (b) surveys

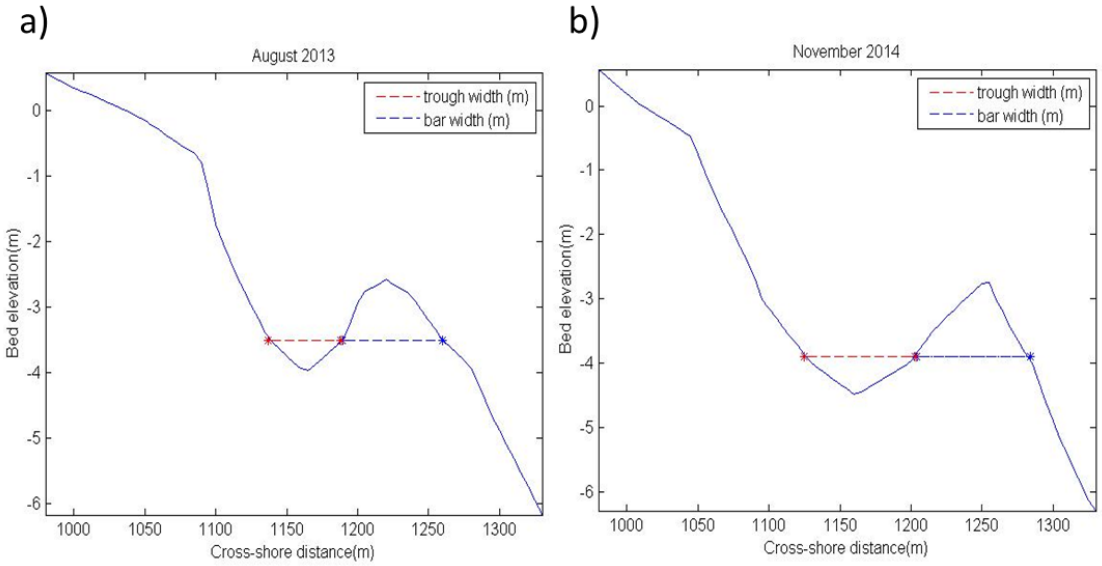

Transverse bar and rip (head and north coast of the Sand Motor)

The head of the Sand Motor exhibited a transverse bar and rip morphology for the major part of the surveying period. Particularly, the three transverse bars occurring in the region for the selected August 2013 bathymetry, are also observed in previous surveys, being recorded for the first time in December 2012. During following surveys the bars are observed to develop (i.e. to grow), displaying biggest dimensions in August 2013. After this period, morphology in the region becomes more fluctuant in time: sand bars migrate both in the cross-shore and longshore direction, and vary between being attached or detached to the shoreline from one survey to another.

Given the complex 3D nature of the bathymetric features, a transverse bar and rip morphology cannot be described in the same was as and LBT morphology. Given their irregular shape, dimensions of the sand bars in the longshore direction also need to be specified, not only in one but in various positions in the cross-shore.
Out of the three transverse bars displayed in figure 3.5, only the bar in the middle, and the one located to its left are measured, by defining a shore normal transect approximately at the centre of each shoal. Given the curvature in the coastline, the bar located in the right extreme differs considerably with respect to the other two and therefore it was not considered. Measurements were performed as follows.

- Bar crest depth and cross-shore distance
  Transects were set in such a way that they would intersect the shallowest points in the bar (figure 3.5). Its position in the cross-shore was defined as described above.
- Bar width in cross-shore direction
  The bars were defined as the areas within the 1.75m depth contour that protrudes from the coastline. This is approximately the deepest contour that consistently displays the transverse bar shape among all the shoals. Width in the cross shore direction was measured from outside the bar (depicted in blue in figure 3.6), from the point where this contour aligns with the coast, to the seaward limit of the bar at the end of the transect.

- Bar width in longshore direction (BWLD) and spacing of rip channel(SRC)
  Three previously defined cross-shore positions were set to measure the inner distance between the 1.75m isobath in the longshore direction (black lines in figure 3.5). Spacing of rip channel was defined as the outer distance between the contours in the same three cross-shore positions (grey lines in figure 3.6)
- Rip channel depth
  Since the depth in the rip channels did not vary significantly at different cross-shore distances, only the average figure is recorded.
- Slope
  The slope seaward of the bar was again determined from the sea ward limit of the bar to an approximate depth of 6m following coast normal transect, while the slope in the swash zone was determined from the crest of the bars to the shoreline (i.e. 0m isobath).

Figure 3.5 Bed elevation with respect to NAP and measuring transects (T1 and T2 for the left and middle bar respectively) for the TBR morphology at the head of the Sand Motor, August 2013

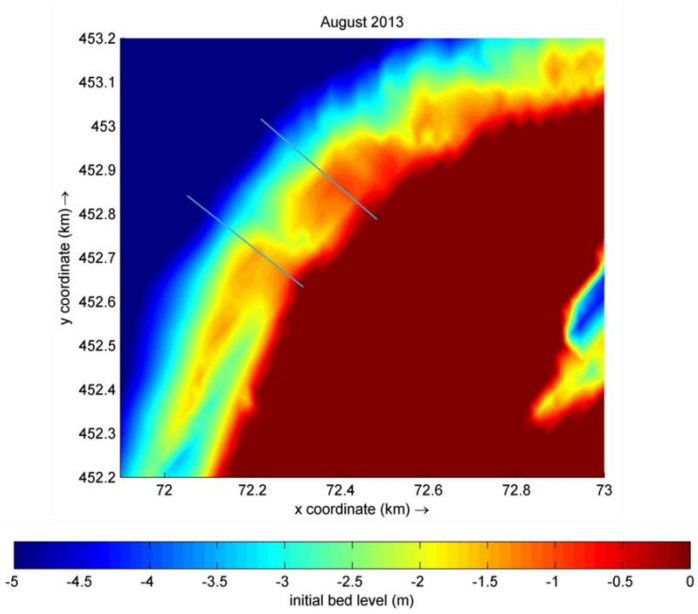

Figure 3.6 Representation of measurements in the TBR morphology at the head of the Sand Motor. The 1.75m isobath (depicted in brown) defines the limits of the transverse bars. BWLD 1 2 and 3 are depicted in black, and SRC 1 2 3 are depicted in grey. Blue transect represents measurement of the bar width in cross-shore direction.

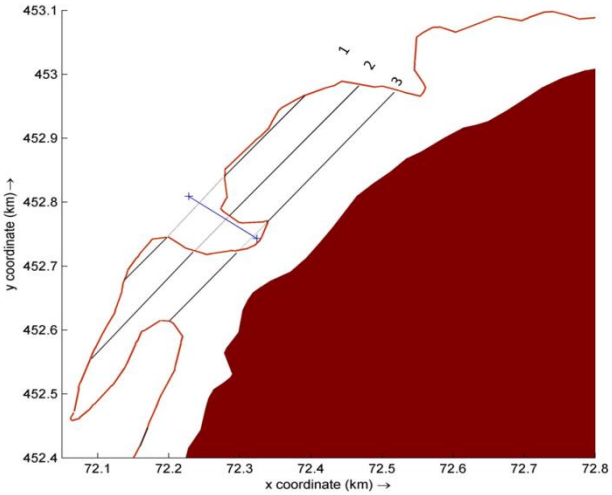

The north region of the Sand Motor exhibits a series of shoals along the coast. Three of them (figure 3.7) resemble the TBR state observed at the head of the Sand Motor in the sense that they are positioned perpendicular to the coast and separated by deeper rip channels. Nevertheless, these bars are smaller and more regular in shape and size, with the exception of a smaller circular shoal that is somewhat detached from the shore. This type of morphology was only present for a short period (surveys April- to August 2013). The region displayed the most dynamic nearshore morphology throughout the analysed surveys, alternating between offshore parallel bars with crescentic patterns, transverse bars, and also complex and paternless features.

Parameters were determined for each of the three shoals in a similar way than in the precedent morphology .Only those parameters which are measured in a different way in the middle shoal are mentioned above.

- Bar width in cross-shore direction
  For the disconnected shoal in the centre, the width is taken as the inner distance between the 1.75m isobath that surrounds the shoal following the coast normal transect.
- Bar width in longshore direction (BWLD) and spacing of rip channel(SRC)
  Similar to above, these parameters were measured at three cross-shore positions. However BWLD3 and SRC3 (located closest to the shore) are only determined for the left and right bars, since the middle bar at this point is no longer present at this position (figure 3.8). Instead, a deeper region that can be defined and measured as a trough is observed.

Table 3.2 contains the measurements of the above mentioned features of the TBR morphologies.

Figure 3.7 Bed elevation with respect to NAP and measuring transects (T1, T2 and T3 for the left middle and right bars respectively) for the TBR morphology at the head of the Sand Motor, August 2013

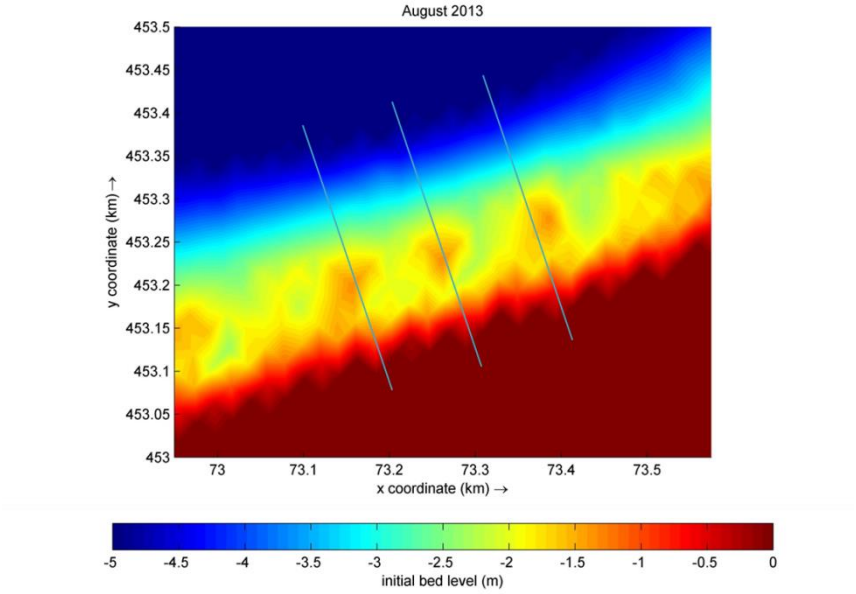

Figure 3.8 Representation of measurements in the TBR morphology at the north coast of the Sand Motor. The 1.75m isobath (depicted in brown) defines the limits of the transverse bars. BWLD 1 2 and 3 are depicted in black, while SRC 1 and 2 are depicted in grey. Blue transects represent bar width in the cross-shore direction.

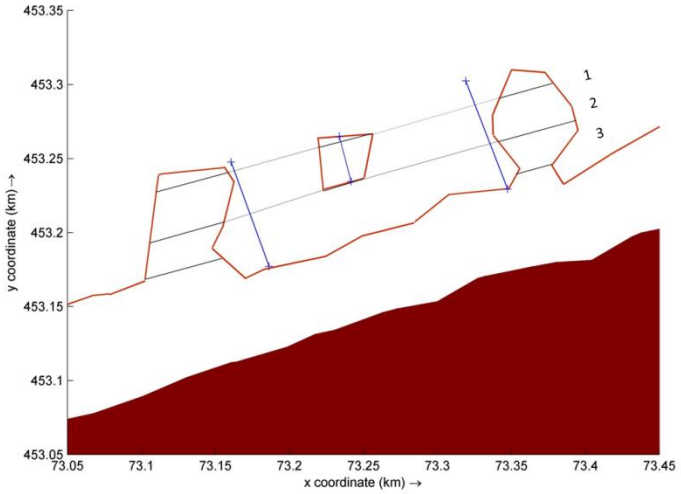

Table3.2 Measured parameters for the TBR features at the head and northeast coast of the Sand Motor observed on 23-August-2013. Depths are expressed as positive values.

Parameter	TBR head		TBR northeast		
	T1 (Left bar)	**T2** (Middle bar)	**T1** (Left bar)	**T2** (Shoal)	**T3** (Right bar)
Bar crest depth (m)	1.42	0.9	1.35	1.36	1.38
Cross-shore distance to crest (m)	198	105	107	103	116
Bar width cross-shore direction (m)	102	97	82	33	83
LBW1 (m)	92	167	50	38	36
LBW2 (m)	219	273	52	28	53
LBW3(m)	146	278	53	-	25
Cross-shore distance to LBW1 (m)	199		120		
Cross-shore distance to LBW2 (m)	156		90		
Cross-shore distance to LBW3 (m)	110		65		
Rip channel depth (m)	2.2		2.05	-	2.1
SRC1 (m)	121		63	-	77
SRC2 (m)	77		69	-	94
SRC3 (m)	54		-		
Slope seaward of bar	0.023	0.021	0.025	0.0246	0.0246
Slope swash zone	0.016	0.011	0.029	0.03	0.033

3.3 Construction of bathymetries

3.3.1 Bathymetries based on the observed Beach States at the Sand Motor

Idealized bathymetries were created on the basis of the identified key characteristics of the beach states observed along the three regions of the Sand Motor in order to investigate their potential impact in longshore sediment transport. Assembling of the bathymetries required a number of steps:

- Additional measurements with multiple transects.

The use of coast normal transects in the section above was useful not only to determine dimensions of the features but also their relative position in the cross-shore and longshore direction. In order to acquire enough data to create the bathymetries, several additional transects had to be set (especially for the transverse bar morphologies) so that the extension of each feature was covered and the position of determined depth contours (in *x* and *y* direction) was recorded. In this way the position of the coastline (i.e. 0m isobath) and remarkable points of inflexion in the isobaths that give shape to bars and troughs, contributed to replicate better the morphologies of interest.

- Replicate measured beach states to obtain repeated bathymetry patterns.

Once enough bathymetric data for each of the selected beach states was collected, the complete data sets were reproduced several times in the longshore direction making sure that the length scales between features remained in accordance to those observed in the original data. Hence, the created bathymetries show long stretches of coast with a particular beach state that appears continuously along the coast.

- Adjusting bathymetries into computational domains

Rectangular computational grids, with a grid cell resolution of 5x5 m were created with the RGFGRID module of Delft3D to interpolate the bathymetry data. Size of the grids varied depending on the dimensions of the different beach states, however in the longshore direction they were set to the particular extension (i.e. in the order of 10^3m) to which a characteristic sediment transport pattern could be observed along the whole extension after the hydrodynamic simulations were performed. This is further addressed in section 4.2.

In the cross-shore direction, the recorded transect data from each morphology was used until a depth of approximately 6.2m. The position of the coastline was adjusted inside the computational grid so that for all the bathymetries, the 6.2m depth contour would be located at a same grid y coordinate. From this point offshore, the bathymetries were extended until a depth of 10 m, using a constant slope of 0.2, i.e. a representative offshore slope in the Delfland coast. The above was done in order to address two particular situations that could occur while executing wave and sediment transport simulations: *1)* Different wave refraction patterns resulting after having significantly different depth values at the most offshore points, and *2)* computations of the relevant parameters (i.e. current velocities, sediment transport) being strongly influenced by the seaward boundary. By normalizing all bathymetries in their seaward side with an alongshore uniform slope, and extending them to a common depth that is far from the area of interest, it is ensured that wave conditions are constant for all simulations at the point where the beach state bathymetry data, begins (~6.2m); and that the analysed sediment transport data is not a result of unknown (seaward) boundary effects.

Longshore Bar and Trough bathymetries

Two bathymetries were created from the surveys in August 2013 and November 2014. The four measured transects in the August 2013 survey extending over a length of 80m in the alongshore direction were consecutively repeated to create LBT1 (3.9a), forming a nearly straight bar and trough. Meanwhile, the characteristic rhythmic patterns in the crest of the bar for the 2014 survey were observed to be repeated approximately every 120m., therefore two more transects were set to produce LBT2 (figure 3.9b).

Figure 3.9 LBT1 (a) and LBT2 (b) bathymetries created after the Longshore Bar and trough morphologies observed in August 2013 and November 2014 at the Sand Motor.

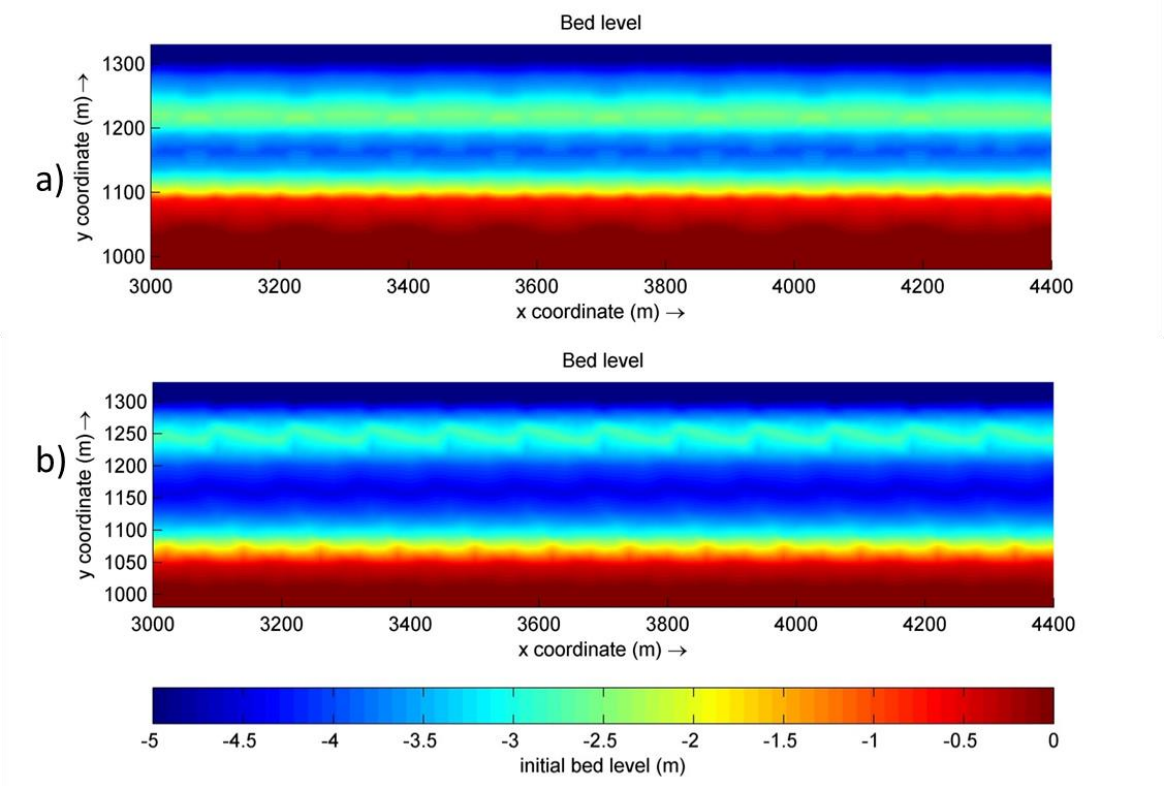

Transverse bar and rip, head of Sand Motor

Only one of the transverse bars, the middle bar (measured with transect 2, figure 3.5) was considered for constructing a representative bathymetry of this region. The bar to its right has a considerably different position in the cross shore given the curvature of the coastline, and therefore a straight coastline would not be formed if this bar was included in the bathymetry. Furthermore, the bar in the left extreme (measured with transect 1, figure 3.5) is extended southwards into a LBT-like morphology, and since the aim for construction of this bathymetry was to analyse sediment transport patterns strictly for a transverse bar and rip morphology, it was only the rip channel spacing between the left and the middle bar which was considering when assembling the bathymetry. TBR1 is depicted in figure 3.10. Since the length scale of this particular feature is large in relation to the others a longer grid and bathymetry (in the alongshore direction) were created.

Figure 3.10 TBR1 bathymetry created after the morphology observed at the head of the Sand Motor in August 2013

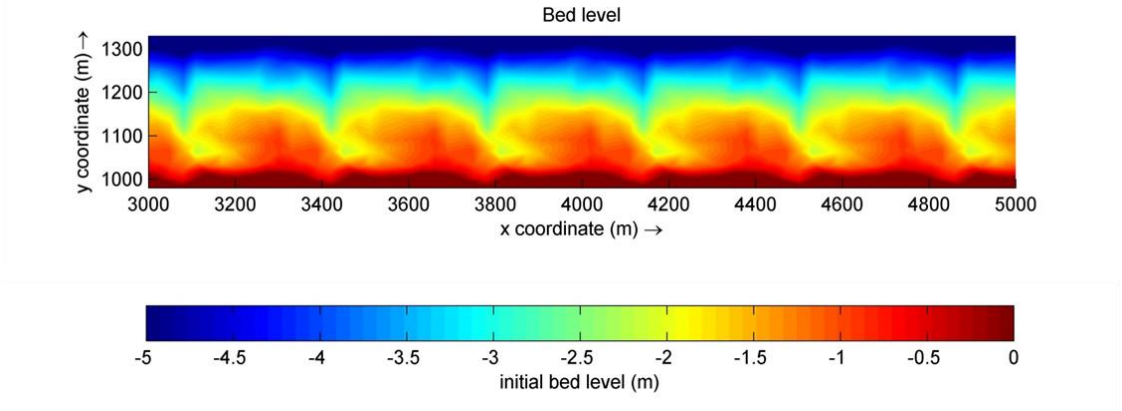

Transverse bar and rip, north coast of Sand Motor

TBR2 presents an alternating pattern of transverse bars and shoals (figure 3.11).To assemble this bathymetry, only the dimensions of the middle shoal and right bar (transects 2 and 3 respectively, figure 3.7) were considered. However, length scales of both rip channels (i.e. rip channel spacing between the left bar and shoal, and between right bar and shoal, as indicated in table 3.2) observed in this morphology were taken into account.

Figure 3.11 TBR2, created after the morphology observed at the north coast of the Sand Motor in August 2013

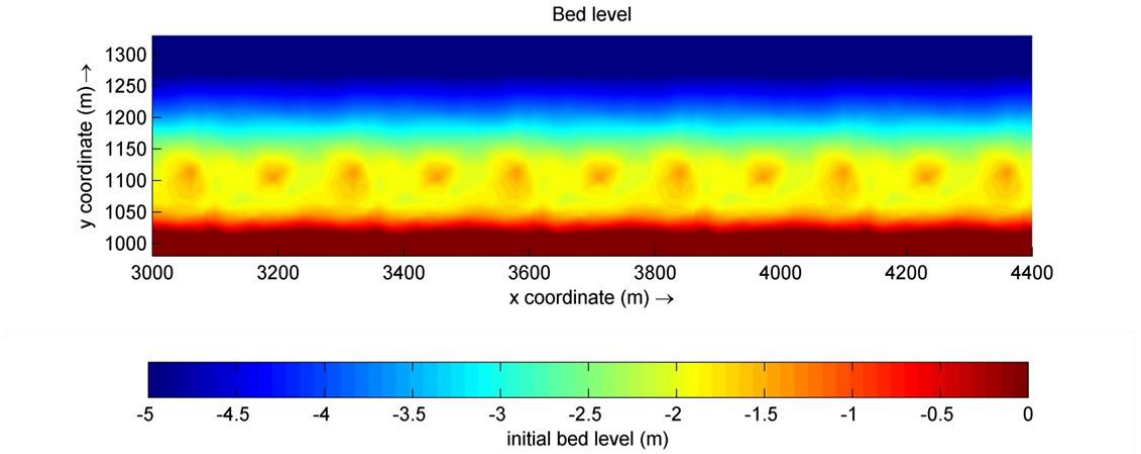

3.3.2 Quantification of morphological variability

One of the aims in this study was to investigate the extent to which morphological variability can impact net longshore sediment transport. The simulation bathymetries described in the previous section, present a range in alongshore morphological variability: From completely alongshore uniform, to rhythmic and highly variable features that are displayed along the coast. The σ_z^2 parameter which estimates the total alongshore morphological variability was then estimated for the 4 alongshore variable bathymetries after de Schipper *et al.* *(*2013).

For the computation of this parameter, an alongshore averaged bed elevation profile was defined, to which the actual bed level in each *x* coordinate was subtracted, in this way the height of level variability (z_{var})was obtained. The bulk alongshore variability metric was then obtained

$$\sigma_z^2 = \frac{1}{l_y L_x} \int_0^{L_y} \int_0^{L_x} (\, Z_{var}(x,y)\,)^2 dxdy$$

Where L_y and L_x are the cross-shore and longshore extent of the bathymetry domain.

The alongshore variability in morphology is greatest for TBR1, followed by TBR2 where σ_z^2 is almost and order of magnitude lower and similar to that in LBT2, finally LBT1 exhibits the lowest variability (table 3.3)

Table 3.3 Total alongshore morphological variability for each of the simulation bathymetries.

	LBT1	**LBT2**	**TBR2**	**TBR1**
σ_z^2	9.9E+05	3.3E+04	4.1E+04	3.1E+03

3.3.3 Alongshore uniform bathymetries

Based on the previously estimated averaged profiles, additional bathymetries characterized to be completely alongshore uniform were created (figure 3.12). Simulations of sediment transport for situations in which morphological variability is absent would provide an indication of the effect of a mean profile slope and shape in the computed transport rates.

The swash zone slope for the alongshore averaged profiles can be appreciated in figure 3.12. The LBT morphologies exhibit the steepest slopes (0.034 and 0.03 for LBT1 and LBT2 respectively), followed by TBR2 (0.016) while the mildest is that for TBR1 (0.012).

Figure 3.12 Alongshore uniform bathymetries and beach profile: LBT1$_{uniform}$ (a), LBT2$_{uniform}$ (b), TBR2$_{uniform}$ (c) and TBR1$_{uniform}$ (d)

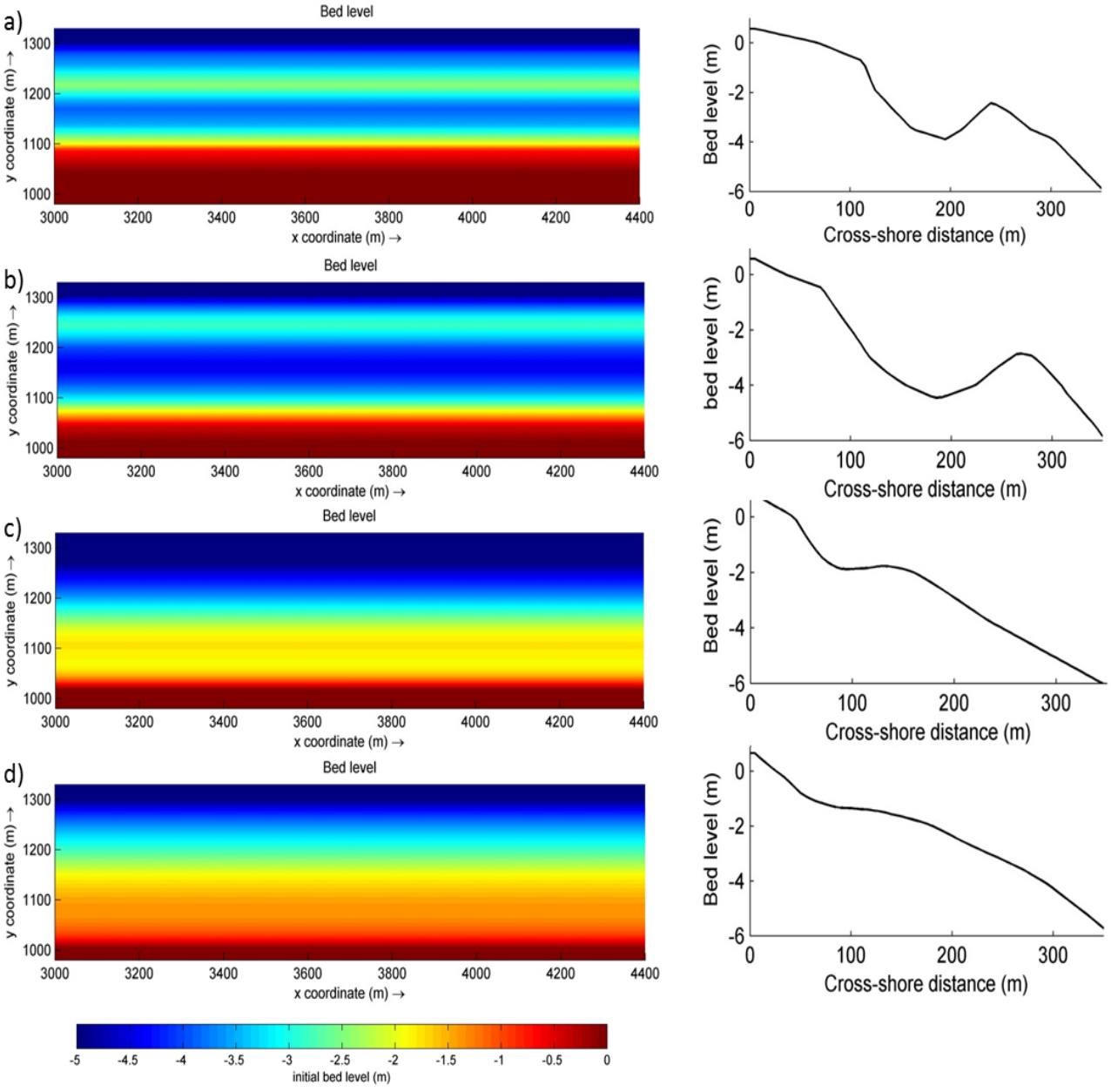

3.4 Association of beach states with wave conditions

Typical wave conditions at the Dutch coast are characterized predominantly by locally generated seas. Given the configuration of the North Sea and the position of the Dutch coast with respect to England, there is a relatively short fetch towards the direction of the main wind condition, i.e. winds that blow from the southwest (Kaji, 2013); while larger fetches enable longer swell waves to approach the coast from the north and the northeast.

Figure 3.13 depicts a computed wave climate time series (from a wave transformation table (Deltares, 2015)) from August 2010 to November 2014 at a 10m water depth in front of the coast of the Sand Motor. Since the Dutch coast is oriented roughly southwest-northeast, incoming waves range in directions from approximately 30 to 200 degrees with respect to the north, but are most common from directions between 270 to 330, this results in both positive and negative angles of wave incidence with respect to the shore coast normal. Significant wave heights are most frequent between 0.5 to 1.5m with an average of 0.9m, while the average wave peak period is 5s. Most energetic conditions occur typically between October and January where high waves (i.e. significant wave heights from 3.5-4m and periods of 8-10s) approach the coast from the west and northwest.
Relatively calm wave conditions (Hs=0.5-1.5m Tp=4-8s) characterized the wave climate at the Sand Motor during August 2013, period for which the bathymetric survey used for the construction of 4 of the simulation bathymetries was performed, while for November 2014 (bathymetry data used to construct LBT2) more energetic events occurred with significant wave heights up to 2m.

Figure 3.13 Computed wave climate for the Sand Motor: Time series from August 2010 to November 2014 at a 10m water depth. The months of August 2013 and November 2014 are highlighted with red boxes.

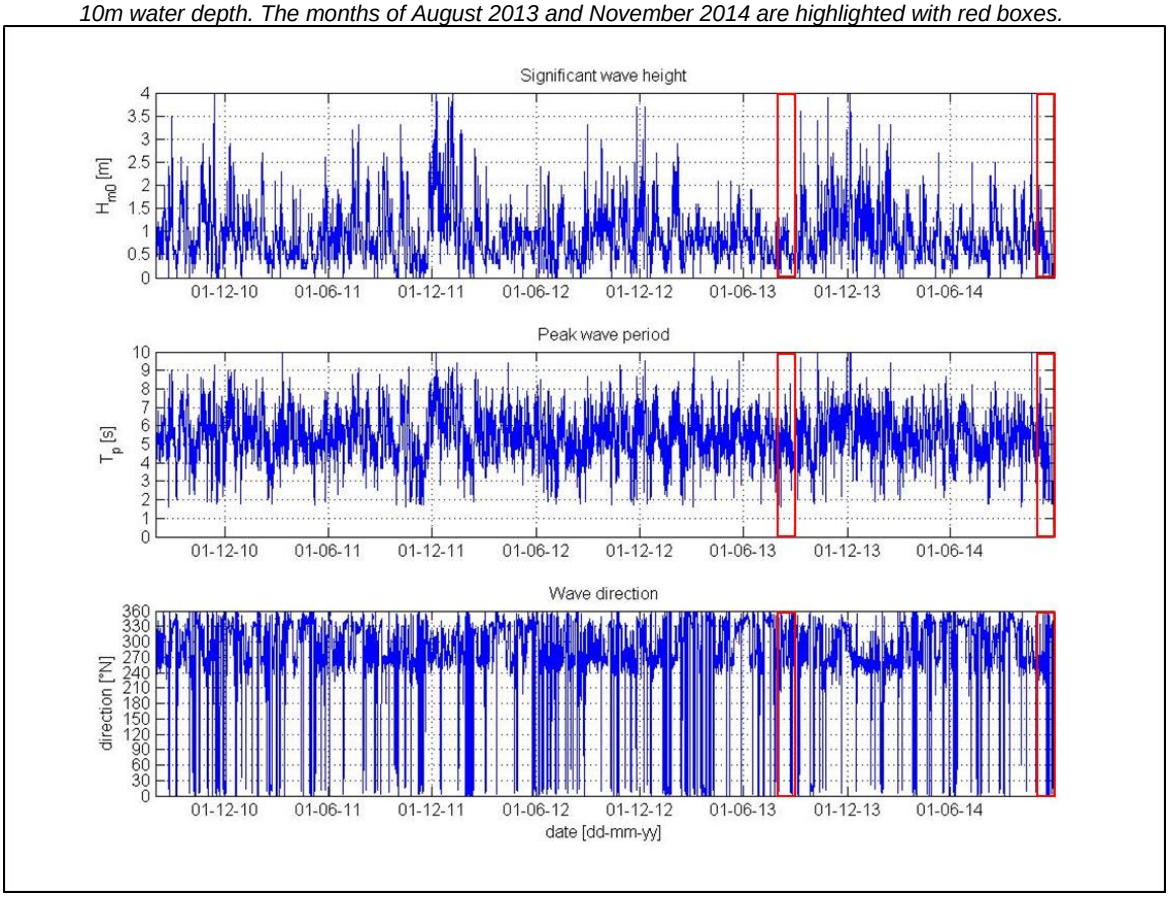

4 Model investigation of the impact of beach states on sediment transport

4.1 Introduction

After having assembled the morphological information that embodies observations at the Sand Motor, the next phase in this study is to investigate how net longshore sediment transport varies for each situation. This was carried out with the use of a numerical model capable of predicting longshore sediment transport. Simulations included a range of wave climate scenarios chosen specifically to assess sensibility to diverse hydrodynamic forcing conditions. Section 4.2 in this chapter describes the followed modelling approach. Prior to analysis of sediment transport, model set up involved execution of several sets of simulations in order to achieve the optimal model settings, this is elaborated in section 4.3. Section 4.5 include the results of the different analysis and finally, discussions and conclusion are given in section 4.6.

4.2 Modelling approach

The use of numerical models allows predicting and understanding hydrological and morphological processes occurring over a variety of coastal environments. For this study, the use of a process based model, Delft3D, provided the means to analyse and compare sediment transport rates in very different morphologies and under a range of hydrodynamic conditions. Such type of study is hard to perform with field experiments as the specific combinations of hydrodynamic forcings and beach states to which sediment transport rates are compared might not occur synchronously within the time and spatial scales to which campaigns take place. Additionally, numerical simulations permit isolation of the different forcings occurring on the field (e.g. waves, tides, wind) and with this sediment transport driven exclusively by wave motions and wave generated currents can be assessed.

Initial sediment transport was simulated for the 8 created bathymetries by imposing a number of wave climate scenarios with the aim of investigating *1)* if there is a response in net longshore transport to the morphodynamic state of the beach, *2)* how sensible such response is to different wave forcings and *3)* how important the mean profile shape and alongshore morphological variability are for the determination of transport rates in each situation.

1 Qualitative and quantitative analysis of longshore sediment transport
In order to get a first estimate of how the existence of different beach states affects net longshore transport both a qualitative and quantitative analysis was performed for a reference wave condition. The former was made through visual examination of map plots of the relevant parameters: depth averaged velocity and total sediment transport, of main importance, while wave height and wave dissipation maps contributed to a better understanding of the first two. Additionally, cross shore transects showing the normal distribution of wave height; longshore current and longshore sediment transport were inspected. These two types of plots were found to be rather useful for identifying under which circumstances net longshore sediment transport is impacted by an alongshore varying topography.

A bulk longshore sediment transport rate (Q) was determined for simulations in the different bathymetries by integrating the total longshore transport per individual cross sections and then averaging along an extension of the computational domain (see section 4.3.2). The longshore total transport is defined as the sum of bed load and suspended load of sediment that is transported in the longshore direction. For convenience of the reader the bulk transport rate Q is expressed in units of m^3/year.

2) Sensitivity of net longshore transport to varying hydrodynamic conditions
The same qualitative and quantitative analysis was performed for sets of simulations in which different combinations of wave height and wave angle of incidence were imposed. As observed at the Sand Motor, the transverse bars in the created bathymetries, are somewhat oblique with respect to the coastline: The big bars in TBR1 are oriented towards the northeast (in the computational domain), and to a minor extent, the shoals in TBR2 are slightly tilted towards the east and spacing between rip channels is not completely symmetric. For this reason it was considered important to check sensibility of sediment transport not only for increasing/decreasing wave height and wave angles, but also to positive and negative angles of wave incidence.

3) Relative contribution of profile slope and alongshore variability in morphology to sediment transport
The computed transport rates for the alongshore uniform and the alongshore variable morphologies were compared in order to identify the importance that the mean profile slope and morphological variability have for determining sediment transport for the different simulated situations.

4.3 Numerical model

4.3.1 Description of Delft3D

Delft3D is a numerical modelling software suite that performs simulations of flows, sediment transports, waves, morphological development, water quality and ecology in coastal, rivers and estuarine areas based on fundamental mechanisms and processes describing each phenomenon. It is composed by a number of modules, each of which addresses specific domains of interest. Delft3D-FlOW is the hydrodynamic and the core module in the model suite given that it provides the unsteady flow and transport information that is used as a basis in other modules (Deltares, 2014).

Delft3D-FLOW simulates flow and transport phenomena resulting from tidal and meteorological forcing by solving the unsteady shallow water equations in two (depth-averaged) or three dimensions. The system of equations, derived from the three dimensional Navier-Stokes equations for incompressible free surface flow, consists of the horizontal equations of motion, the continuity equation and the transport equations for conservative constituents. Numerically, the partial differential equations are solved by finite differences once they are discretized in space with the use of curvilinear or rectangular grid cells (Deltares, 2014).

Delft3D-WAVE simulates the evolution of random, short crested wind-generated waves in diverse water bodies. This module is based on SWAN (Simulating Waves Nearshore), a third-

generation wave model that uses action density $N(\sigma,\theta)$ (equal to energy density divided be the relative frequency$\frac{E(\sigma,\theta)}{\sigma}$), to describe development of the wave spectrum. Delft3D-Wave solves the action balance equation in stationary mode, with finite difference schemes in the space and spectral dimensions. Geographic space is discretized with a rectangular grid with constant resolutionsΔx, Δy while the spectrum in the model is discretized with constant directional and relative frequency resolutions $\Delta\theta$ and $\Delta\sigma/\sigma$ respectively (Deltares, 2009).
In the present study, these two modules are coupled in an online mode to have a dynamic interaction for which the effect of flow on waves via set-up, current refraction and enhanced bottom friction; and the effect of waves on current via forcing, enhanced turbulence and enhanced bed shear stress (Deltares, 2009) are taken into account.

4.3.2 Model set up

Several simulations with arbitrary wave climate conditions were executed in which key parameters were varied until stable and consistent computations on flow and transport resulted for the set of 8 previously constructed bathymetries. The most important parameters for the model set up were found to be, the extent of the computational domain, the computational time step and the inclusion of the roller model for flow computations, as described below.

Computational domain

A single layer model (2Dh) was used for all simulations in this study as the computational effort of multiple vertical layer models (3D) often becomes too high. Furthermore, the aim of the study is to assess trends in the net longshore sediment transport, therefore depth averaged computations provide sufficient information. Simulations of morphological changes which require resolution of the vertical flow (i.e. driven by strong non uniform vertical structures of the flow (Ranasinghe, et al., 2004)) are beyond the scope of this report.

The computational domain for both flow and wave simulations is defined by rectangular grids for which the *x* coordinates following the longshore direction, while the normal distance to the shore is represented by *y* coordinates (depicted in figure 4.1).Dimensions of the domains both in the cross-shore and longshore direction were critical for reaching consistent computations of velocities and sediment transport (see figure 4.1). As mentioned in section 3.2, resolution of the grids was set to 5 x 5 m for both cases.

In the cross-shore direction the computational domain for all bathymetries was extended up to a distance of 550m and a depth of 10m, in such a way that the offshore boundary, was far from the area of interest and that refraction did not affect the wave field at that point. In the longshore direction, the extension for which regular patterns in the flow and transport were computed by the model (i.e. consistent patterns following the repeating features of the underwater topography) varied for the different bathymetries: for the transverse bar morphologies, larger morphological features required larger extensions (figure 4.1). Consistency (i.e. computed transport rates between same positions in the repeated bathymetric patterns that varied less than approximately 2%) was reached for lengths of 1,600m for the LBT morphologies, and 2,200 and 4,350m for the TBR2 and TBR1 bathymetries respectively.
One wave grid extending 5,200m in the longshore and 570m in the cross-shore direction was used for all the bathymetries. These dimensions were set so as to comprise a large enough domain to avoid wave field disturbances near the flow grid open boundaries (Deltares, 2009).

Figure 4.1 Inconsistency in depth averaged velocity computations for the TBR2 bathymetry with a 1600x350m computational grid: boundary effects result in overestimation of the velocities in the left area of the computational domain

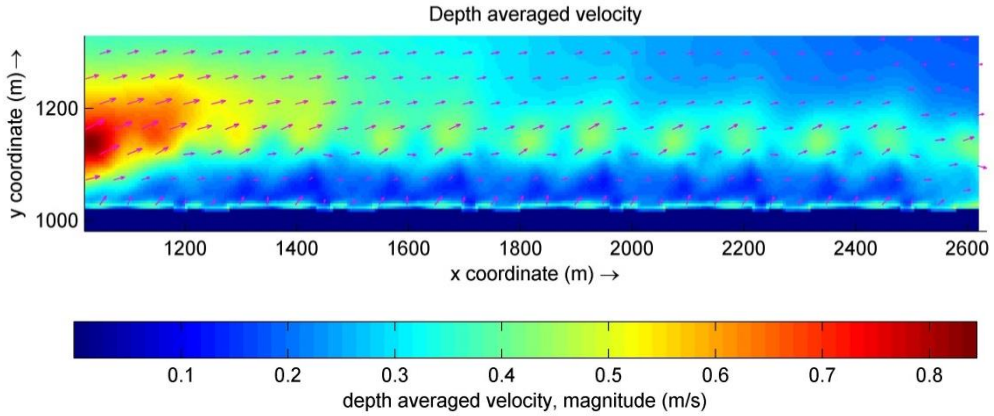

Computational time step

An important parameter that determines accuracy and convergence of the simulations is the computational time step. For a given grid cell resolution, usage of a too large time step can result for example in exceptionally high changes in water level and velocity in the same grid cell between consecutive time steps. A convergence criterion is the Courant-Friedrichs-Lewy (CFL) condition:

$$CFL = \frac{\Delta t\sqrt{gH}}{\{\Delta x, \Delta y\}} < 10$$

Where Δt is the computational time step, g the acceleration of gravity, H is the total water depth, and $\{\Delta x, \Delta y\}$ is a characteristic value of the grid spacing (e.g. the minimal value) in the cross-shore and longshore direction (Deltares, 2014). A number of time steps ranging from 3 to 15s where tested in simulations for all morphologies, and a time step of 6s was found to be the most cost-effective (with respect to accuracy and computational effort). While the courant condition for this time step was not fulfilled in the entire computational domain of the different bathymetries, small differences between simulations with smaller time steps where found: as an example, bulk sediment transport rates varied in the order of 2%; suggesting good convergence in the solutions for the selected time step.

Roller Model

A roller model extension in the Delft3d model suite allows including the effect of rollers on wave dissipation: At the point of breaking, wave energy is first transferred to roller energy before it is dissipated; this causes a spatial lag between the location of wave breaking and the actual dissipation (Reniers, et al., 2004). Even though several studies have proved that including rollers in the wave forcing results in improved simulation of observed longshore currents structures by velocity maxima is shifted landwards in comparison with models with no rollers (Ruessink, et al., 2001); inclusion of the roller model in the simulations for this study resulted in convergence complications that would ended in crash of simulations of determined morphologies. Even when the time step was decreased to 1.5s high inaccuracy of computations remained. Therefore results of current velocity and sediment transport

presented on this study are exclusive of simulations that include the roller model. This however resulted in estimations of lower current velocities and sediment transport rates. Figure 4.2 depicts the errors on the longshore current and longshore sediment transport between simulations with and without inclusion of roller energy for the LBT1 bathymetry. A comparison of the sediment transport rates computed for the several bathymetries showed differences between model schematisations ranging from 40 to 90%.

Figure 4.2 Longshore current (top) and longshore sediment transport (bottom) for LBT1at an arbitrary transect.

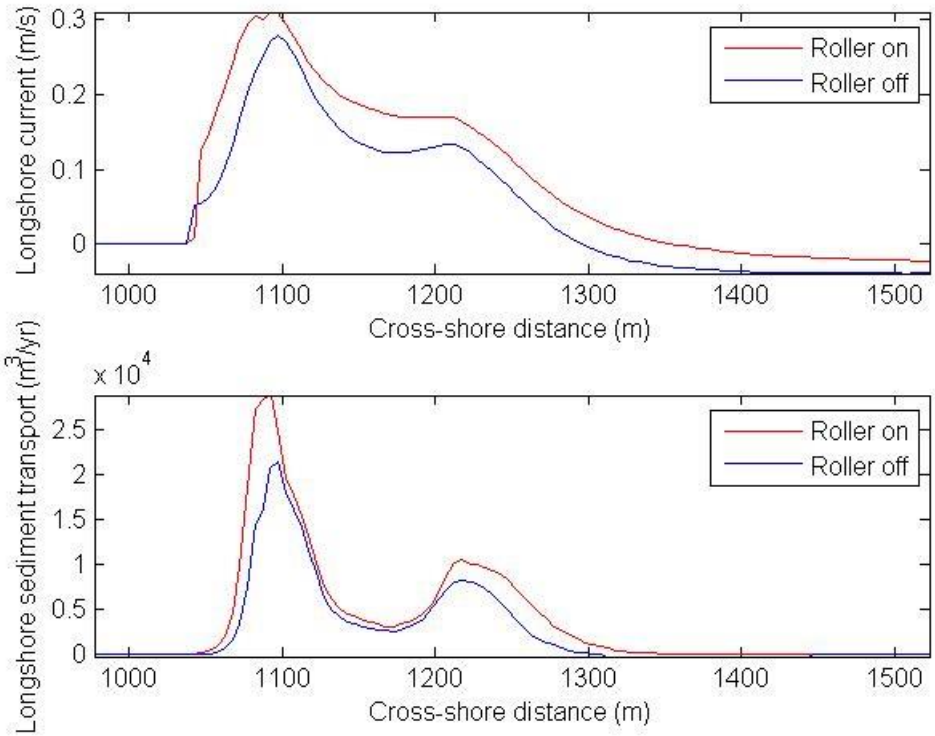

Initial and boundary conditions

Open boundaries are set on Delft3D to delimit the computational domain across a flow field. Conditions prescribed at these boundaries represent the type of forcing on the flow in the areas beyond the modelling domain. A water level boundary was defined at the seaward limit of the domain. Given that the primary focus on this study is on longshore sediment transport driven by wave generated currents, the water level at the offshore boundary was set to zero, to exclude tidal processes. Neumann boundaries, representing and alongshore water level gradient were imposed at both cross-shore boundaries. The gradients in water level are calculated from conditions at the seaward boundary, thus these too are set to zero.

Initial conditions of sediment concentration and water levels are set to zero over the entire computational domain. Since boundary conditions at the start of the simulation match the initial conditions, few disturbances are expected (Deltares, 2014) and hence a smoothing time of 60 min was set to allow damping of the generated transient solution (if any).

The hydrodynamic boundary conditions for the wave module were prescribed via a *wavecon* file, which indicates: the significant wave height (H_s), peak wave period (T_p), wave direction (θ), directional spreading (m), additional water levels and wind speed and direction at specific

time steps. Steady wave conditions were imposed for the simulations. The above is again justified on the focus of the study, and with this the assumption is made that the time scale for the longshore current to reach equilibrium lies well within a time scale of steady wave conditions (i.e. hours before conditions change).
For the initial set up simulations the wave climate is defined by $H_s = 1.5m$, $T_p = 6s$ and $\theta = 355°$ or - $5°$ with respect to the shore normal, from now on the latter will be used. No wind or additional water level were included and the default value for $m = 4$ was used. Simulation time was set to 12 hours for all cases.

Sediment and morphological settings
Sediment characteristics for all simulations were uniform in space. A median grain size diameter (D_{50}) of 278µm was specified. This figure resembles grain size distribution at the Sand Motor as D_{50s} of 215-350 µm have been recorded throughout morphological surveys (Kaji, 2013). The sediment specific density was assumed 2,650kg/m^3 with a dry bed density of 1,600 kg/m^3.
Sediment transport in all simulations is computed with the TRANSPOR2004 formulation (van Rijn , et al., 2004), an improved combination between its antecessors TRANSPOR1993 and TRANSPOR2000 and new approximation formulations.
No morphological changes were allowed during the simulations, as these would affect the distribution of nearshore circulation and sediment transport, especially for the transverse bar morphologies.

4.4 Impact of beach states on net longshore sediment transport for a reference situation

This subsection regards the analysis of the spatial distribution of sediment transport and wave generated currents, as well as the quantification of net longshore transport for each of the alongshore variable bathymetries. The imposed wave climate,$H_s = 1.5m$, $T_p = 6s$ and $\theta = 355°$ or - 5° with respect to the shore normal (at the 10m depth contour) represents a typical sea condition in the Dutch coast. The aim is to identify how sediment transport behaves in the different beach states, under a reference wave climate, in order to allow comparison between simulations with different wave conditions. Quantification of transport in the alongshore uniform bathymetries is given in the following subsections.

Qualitative analysis of flow and sediment transport

The longshore bar and trough morphologies promote the formations of continuous longshore currents with two velocity peaks: the first one located at the initial point of wave dissipation (i.e. the offshore bar) and the second one, higher in magnitude reaching velocities of approximately 0.3 m/s (figure 4.3), located in the swash zone, where the remnant wave energy is ultimately dissipated. Sediment transport follows closely this distribution. The effect of a variable topography appears to be higher in the swash zone, where the rhythmic patterns in the coastline result in a less alongshore uniform longshore current and with this, magnitudes of longshore transport also vary from one place to another (figure 4.5a).

Figure 4.3 Computed depth averaged longshore current and bed level for LBT1

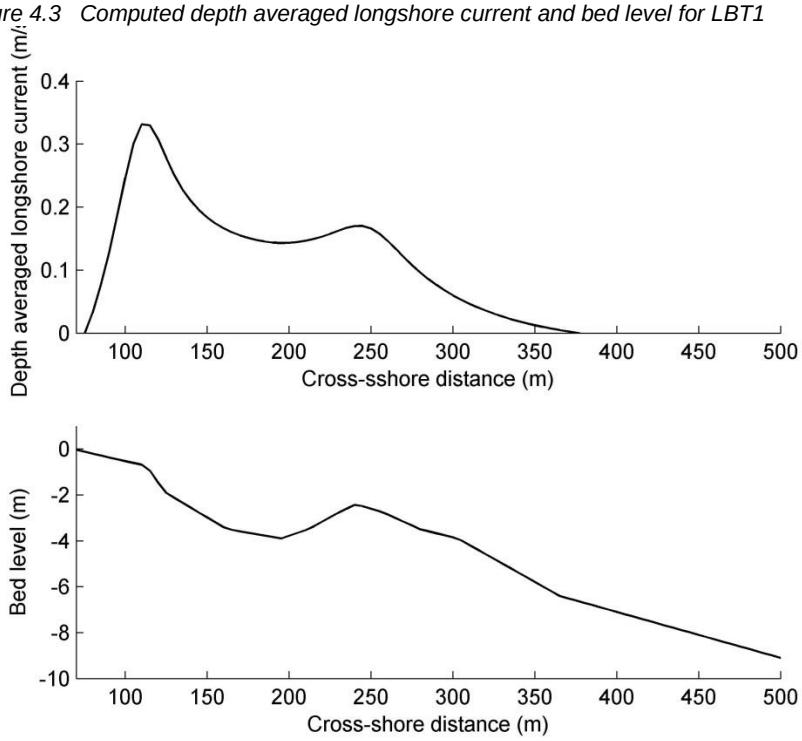

Sediment transport in TBR2 exhibits a higher spatial variation than for the case of the LBT morphologies (figure 4.5b). Along the coast, transport is increased at the seaward end of the shoals (orange patches), where higher wave dissipation occurs and the alongshore component of the flow is strongest with velocities of around 0.3 m/s; in the adjacent deeper rip channels and trough regions, transport decreases and is then directed obliquely

landwards. In the cross-shore direction significant sediment transport takes place over a broad area, given a relatively shallow bed. Figure 4.4 depicts the cross shore distribution of the longshore current and longshore sediment transport for a bar (black curve) and a rip (red curve) profile. It is noted how even in the absence of a shoal waves dissipate and generate a longshore current that is able to transport sediment along the coast.

Figure 4.4 Depth averaged longshore current, longshore sediment transport and bed level for a bar(black curves) and rip (red curves) profile in TBR2.

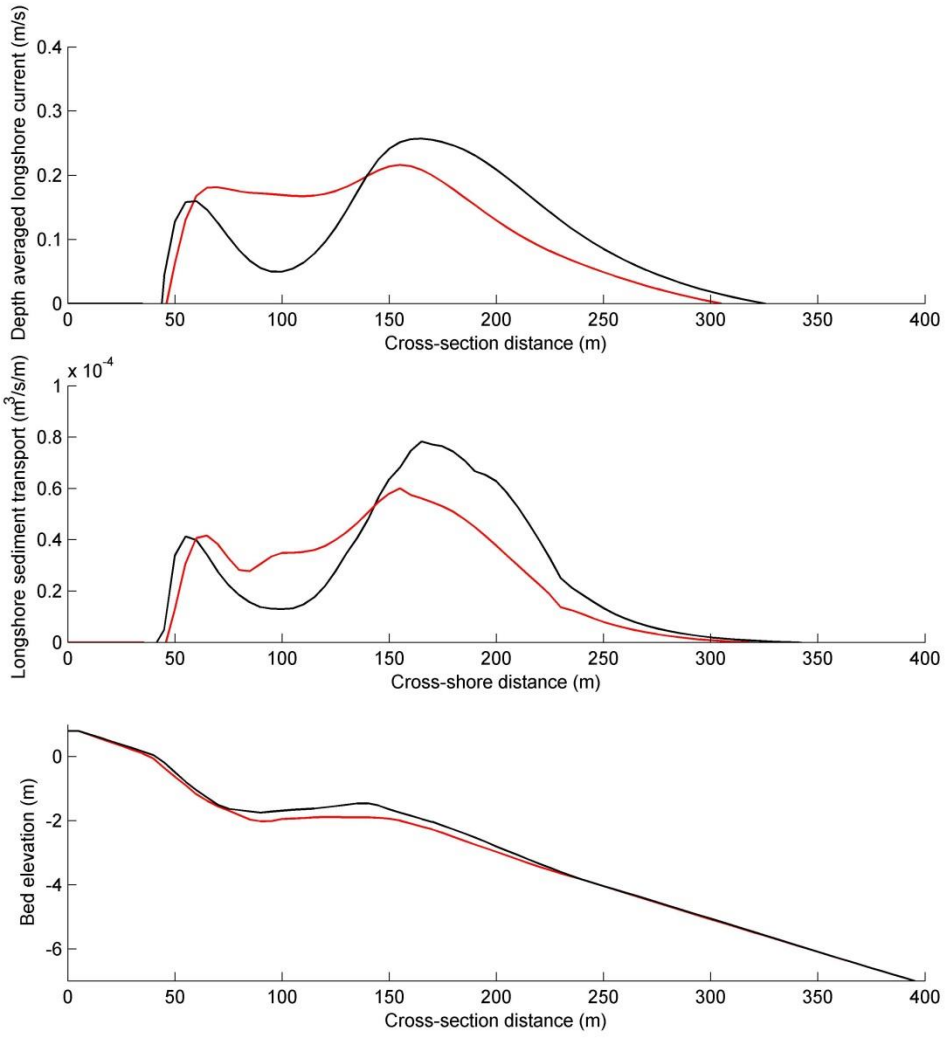

The most complex behaviour on the flow and sediment transport occurs for the TBR1 bathymetry. The strong rip circulation that can be observed in figure 4.6 is a result of the different wave breaking patterns between the transverse bars and the rip channels. As wave shoaling and breaking is enhanced over the former, the water level set up that counteracts the created wave forces is higher to that on the rip channels, where wave breaking is less intense (Bosboom & Stive , 2013). The alongshore gradient in water level then drives an intense flow towards the rip channels (yellow to orange patches) that latter deviates offshore and reaches magnitudes of around 0.8 m/s. This results in positive and negative longshore sediment transport. The former is associated with the current that feeds the rip and flows in the same direction as the longshore current, resulting in velocities of approximately 0.5m/s.

Significant negative transport occurs in the seaward end of the bar, where the rip current deviates and flows opposite to the longshore current thus completing a vortex circulation.

Figure 4.5 Longshore sediment transport simulated for the LBT2(a) and TBR2(b) bathymetries.

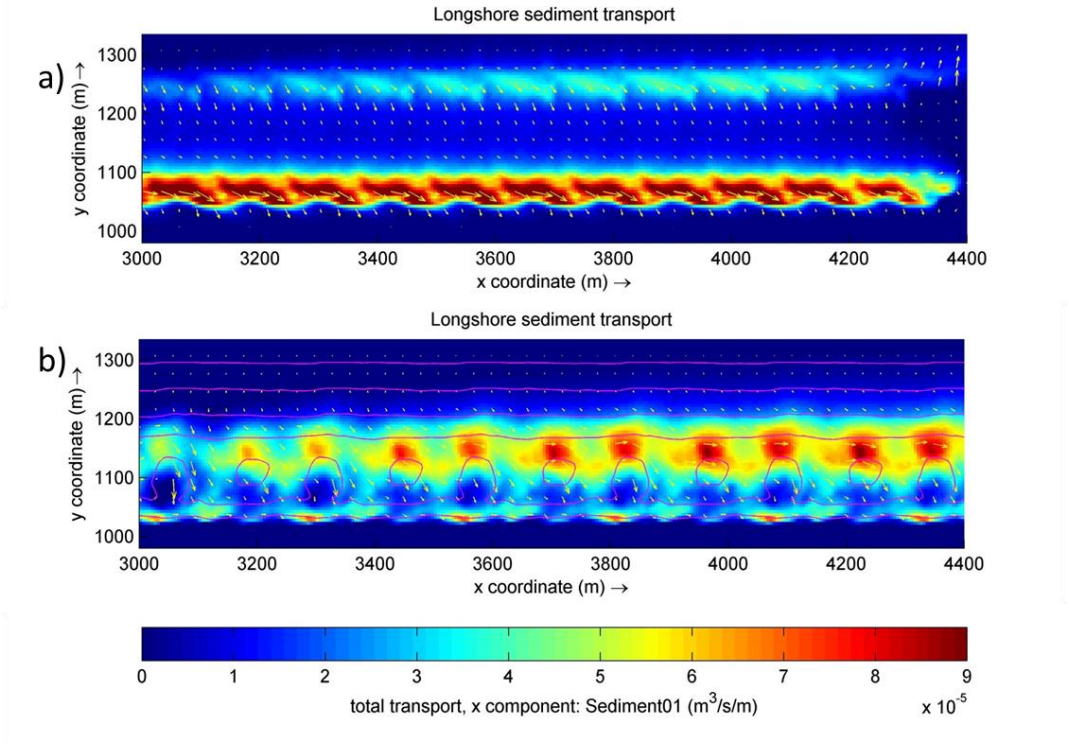

Figure 4.6 Depth averaged velocity (a) and longshore sediment transport (b) simulated in TBR1

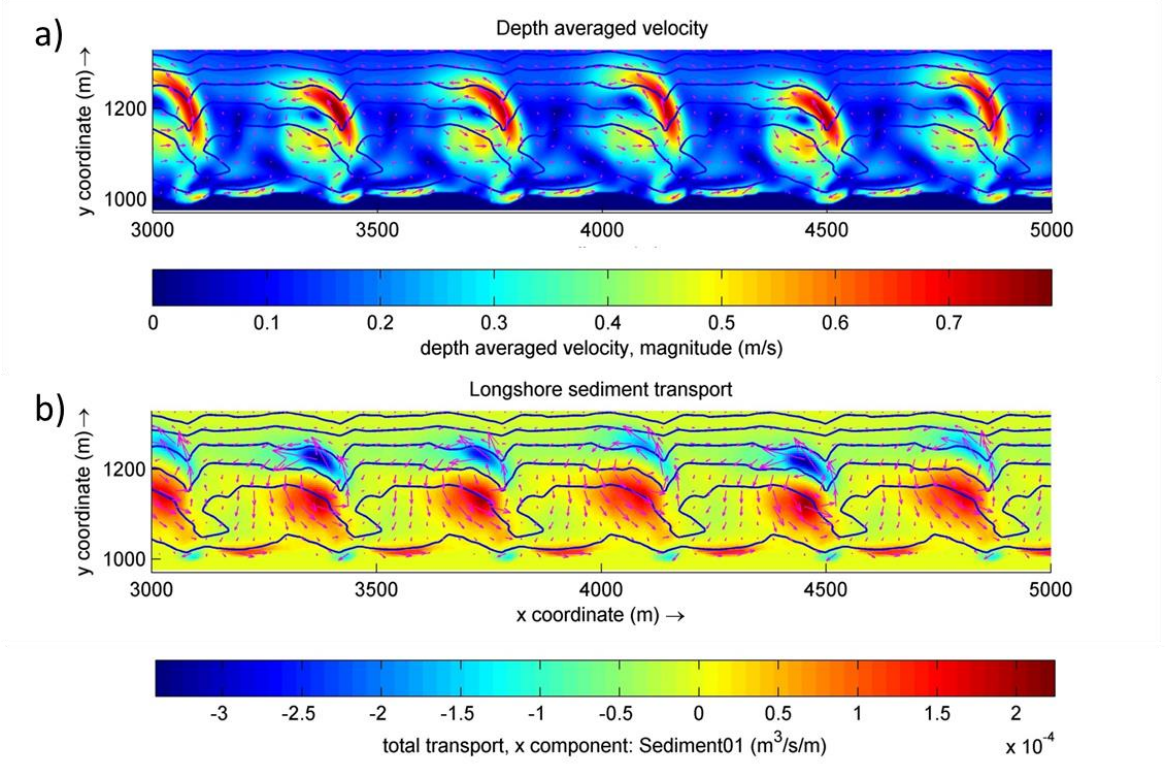

Quantification of net longshore sediment transport

Table 4.1 provides the estimated Q for each bathymetry. Net longshore transport is highest for TBR2 but is fairly similar (about 6% higher) to that in the LBT morphologies. Despite the higher variation in transport magnitudes along the coast observed in the former, the shallower nearshore features promote transport rates comparable to the ones in the more uniform bathymetries. As for TBR1, a negative Q results from the complex rip circulation, however this figure is an order of magnitude lower than in simulations with other bathymetries, indicating that even when the net value is negative, the majority of the transport takes place within closed cells and little sediment is transported along the coast.

Table 4.1 Net longshore transport rates simulated for each bathymetry under incidence of waves with H_s=1.5 T_p=6s andΘ=5° at 10m water depth.

	LBT1	LBT2	TBR2	TBR1
$Q\ [m^3/yr]$	2.48E+05	2.49E+05	2.67E+05	-6.50E+04

The above findings suggest that the response of net longshore transport trough a range of morphological configurations depends not only on the degree of morphological variability along the shore. Wave dissipation and the resulting longshore current that drives sediment transport, depends to a high extent on the profile slope, an also important factor that characterizes the state of the beach. In this way, the general slope of the profile is equally or even of higher relevance when determining the response of net longshore transport.

4.5 Sensitivity of net longshore transport to wave angle and wave height

4.5.1 General

In order to investigate if the response in net longshore transport for different beach states found above still holds when subject to different hydrodynamic conditions, six combinations of wave height and wave angle were tested in the different bathymetries; however for each combination both a positive and a negative angle of wave incidence were considered for simulations. Negative and positive wave incidence is defined as waves approaching from the northwest and northeast of the computational domain respectively. This made a total of 12 different wave conditions to be imposed in the 8 created bathymetries. Table 4.2 provides this information. Only significant wave height and angle of incidence were varied since these appear to be the parameters determining the sensibility in nearshore circulation patterns (Yu & Slinn, 2003).

Table 4.2 Significant wave height, angle of wave incidence with respect to the shore normal, and peak wave period at 10m depth imposed for the sensitivity analysis.

	Negative angle, test *a*			**Positive angle, test *b***		
	H_s [m]	Θ [°]	T_p [s]	H_s [m]	Θ [°]	T_p [s]
Reference High waves low angle	1.5	-5	6	1.5	5	6
Test 1 High waves medium angle	1.5	-20	6	1.5	20	6
Test 2 High waves low angle	1.5	-45	6	1.5	45	6
Test 3 Low waves high angle	1	-5	6	1	5	6
Test 4 Low waves medium angle	1	-20	6	1	20	6
Test 5 Low waves low angle	1	-45	6	1	45	6

In the following subsections the qualitative and quantitative sensitivity analysis of sediment transport for the modelled scenarios are described for the alongshore variable morphologies. The corresponding analysis for the alongshore uniform bathymetries will be addressed in section 4.6. In the former, a comparison will first be made for simulations with increasing wave angle (section 4.5.2), comparing the reference, test 1 and test 2 simulation sets; while sensitivity to wave height (section 4.5.3) is addressed by comparing with simulations in test 3, test 4 and test 5.

It is important to mention that the estimated bulk transport rate for a same bathymetry and same simulation test but with opposite wave angle (i.e. positive, negative) was found to deviate even for the alongshore uniform bathymetries, where no variation was expected. For most of these simulations a variation in the transport magnitudes was equal or lower than 3%, however in 4 specific cases (refer to Appendix B) transport rates deviated up to 13%. This was therefore considered the accuracy of the model to simulate longshore sediment transport. The magnitudes of Q for simulation tests with a positive and negative wave angle (for the alongshore uniform bathymetries only) were then averaged to allow a

consistent comparison between simulations. For the sake of comparison, transport rates are now addressed as normalized rates (Q_{norm}) with respect to the idealized LBT1$_{uniform}$.

4.5.2 Sensitivity to angle of wave incidence

Reference test-b: High waves, low angle

The qualitative description of patterns in longshore transport for the reference situation (with a negative wave angle) was described in the previous section, to recapitulate the estimated bulk transport rates, now expressed as Q_{norm} were 0.88, 0.95 and -0.23 for the LBTs, TBR2 and TBR1 respectively. Even though, the estimated Q_{norm} for LBT1, LBT2 and TBR2 deviated for simulations with a positive wave angle of incidence (1.04, 1 and 1.08 respectively), the spatial distribution of sediment transport appear to be very similar in both cases. Furthermore given the estimated accuracy of the model, it is concluded that sediment transport in these three bathymetries does not vary significantly for the particular wave conditions imposed in this test.

Nevertheless, this was not the case in TBR1. Where the flow and sediment transport patterns do exhibit significant changes. Rip circulation is also generated for this situations, however this time the rip flows in the same direction as the longshore current, and thus enhances sediment transport. In contrast to the situation with a negative wave angle, the offshore directed flow is now fed from both sides of the rip channel: The feeder current to the left of the rip flows opposite to the longshore current (figure 4.7a). Both currents converge over the channel with velocities of approximately 0.3 m/s and then deviate seawards with a trajectory that follows the depth contours.
Longshore sediment transport in opposite directions also occurs in this case: positive transport (i.e. against direction of the longshore current) is now restricted to the location were the feeder currents are active, while negative transport (in the direction of the longshore current) is predominant in space and being significantly enhanced by the rip current (figure 4.7b). This results in a Q_{norm} of 1.45, which is significantly above the transport rates for all the other bathymetries.

Summary of simulations in reference test

-Wave conditions: H_s=1.5m T_p=6s θ=-5 and 5°.

-Q_{norm} test a: LBT2, LBT1 :0.88 →TBR2: 0.95 →TBR1:-0.23

-Q_{norm} test b: TBR1: 1.45 →TBR2: 1.08 →LBT1: 01.04→ LBT2: 1

-High variability in the spatial distribution of sediment transport results in significant increase of net longshore sediment transport in the case of a positive wave angle, and a decrease for a negative angle.

Figure 4.7 Depth averaged velocity (a) and longshore sediment transport (b) for TBR1 in test b

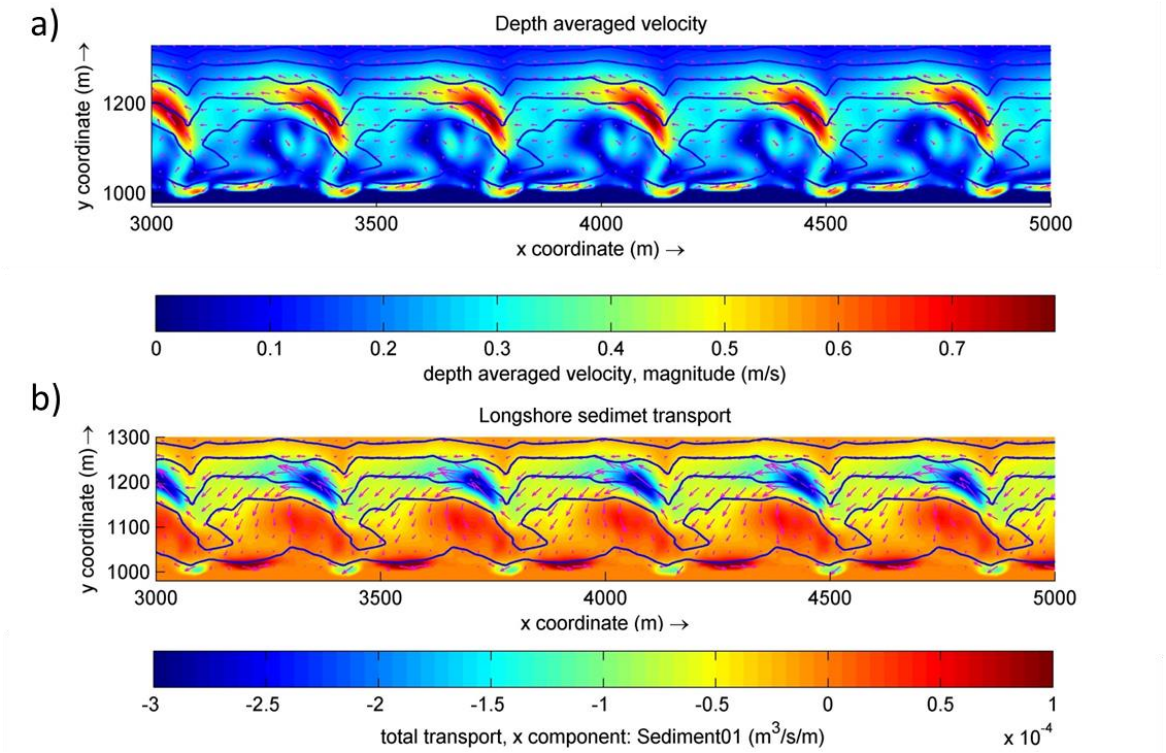

Test 1: High waves, medium angle

The LBT morphologies exhibit the highest longshore transport rates (Q =1x10^6 m^3/year). For both positive and negative wave angle simulations Q_{norm} values were estimated to be very close to 1. For an increasing wave angle the longshore current peaks with velocities of around 0.8m/s (for both LBT1 and LBT2) in the swash zone and appears to be more uniform along the coast a similar behaviour is observed for longshore sediment transport (figure 4.8a).

Velocity and transport vectors for TBR2 also indicate a higher influence of the longshore current as the angle of wave incidence has increased: the previously observed deviation of the vectors in deeper areas is now even more reduced (figure 4.8b). As before, the highest sediment transport takes place in proximity to the crest of the connected and disconnected shoals; however this difference appears to be reduced for this situation. Very limited transport occurs in the swash zone as compared to the LBT morphologies given the more dissipative character in the upper nearshore areas for this bathymetry. The normalized net transport rates Q_{norm} are estimated as 0.73 in test *a* and 0.82 for test *b,* despite the fact that qualitatively, no difference in the behaviour of sediment transport and depth averaged velocities is displayed between the two situations. In any case, a more significant reduction in the transport occurs for this bathymetry, and given that no increased alongshore variation in sediment transport is observed, it becomes apparent that this reduction is more influenced by the general slope and shape of the beach profile, rather than the alongshore variation in morphology.

Velocity and sediment transport for TBR1 show a higher variability along the coast than TBR2, and again different patterns for both parameters are observed when waves approach at a negative and positive angle. Even though a cell-like circulation that promotes longshore transport in opposing directions occurs now that the angle of wave approach has increased to 20° at the seaward boundary of the computational domain, the longshore current and sediment transport exhibit undulating trajectories that follow the underlying depth contours of the seaward limit of the bars.

In the case of a negative wave angle (test *a*), the flow describes more meandering trajectories, and it is especially accelerated (velocities of 0.5m/s) in the locations where a feeder current was present in the case of smaller angle of incidence resulting in an increase of sediment transport in the same location (figure 4.8c), after bypassing the rip channel the magnitude of the longshore current decreases and it is directed slightly more towards the offshore. On the contrary, when waves approach at a positive angle from the shore normal (test *b*) the more uniform longshore current accelerates after it has bypassed the rip channel (velocities of 0.65m/s) suggesting that there is still some influence of flows that generate after different wave breaking patterns between the bars and rip channels that enhance the longshore current. Sediment transport is also increased at these locations (4.9) and the magnitudes are somewhat larger than for test *a*. This is reflected in the net transport rates, Q_{norm} which are 0.66 in test *a* and 0.82 in test *b*.

It is evident that the alongshore variability in morphology is reflected in the patterns of nearshore circulation, nonetheless the extent on which this affects and reduces or increases sediment transport cannot be fully determined qualitatively. Similar to TBR2, the milder slope on the transverse bars (~0.01), which are predominant in space for TBR1, promotes higher wave dissipation and entrainment of sediments at a distance from the coast, unlike the LBT morphologies where the steeper beach face and swash zone (~0.04) result in wave dissipation restricted to a very narrow area, giving rise to higher longshore transport following longshore velocities of approximately 1m/s.

Summary of simulations in test 1

-Wave conditions: H_s=1.5m T_p=6s θ=-20 and 20°.

-Q_{norm} test *a* LBT2: 1.04→ LBT1: 0.99 →TBR2: 0.73 →TBR1: 0.66

-Q_{norm} test *b*: LBT1: 1.01→LBT2: 1→TBR2: 0.82→ TBR1: 0.81

-Reduction of transport for TBR2 appears to be driven by the general profile slope

- Distribution of longshore transport varies in the longshore direction as a response of the 3d patterns in bathymetry; nonetheless it is not clear to which degree the latter influences the reduction in sediment transport.

4.8 Longshore sediment transport maps for a) LBT2 b) TBR2 and d)TBR1 bathymetries in test a. Isobaths are depicted in pink. A scaling factor of $8x10^4$ is used to represent transport vectors

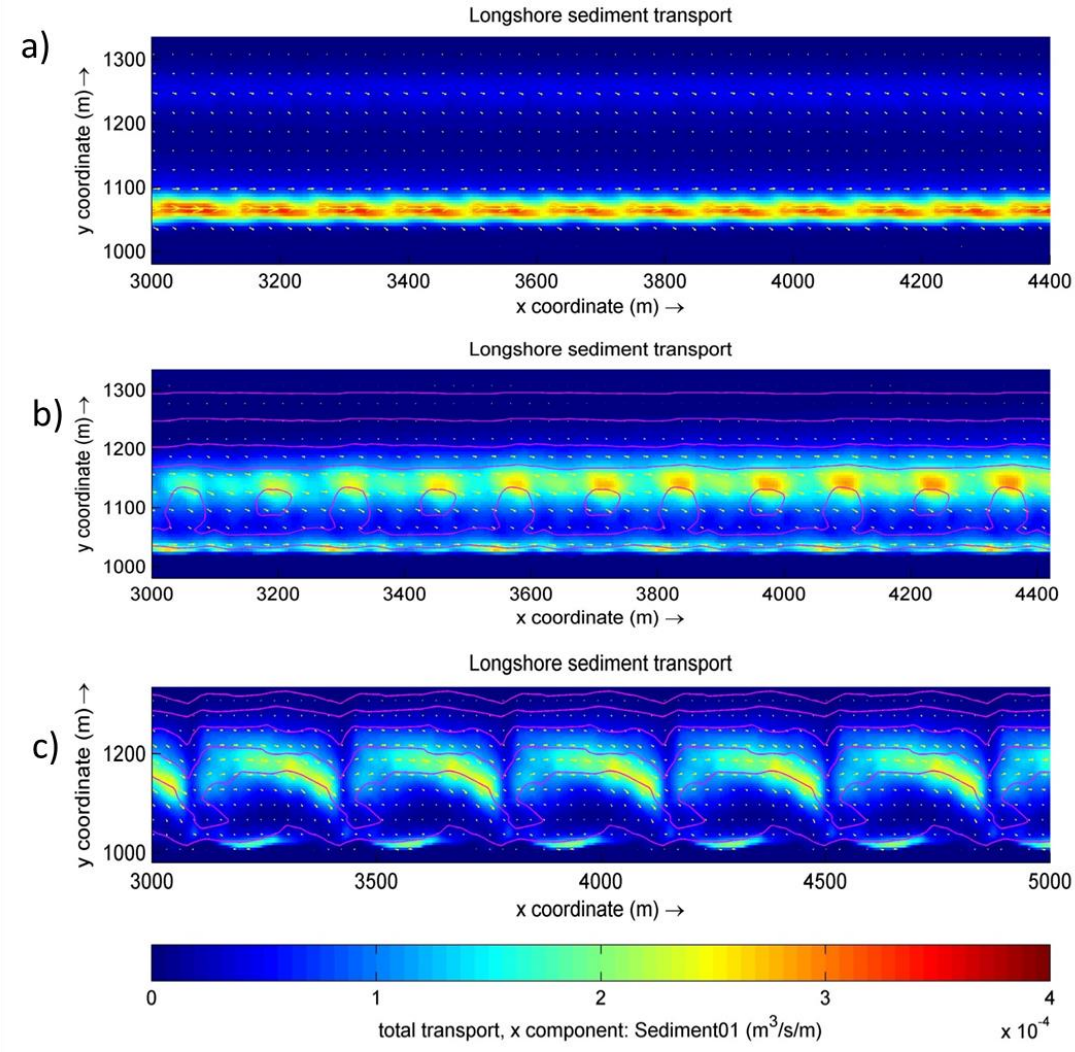

Figure 4.9 Longshore sediment transport in TBR1 for test b

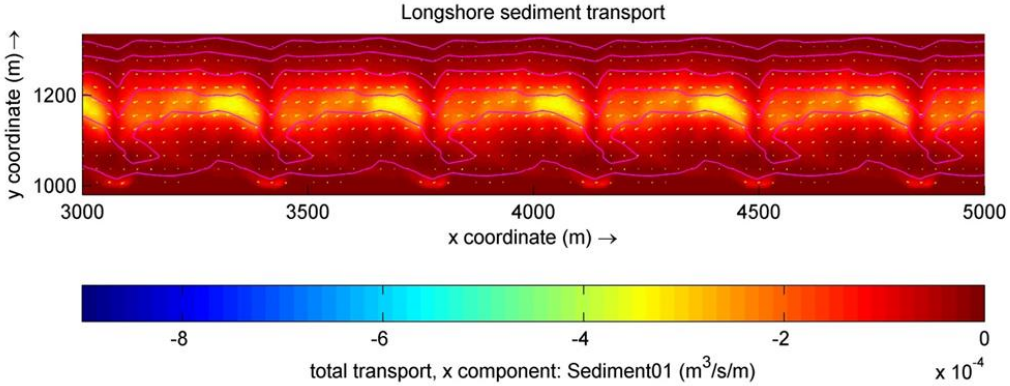

Test 2: high waves, high angle

The wave conditions imposed in this simulation set resulted in the highest hydrodynamic forcing and sediment transport rates (in the order of 2.6x10^6 m^3/year). As for the previous cases, magnitudes of sediment transport are largest for the LBT bathymetries (Q_{norm}=0.95 – 1.04). For waves approaching at an angle of 45°, the generated flows are completely alongshore directed (i.e. no cross-shore component in the velocity is present) and reach maximum values of approximately1.2 m/s in the swash zone, as can be seen in the velocity map in figure 4.10; sediment transport presents a very similar behaviour.
The intense longshore current also dominates over the transverse bar morphologies. Even for TBR1, the meandering circulation is now replaced by straight trajectories that are barely deviated seaward in proximity of the deeper rip channels in both tests *a* and *b*. The net transport rates for this bathymetry are 0.45 in test *a* and 0.57 in test *b,* where again slightly higher transport is observed at the seaward end of the bars. The relatively uniform patterns observed in circulation and sediment transport (figure 4.11b), suggest that that the three-dimensional character of topography contribute scarcely to this reduction.
Longshore transport for TBR2 now presents a slightly different distribution in the cross-shore direction: whereas before little sediment was transported close to the coastline, a transport peak in the swash zone of equivalent magnitude than the associated with the shoals is now developed (figure 4.11a). This is related to the wave dissipation patterns under such oblique wave incidence. Figure 4.8a also shows that transport magnitudes along the different bathymetric features are also more homogeneously distributed. Following from this, morphological variability is assumed to be of minor importance on the determination of longshore sediment transport (Q_{norm}=0.57 test *a*, 0.59 test *b*) for the imposed wave conditions.

Figure 4.10 Depth averaged velocity for LBT1 in test a

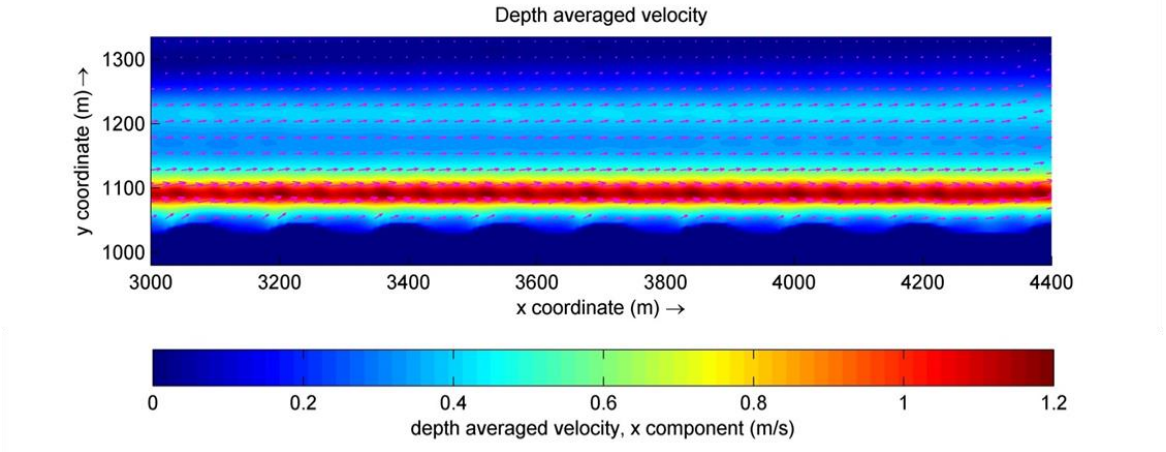

Figure 4.11 Longshore sediment transport for the TBR2 (a) and TBR1 (b) bathymetries. Depth contours depicted in pink

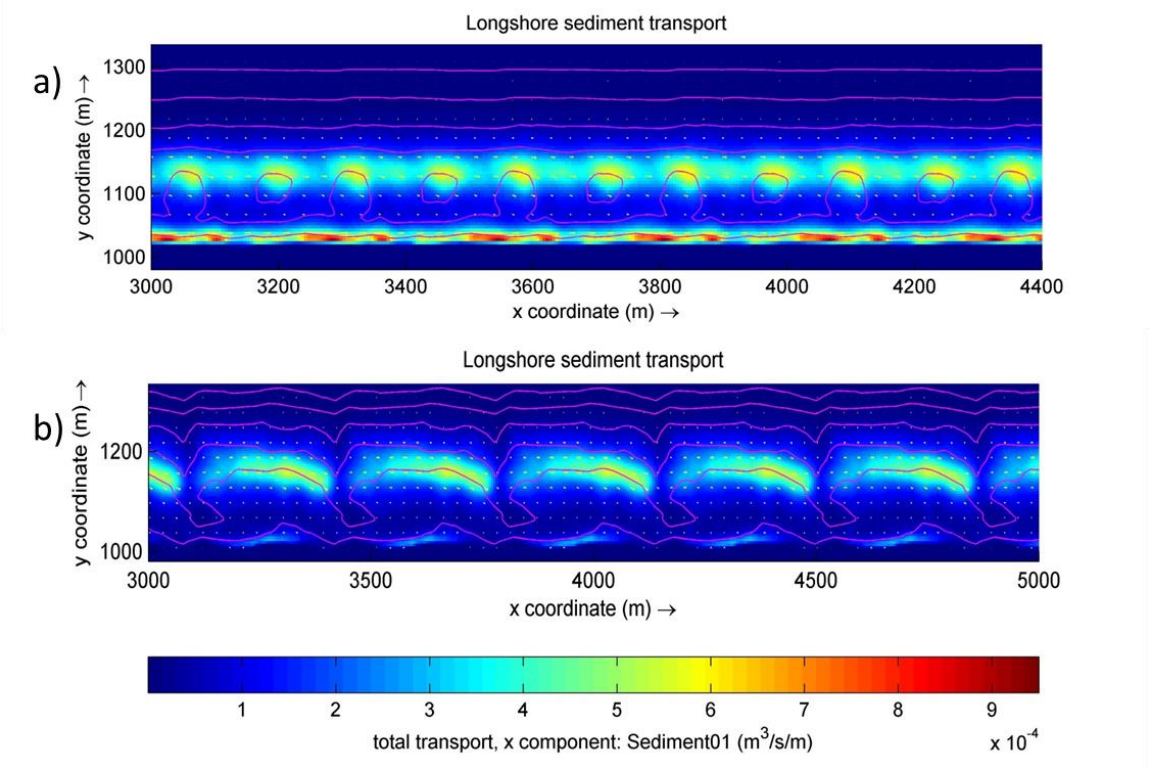

Summary of simulations in test 2

-Wave conditions: H_s=1.5m T_p=6s θ=-45 and 45°.

-Q_{norm} test *a* LBT3: 1.02→ LBT2: 0.95 →TBR2: 0.57 →TBR1: 0.45

-Q_{norm} test *b*: LBT3: 1.04→LBT2: 0.98→TBR2: 0.59 →TBR1: 0.57

-The alongshore variability in morphology for all beach states does not seem to have considerable effects on the spatial distribution of longshore sediment transport, indicating a higher influence of the profile configuration on dictating sediment transport rates. Nonetheless this is further address in following sections.

4.5.3 Sensitivity to decreasing wave height

Test 3: Low waves high angle

As lower waves approach to the coast, the cross-shore distribution of sediment transport exhibit some changes in the LBT morphologies: the offshore bars are now too deep to enhance significant breaking (especially for LBT2, were the bar crest depth is 2.7m), sediment transport is now restricted to the area where waves ultimately break near the shore and a longshore current that transports sediments with velocity of 0.3m is

generated (figure 4.11a). No difference is observed in the behaviour of the flow and sediment transport between simulations in test *a* and *b.*
Q_{norm} for LBT1 and LBT2 bathymetries in this simulation does not reflect any significant changes than for the previous simulation of sediment transport under a low wave angle of incidence (i.e. the reference tests), values range from 0.92 to 0.97, given the estimated level of uncertainty of the model to compute sediment transport, an interpretation cannot be made regarding whether sediment transport is enhanced over one of these bathymetries.

Figure 4.12 Depth averaged velocity in the LBT1 bathymetry for test a

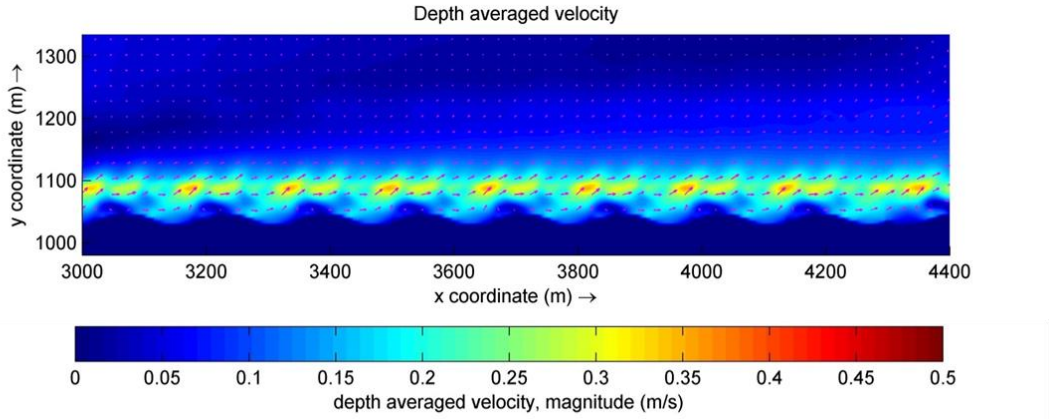

Circulation in TBR1 in tests *a* and *b* is again characterized by a system of feeder and rip currents. With smaller waves, the formed eddy circulates over a more reduced area and its position is shifted landwards, according to the new position of wave breaking. Velocity of the rip currents is reduced only moderately (0.6-0.7 m/s vs 0.8m/s), while the feeder current for test *b* is observed to be of higher magnitude than in the reference test-b (where waves were 1.5m high). As before, Q_{norm} is significantly reduced for test *a*, and increased for test *b* (figure 4.13).

Figure 4.13 Longshore sediment transport in TBR1 for test a (a) and b (b)

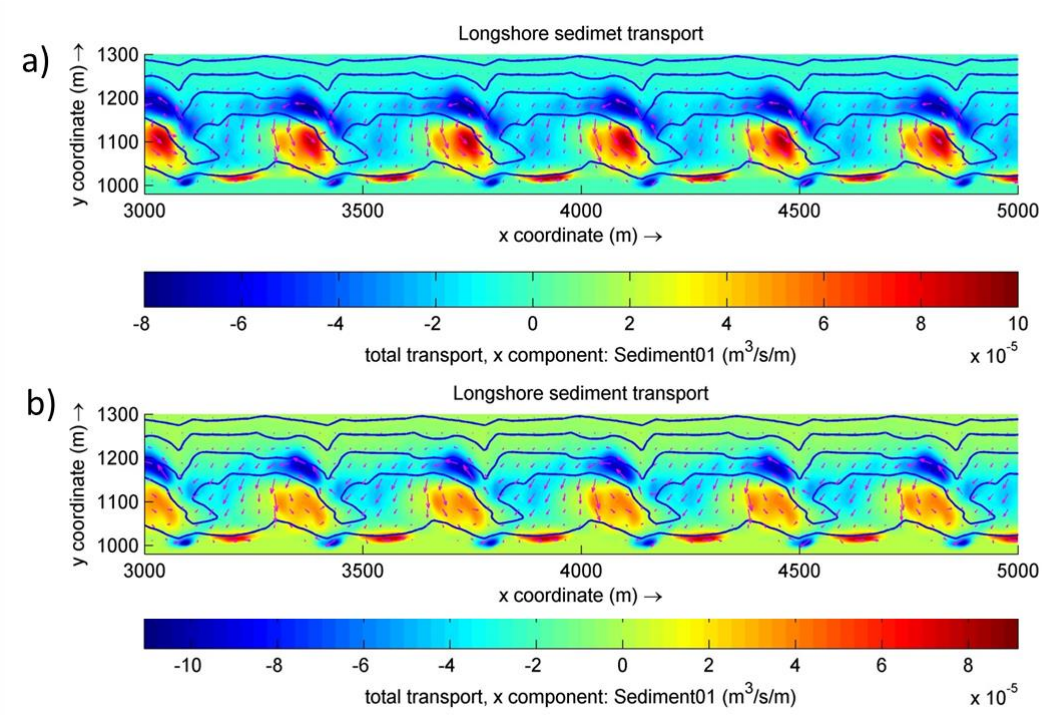

Flow and sediment transport in TBR2 for this simulation test now exhibit considerably different patterns than in the reference test. The meandering longshore current present for that case is now replaced by more onshore and offshore directed flows over the sand bars and rip channels respectively (figure 4.14). This is associated with the fact that the higher waves in the reference simulation dissipate seaward of the shoal crests, in deeper regions (highest dissipation occurred over the 2m isobath) where the depth contours are more uniform in the longshore direction and with this, the variations in the patterns of wave breaking do not exert a strong enough forcing to generate a rip circulation. Dissipation in test 3 on the contrary, takes place very close to the bar crests where the bathymetry is more variable, and alongshore gradients of wave forcing stimulate the described circulation.

The slight inclination of the shoals and asymmetry of the rip channels in this bathymetry appears to have some influence in the flow: Although magnitudes remain fairly similar, a stronger normal component in the velocity is observed in the case of waves approaching at a negative angle (test b). This is reflected in lower longshore sediment transport rates in test *b* than in test *a*.

Figure 4.14 Depth averaged velocity in TBR2 for test a (a) and b (b)

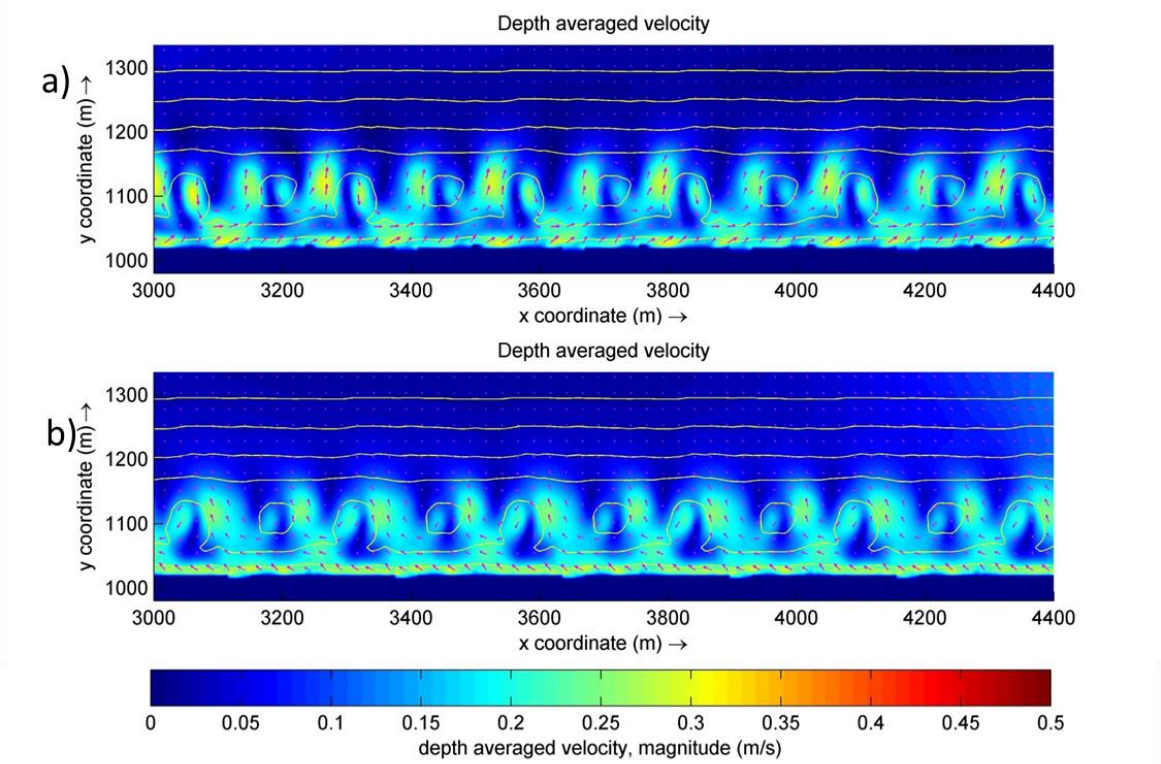

Magnitudes of the onshore and offshore velocities depend on the dimensions of the underlying features: Onshore flow is higher over the shore connected transverse bars, attributed to higher dissipation rates over it, and is lower over the smaller disconnected circular shoals. As for the offshore directed currents, magnitude of the flow was found to be related to the rip channel spacing only for test *a:* flow in the rip channels located at the downdfrift side of shore attached shoals (rip channel spacing 94m, as presented in table 3.2) exhibit slightly lower velocities than the ones downdrift of a disconnected shoal (rip channel spacing of 69m). A longshore current of equivalent magnitude is generated in the swash zone, which appears to be more uniform in the longshore direction for test *a.*

The pattern in wave generated currents is not as strongly reflected in sediment transport over the bars and rip channels (figure 4.15) given probably by the fact that velocities only reach magnitudes of 0.25-0.3 m/s, which does not appear to provide the enough forcing to entrain sediment significantly, especially for the deeper rip channels. In any case, longshore sediment transport takes place mainly in the swash zone, where the more uniform longshore current for test a results in a normalized transport rate of 1, while Q_{norm} in test b is reduced to 0.84.

Figure 4.15 Longshore sediment transport in TBR2for test a (a) and b (b)

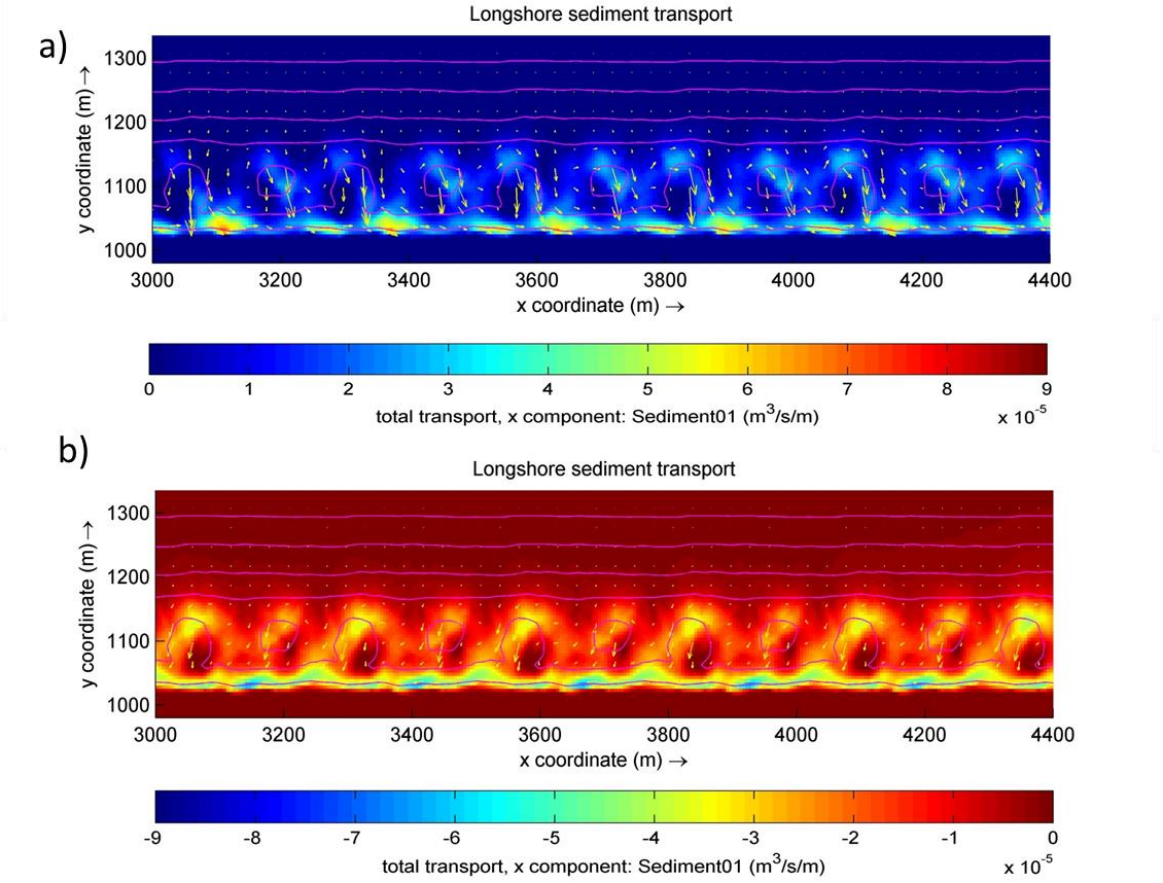

Summary of simulations in test 3

-Wave conditions: H_s=1.0m T_p=6s θ=-5 and 5°.

-Q_{norm} test *a* LBT1:0.93→ LBT2: 0.92 →TBR2: 0.84 →TBR1: -0.35

-Q_{norm} test *b*: TBR1: 1.24→TBR2: 1→LBT1:0.97→LBT2:0.96

- Net sediment transport rates varied similarly than in the reference test amongst the LBTs and TBR1 bathymetries. Reduction in sediment transport related to effects of an alongshore variable topography is observed in TBR2 in the case of waves approaching at a negative angle to the shore normal.

Test 4: Low waves medium angle

For this simulation set, the normalized net transport rates in the longshore bar and trough morphologies, suggests enhancement of sediment transport for LBT1 (Q_{norm} =0.97 test a and b). Under the imposed wave conditions, waves approach the shoreline with a very similar height (given very limited dissipation over the bar) and it is the slightly steeper slope in the swash zone for LBT1 (~0.037 vs ~0.031) that results in a narrower breaker and thus a concentration of wave energy that promotes higher sediment transport (figure 4.14).

Figure 4.14 Cross-shore distribution of longshore transport for LBT2 and LBT3 in simulation test 5

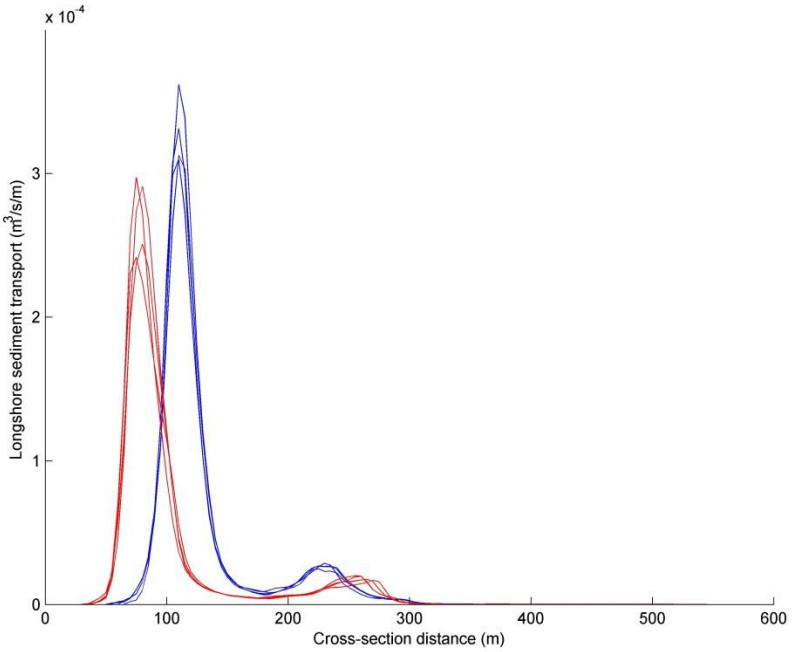

Circulation and sediment transport for TBR2 have now reduced their alongshore variability, even though the flow describes meandering trajectories (figure 4.15a), sediment transport is more homogeneous in space and starts to become more important in the swash zone (figure 4.16a). No significant differences were found between tests *a* and *b*, in which the normalized transport rates were found to be 0.71 and 0.78, similar figures to those found in test 1.

As for TBR1, circulation and sediment transport patterns in the nearshore are again sensible to the direction of wave approach: For both a positive and negative angle of wave incidence the alongshore component of the flow is weakened and the resulting currents are more influenced by the underlying topography than in the situation where higher waves approach at the same angle to the coast. When the angle of wave incidence is negative, circulation is characterized by what could be a transition between a meandering longshore current and a rip circulation (figure 4.15b). Offshore velocities are generated above the rip channels, nevertheless these do not reach such high magnitudes and no vortex circulation is present, as in the case in the reference case and test 3 with almost normal wave incidence. The highest velocities are associated with the feeder current that flows in the same direction as the longshore current (~0.4 m/s) and after describing an offshore trajectory over the rip

channel, the flow is again redirected parallel to the coast. Despite the fact that no significant sediment transport towards the offshore, or opposing the direction of the longshore current occurs (figure 4.16a), the large spatial variation in the flow field is attributed to influence the outcome in net longshore transport Q_{norm} =0.47.

In the case of a positive wave angle, no pure offshore velocities are generated over the rip channel, however the longshore current exhibits very sinuous trajectories, and it is accelerated in proximity of the rip channel (figure 4.15c). Highest sediment transport occurs in these locations (figure 4.16b). Additionally low sediment transport that opposes the direction of the longshore current takes place due to a weak eddy that is formed in the location where the stronger feeder currents occur in the case of test *a*.

Occurrence of the offshore and sinuous currents that impact net sediment transport rates is a result of a balance between longshore and cross-shore hydrodynamic forcings: Low waves that approach the coast are able to propagate further landwards before breaking, after having been more affected by refraction processes. Influence of the non-uniform bathymetry is higher at the moment of dissipation and the forcings generated by the previously described longshore gradients in water levels are sufficient to destabilize the longshore current.

Figure 4.15 Depth averaged velocity for TBR2 in test a (a), TBR1 test a(b) and TBR1 test b(c).

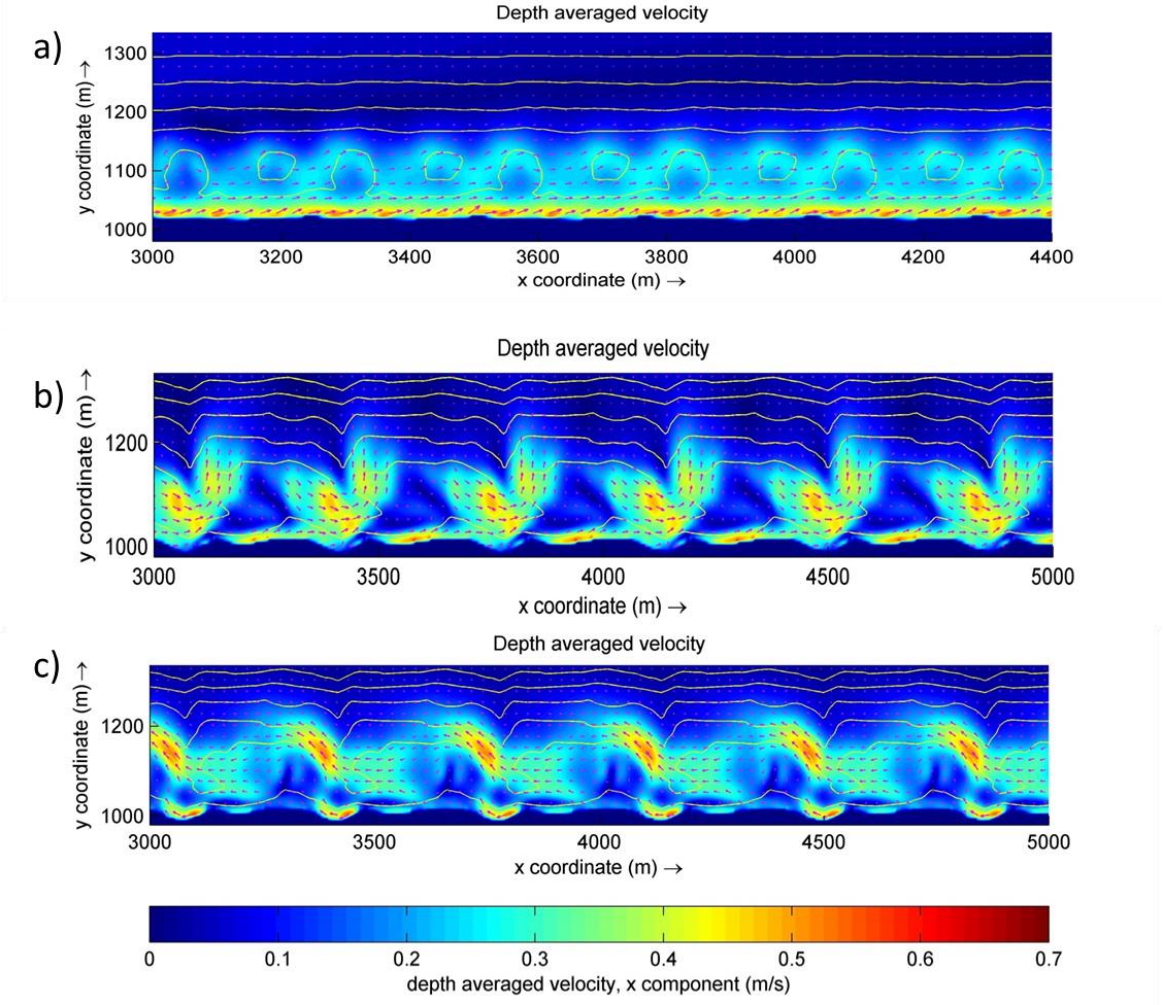

Figure 4.16 Longshore sediment transport for TBR2, test a(a) and TBR1 test a(b) and b(c)

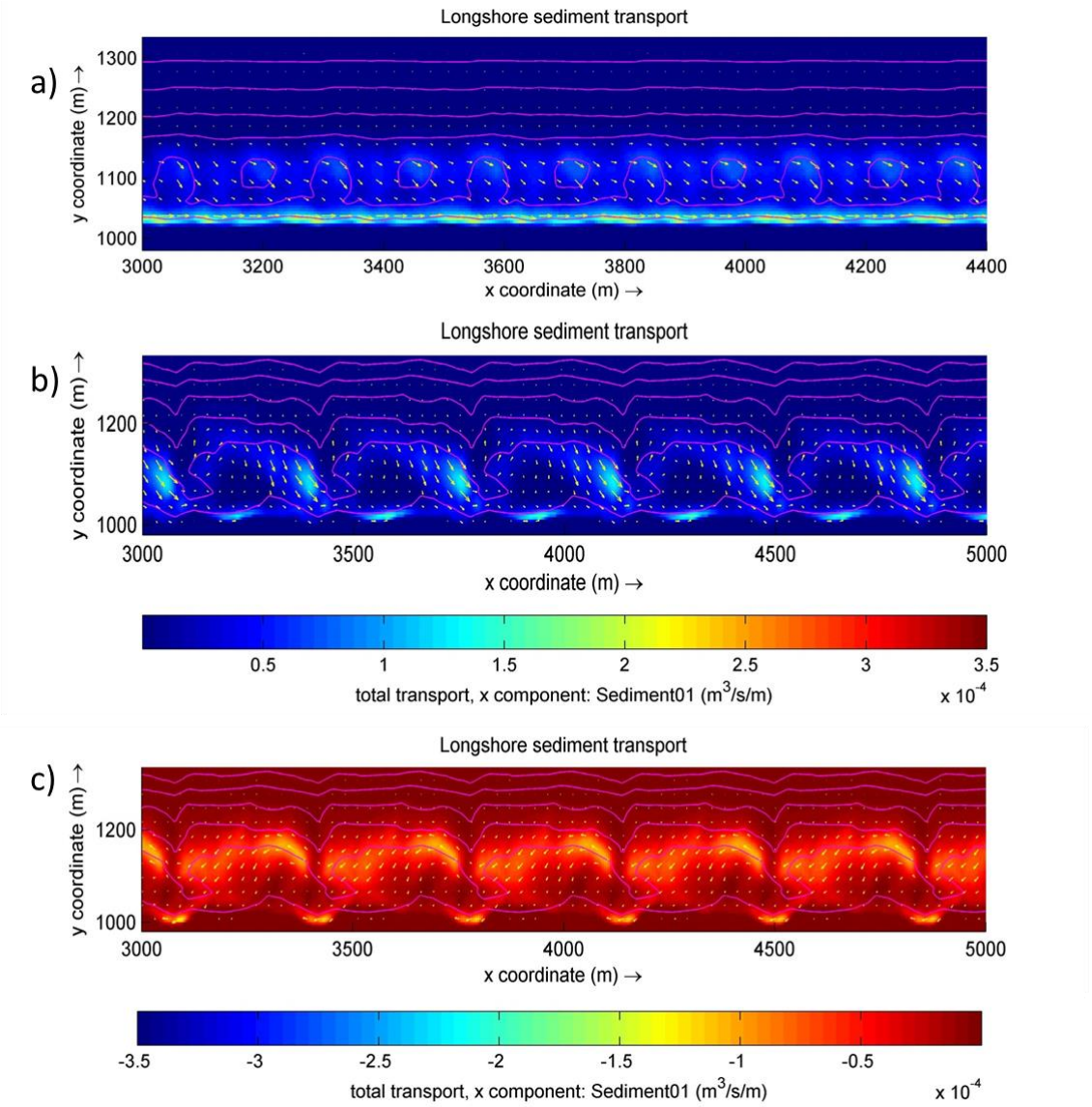

Summary of simulations in test 4

-Wave conditions: H_s=1.0m T_p=6s θ=-20 and 20°.

-Q_{norm} test *a* LBT1:0.97→ LBT2: 0.85 →TBR2: 0.71 →TBR1: 0.47

-Q_{norm} test *b*: LBT1: 0.97→ LBT2: 0.88 →TBR2: 0.78 → TBR1: 0.66

- Higher sediment transport for LBT1 than for LBT2 was found due to a different swash zone slope.

-The normalized net transport rate for TBR2 resembles that of simulations in test 1, no sensibility to a decreasing wave height was found.

-TBR1 exhibits variability in the spatial distribution of the flow and sediment transport driven by an alongshore variable morphology

Test 5: Low waves high angle

As expected, the flow field and sediment transport patterns for all bathymetries under the wave conditions imposed in test 5, become less variant in space suggesting that the alongshore variability in morphology has small influence on determining sediment transport patterns, this is . For LBT1 and LBT2, the rhythmicity of the coastline appears to be of minimal influence. This can be appreciated in the velocity map in figure 4.17. A continuous velocity peak occurs along the coast and vectors describe purely straight trajectories, net transport in LBT2 (Q_{norm} =0.84 ,0.88) is again reduced with respect of LBT1 (Q_{norm} = 0.95, 0.96).

In TBR2, the previously meandering behaviour of the flow has now turned into uniform circulation with very small variation between rip and shoals (figure 4.17b), as occurred in the case of incident waves of 1.5m height. Normalized transport rates are 0.56 and 0.78.

Meandering currents flow over the TBR1 bathymetry in tests *a* and *b*; nevertheless this time the longshore current carries enough inertia to flow over the rip channel. These circulation patterns are followed closely by the patterns in which sediment is transported and very similar transport rates are found for both tests (Q_{norm} = 0.95, 0.96). Both transverse bar morphologies appear to have shifted their velocity and transport peaks towards the swash zone. This is consistent with observation in test 3, indicating that dissipation of wave energy is translated landwards not only for a decreasing wave height, but also for an increasing wave angle.

Figure 4.17 Depth averaged velocity in test a for LBT1(a), TBR2(b) and TBR3(c)

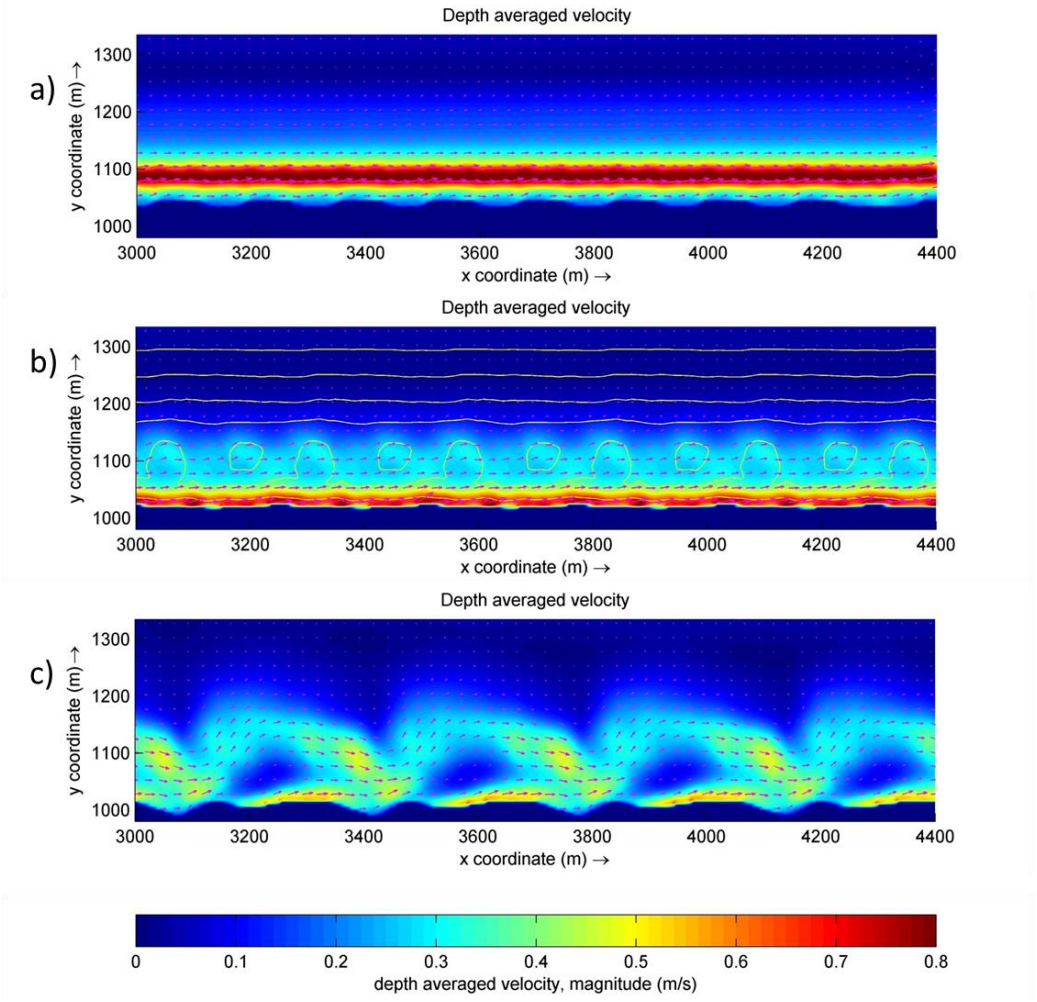

Summary of simulations in test 5

-Wave conditions: H_s=1.0m T_p=6s θ=-45 and 45°.

-Q_{norm} test *a* LBT1:0.95→ LBT2: 0.84 →TBR2: 0.56 →TBR1: 0.36

-Q_{norm} test *b*: LBT1: 0.96→ LBT2: 0.88 →TBR2: 0.60 → TBR1: 0.39

-A reduced spatial variation in patterns of flow and transport is exhibited in all bathymetries indicating that the profile shape has a higher influence on determining sediment transport.

Table 4.4 and figure 4.18 provide a summary of the estimated normalized transport rates in simulations for the alongshore variable bathymetries. The highest transport rate is in the order of 2.7x10^6 m^3/year and it corresponds to simulations in the LBT2 bathymetry under high waves approaching at a high angle from the shore normal (test 2). Following in magnitude are simulations in test 1 (LBT2 ~ 1 x10^6 m^3/year), while the lowest transport rates occurred under low waves and low angle of incidence (test 3:LBT2 ~ 8.6 x10^4 m^3/year).

Table 4.4 Normalized transport rates in the alongshore variable bathymetries for the different wave height and wave angle simulations

	Negative angle, test *a*				**Positive angle, test *b***			
Test	LBT1	LBT2	TBR2	TBR1	LBT1	LBT2	TBR2	TBR1
Q_{norm} **Reference test: High waves, low angle**	0.88	0.88	0.95	-0.23	1.04	1.00	1.08	1.45
Q_{norm} **Test 1 High waves, medium angle**	0.99	1.04	0.73	0.66	1.01	1.00	0.82	0.82
Q_{norm} **Test 2 High waves, high angle**	0.95	1.02	0.57	0.45	0.98	1.04	0.59	0.57
Q_{norm} **Test 3 Low waves, low angle**	0.93	0.92	0.84	-0.35	0.97	0.96	1.00	1.24
Q_{norm} **Test 4 Low waves, medium angle**	0.97	0.85	0.71	0.47	0.97	0.88	0.78	0.66
Q_{norm} **Test 6 Low waves, high angle**	0.95	0.84	0.56	0.36	0.96	0.88	0.60	0.39

Figure 4.16 Normalized transport rates in the alongshore variable bathymetries. Subfigures a and b depict simulations with a negative wave angle while b and d represent simulations with a positive wave angle.

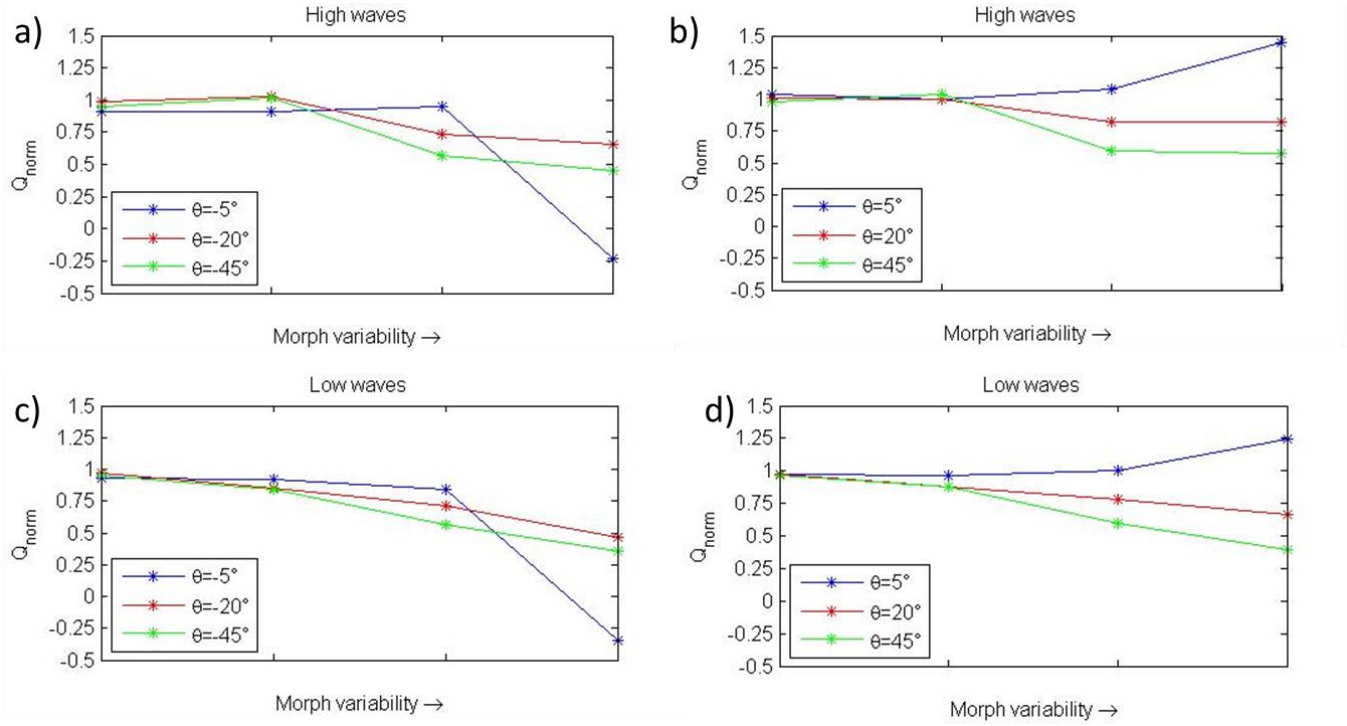

4.5.4 Discussions

After this qualitative and quantitative analysis it was found that net longshore sediment transport did vary significantly between the alongshore variable morphologies. Furthermore, the degree to which transport rates vary amongst them was found to be sensible to the incoming wave height and angle of incidence.

Cell-like and rip circulation patterns appear to reduce the capacity of the longshore current to mobilize sediments along the coast. Generation of these type of circulations was found to be depended on the combination of wave angle and wave height: For a small wave angle and a relatively weak longshore current, longshore gradients in wave energy dissipation will generate a rip circulation that will dominate circulation in the nearshore. As wave angle increases, and so does the magnitude of the longshore current, it becomes harder for the topographically controlled rip currents to develop (Bruneau, et al., 2009).In this study, generation of rip circulation that hampers or enhances longshore transport rates for both TBR1 and TBR2 bathymetries was found to be favoured by a smaller wave height.

This might appear contrary to conclusions reached in field and numerical studies regarding rip current generation, where higher waves appear to enhance rip circulation (Houser, et al., 2013; Aagaard, et al., 1997). However such conclusions were reached on the basis of the extent of wave dissipation over the studied longshore or transverse bar. Regardless of the fact that the amount of energy dissipation over the bars in TBR1 and TBR2 is lower for 1m waves, the position of wave breaking appears to be more dominant for the generation of rip circulation. In this case, 1m waves break and dissipate their energy over more irregular bathymetry, hence generating larger gradients in the wave forcing and promoting stronger rip circulation.

Moreover, a very important morphological aspect that was found to determine the outcome in net longshore transport was the asymmetry and orientation of the transverse bars and rip channels given that these can promote reduction (for the cases where the rip flows against the direction of the longshore current) or enhancement (when the rip and longshore current flow in the same direction) of net transport rates. In this study transport was favoured under a positive wave angle in both TBR morphologies even though it was only in the case of TBR1 that the offshore directed currents flowed over a narrow and well defined rip channel. For the case of TBR2 a moderate tilting of the transverse bars and the asymmetry between the two deeper channels between them promoted more normal circulation and sediment transport patterns for the case of a negative wave angle and therefore lower longshore transport rates than the ones estimated in the case of a positive wave angle.

A reduction of transport rates for the TBR bathymetries that was not associated with generation of 3D nearshore circulation patterns was also found, especially for the cases where very oblique waves approached the coast. These should then be explained by the effect that the mean profile slope has on wave energy dissipation and hence in the cross-shore distribution of the longshore current and longshore sediment transport. However this is further addressed in the following section.

Based on the estimated transport rates, a response between the more uniform LBT bathymetries is still not clearly identified. In the case of a nearly normal wave incidence, transport and velocity maps showed more alongshore variation in the magnitudes of these parameters than compared with the cases with more oblique wave incidence; in the same way, variation in the transport rates between LBT1 and LBT2 due to their (slightly) different slope in the swash zone was expected. However it could not be determined whether this impacts the transport rates significantly or not. It is likely that the accuracy of the models to simulate sediment transport is lower than the accuracy needed to identify the smaller variations in the transport rates.

4.6 Differentiation between profile slope and alongshore variability of morphology

4.6.1 Net longshore sediment transport for alongshore uniform bathymetries

As mentioned above, simulations of sediment transport over alongshore uniform bathymetries were performed in order to discriminate between the effects that the mean profile slope and the 3D characteristics of the morphology have on net transport rates. The same wave climate conditions as in table 4.2 were imposed and for each test, and the estimated $\boldsymbol{Q_{norm}}$ under a positive and a negative wave angle were averaged (see appendix). For these simulations, transport rates between the different bathymetries were also found to be sensible to wave height and wave angle. Table 4.5 provides the $\boldsymbol{Q_{norm}}$ in each of the alongshore uniform bathymetries.

Test	$LBT1_{uni}$	$LBT2_{uni}$	$TBR2_{uni}$	$TBR1_{uni}$
$\boldsymbol{Q_{norm}}$ **Reference test: High waves, low angle**	1.00	0.99	1.09	1.10
$\boldsymbol{Q_{norm}}$ **Test 1 High waves, medium angle**	1.00	1.04	0.82	0.76
$\boldsymbol{Q_{norm}}$ **Test 2 High waves, high angle**	1.00	1.00	0.64	0.51
$\boldsymbol{Q_{norm}}$ **Test 3 Low waves, low angle**	1.00	0.97	1.18	1.16
$\boldsymbol{Q_{norm}}$ **Test 4 Low waves, medium angle**	1.00	0.91	0.84	0.73
$\boldsymbol{Q_{norm}}$ **Test 6 Low waves, high angle**	1.00	0.90	0.76	0.47

Regarding $LBT1_{uni}$ and $LBT2_{uni}$, a decrease in the transport rates of approximately 10% is observed in the cases of small waves and medium to high wave angles. This is consistent with what was found for the simulations in the alongshore variable bathymetries: A relatively steeper slope results in a narrower breaker and thus a stronger longshore current transporting a higher amount of sediment along the coast.

A more significant variation is found between the LBT and TBR bathymetries: For nearly normal wave incidence a similar value of $\boldsymbol{Q_{norm}}$ was found for all bathymetries, nevertheless, the profile shape and slope of TBR2 and TBR1 uniform promote moderately higher transport rates. Moreover for an increasingly oblique wave incidence transport rates decrease for these two bathymetries, where values of $\boldsymbol{Q_{norm}}$ are around 50% lower than in the LBT cases. An explanation to this was found after analysing qualitatively how wave energy dissipates across the shore and the resulting distributions of the longshore current and sediment transport: Even for simulations under a same wave height, when the angle of wave incidence increases, wave dissipation becomes more important closer to the shoreline and sediment transport is focused in such area. This is depicted in figure 4.17 where under a small wave angle (4.17a) significant transport occurs over the offshore bar and the swash zone in the case of $LBT1_{uni}$ (blue curve), while for $TBR1_{uni}$ a more uniform slope and a shallower nearshore promotes sediment to be transported at comparable rates over a broader area (red curve). However for a large wave angle (but same wave height), dissipation over the offshore bar in LBT1 is reduced and with this, the majority of energy carried by the waves ends up by being dissipated abruptly in the swash zone, promoting considerably stronger current and

higher sediment transport than in the case of $TBR1_{uni}$ (figure 4.17 b), where wave energy is still being dissipated gradually following from a milder profile slope.

Figure 4.17 Cross-shore distribution of longshore sediment transport for $LBT1_{uni}$ (blue curves) and $TBR1_{uni}$ (red curves) under a small and high wave angle(a and b respectively).

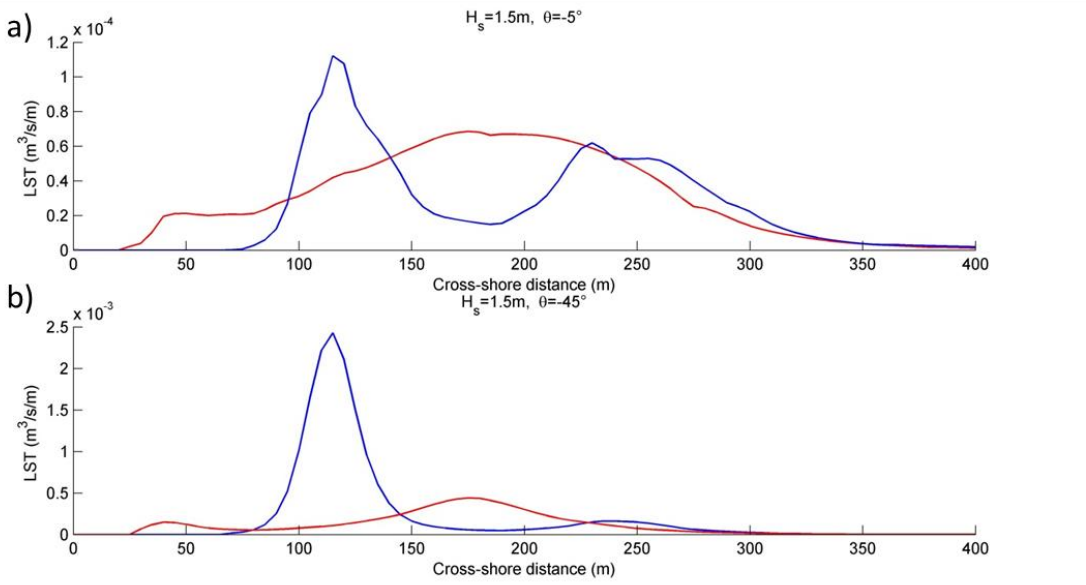

4.6.2 Profile shape versus alongshore variability in morphology

Comparison between the estimated $\boldsymbol{Q_{norm}}$ in the alongshore variable bathymetries and their respective alongshore uniform versions confirmed the suggestions formulated in section 4.5 where for an increasing wave angle, a stronger longshore current and more homogenous sediment transport patterns will take place and net transport rates between alongshore uniform and alongshore variable morphologies will be more alike (figures 4.18 and 4.19), then, the slope in the swash zone determines the outcome of transport rates: higher transport will occur for steeper slopes, i.e. the LBT morphologies.

Meanwhile, rip and cell like circulation promoted by 3D bathymetric features impacts net longshore transport more significantly in the cases of nearly normal wave incidence (figure 4.18 and 4.19 a and b), where $\boldsymbol{Q_{norm}}$ in the absence of morphological variability is similar for all bathymetries. For the additional situations in which a rip was generated (i.e. small waves and medium wave angle in TBR1), net transport is impacted to a smaller extent only for the case where rip and longshore current flow in opposing directions, resulting in a further reduction in $\boldsymbol{Q_{norm}}$ from what is already dictated by the effect of the swash zone slope (figure 4.18d). This again highlights the importance of the orientation and asymmetry of transverse bars and rip channels with respect to the incoming wave crests.

Moreover, additional situations were identified in which sediment transport rates were reduced by an alongshore variable bathymetry and such reduction could not be attributed to residual currents or 3D circulation patterns. These are particularly significant in the TBR2 bathymetry under small waves and high wave angle, as it is depicted in figures 4.18f and 4.19f.

Figure 4.18 Q_{norm} for the alongshore variable bathymetries (black curve) and their respective alongshore uniform bathymetries (red curve) in tests a

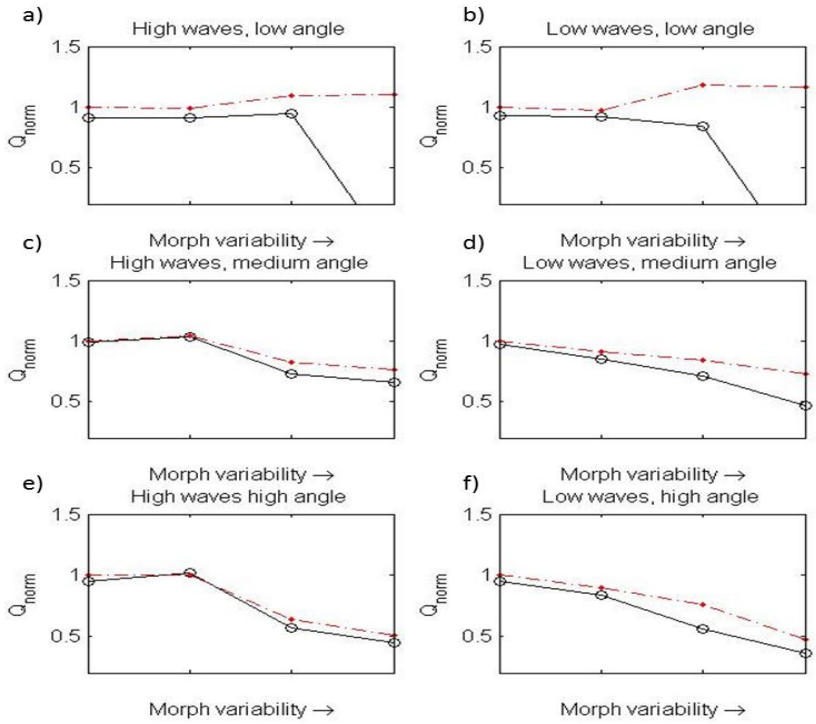

Figure 4.18 Q_{norm} for the alongshore variable bathymetries (black curve) and their respective alongshore uniform bathymetries (red curve) in tests b

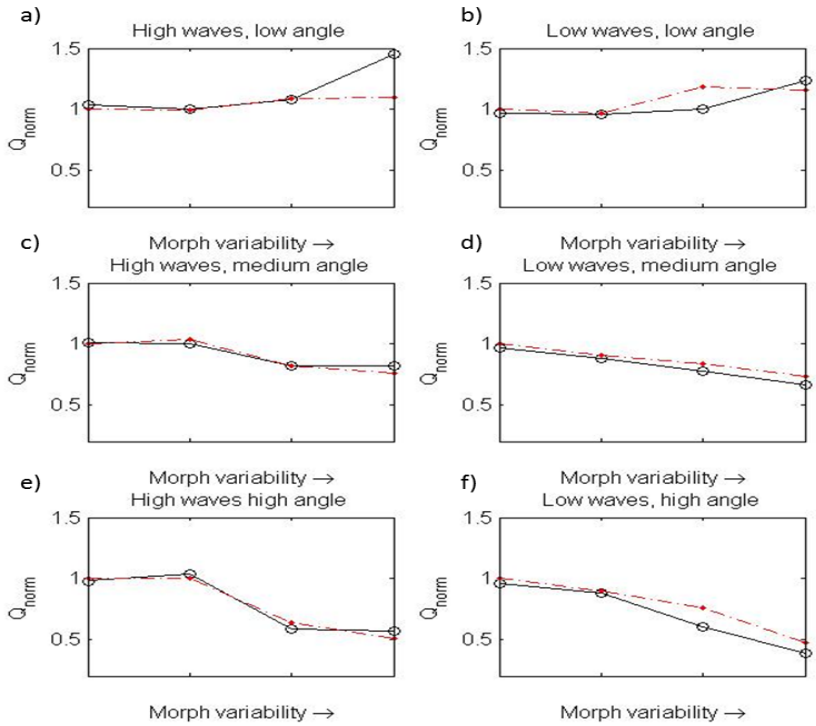

Further investigation is required to find a proper explanation for the above. Some possible reasons might include:

- An insufficient time for sediment to be picked up
- Positions with maximum sediment stirring do not correspond with the position of maximum current velocities
- Reduction of flow velocities due to diffusion of wave energy and longshore current over a wider cross-shore extent

To provide a preliminary insight on this matter figure 4.19 depicts the longshore distribution of the significant wave height, longshore current, equilibrium concentration and longshore sediment transport in TBR2 and $TBR2_{uni}$ for test 5a (low waves, high wave angle) for the point in the cross-shore where maximum velocities and sediment transport occurred, i.e. the swash zone. It appears that in the case of the alongshore variable TBR2, positions of maximum longshore current velocities do coincide with the positions of maximum sediment stirring (depicted in 4.19b and 4.19c respectively).

More contrasting is the reduction of the longshore current velocity and longshore sediment transport with respect to that in the alongshore uniform bathymetry, which might be attributed to the fact that for a more irregular bathymetry there is a larger cross-shore extent in which wave energy is dissipated and thus forcings driving sediment transport are more spread and diffused. Nevertheless, additional and more detailed research is required and therefore conclusions on this topic are not drawn in the present study.

Figure 4.19 Longshore distribution of the significant wave height, depth averaged longshore velocity, equilibrium sediment concentration, longshore sediment transport and bed elevation for TBR2 (blue curves) and its correspondent uniform bathymetry (red curves) after simulations in test 5a (i.e. low waves and high wave angle).

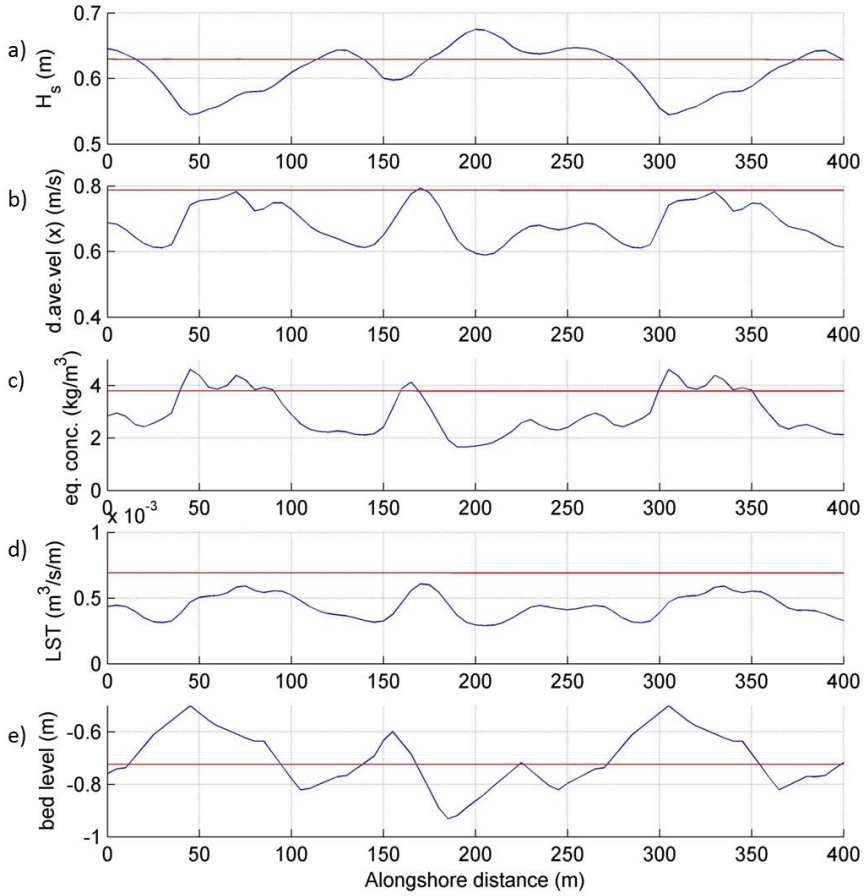

4.6.3 Discussions and conclussions

By performing simulations of sediment transport in alongshore variable and alongshore uniform bathymetries it was possible to identify variation in the net transport rates to the existent morphodynamic state. Morphologically, two factors account for such variations: *1)* the alongshore variability and 3D configuration in the bathymetry and *2)* the slope and configuration of the mean profile. The relative importance of these two depends on the hydrodynamic forcing exerted on the system.

In general, relevance of the profile slope on determining sediment transport behaviours increases as the angle of wave incidence increases, as it could be expected given that a stronger longshore current will prevail over other kinds of circulation patterns that could arise from an alongshore variable morphology.

Furthermore, it was found that a steeper slope in the swash zone promotes higher transport rates, especially under medium and high oblique wave incidence, where wave energy tends to dissipate in proximity to the shoreline, thus more abrupt wave breaking in steeper profiles result in higher longshore current velocities and sediment transport.

Even though generation of rip currents where found to reduce or increase net longshore transport rates in the TBR morphologies with respect to that in the LBT morphologies, a more significant impact was found for the cases where the rip channels and transverse bars were oriented opposite to the direction of the longshore current resulting in significant decrease in net longshore transport rates than the ones estimated in completely alongshore uniform bathymetries.

Regardless of an increase or decrease in the longshore transport, it is important to note that the topographically controlled rip circulations that significantly impact net longshore transport in the TBR morphologies are of relevance for conditions in which the wave angle is small. These are therefore situations in which sediment is transported at low rates (for the TBR as well as for LBT morphologies). The potential of 3D bathymetric features to affect sediment redistribution along the coast is therefore expected to be low for coasts in which wave incidence is persistently oblique. For particular cases where shore-normal waves are dominant, complex bathymetric configurations will impact the above to a larger extent.

5 Conclusions and recommendations

5.1 Conclusions

This study investigated the impact of beach states on net longshore sediment transport. A numerical model was used to estimate transport rates for a range of morphological configurations: from alongshore uniform to complex 3D bathymetries observed in the coast of the Sand Motor; and under diverse wave climate scenarios. The following was found:

- A methodology was developed to assess the impact of beach states on net longshore transport which consisted in computing initial transport rates over coasts with repeating beach state features.

- Typical beach states occurring at the coast of the Sand Motor ranged from relatively alongshore uniform offshore parallel bars, with corresponding swash zone slopes of around 0.035; to rhythmic and asymmetric transverse bars that connect to the shore for which slopes in the swash zone can be as mild as 0.01.

- Net longshore transport was found to be dependent on the morphology of the considered beach states (i.e. “longshore bar and trough” and “transverse bar” states). The variations in transport rates are a function of two morphological aspects:*1)* the alongshore variability and 3D configurations in the bathymetry and *2)* the slope and configuration of the mean profile. And their relative importance on net transport rates is sensible to the hydrodynamic forcing, and the generated nearshore circulation patterns.

- Relevance of the profile configuration on determining sediment transport behaviours increases as the angle of wave approach increases, as a stronger longshore current will be generated and prevail over other types of circulation that could arise from an alongshore variable bathymetry.

- Steeper slopes in the swash zone promote higher transport rates for medium and especially for high wave angles. More abrupt wave dissipation takes place under this conditions resulting in higher longshore current velocities and consequently higher transport rates given that sediment transport is non-linearly dependent on the flow conditions.

- Generation of topographically controlled rip currents that increase or decrease net longshore transport rates depends on the angle of the incoming waves with respect to the coast. Situations with nearly normal wave incidence result in larger potential for rip current development than situations with obliquely incident waves.

- Dependence on wave height for the generation of rip currents that enhance or decrease longshore sediment transport was found to be much smaller in comparison to that for the angle of wave incidence.

- Orientation and asymmetry of the transverse bars and rip channels (with respect to the approaching waves) influence longshore sediment transport as the generated rip circulation can significantly enhance or reduce net transport rates (respectively if the rip flows in the direction of the longshore current or in the direction against it). A more

significant impact on net longshore transport given by 3D bathymetric features was found for the situation with a rip-flow opposite to the direction of the longshore current.

- The potential of 3D bathymetric features on impacting sediment redistribution along the coast is low for situations in which waves persistently approach obliquely to the coast. For coasts on which waves approach predominantly under small angles, a 3D beach state morphology may however exert a larger effect.

5.2 Further research and recommendations

Additional research actions that could improve and enhance the findings in this study include the following:

- Further investigation of why sediment transport rates are reduced as an effect of an alongshore variable morphology for the particular cases mentioned above.

- Inclusion of additional hydrodynamic forcings that occur on the field. Particularly, addition of the influence of a vertical and horizontal tide. Variations in water level driven by the former modulate generation of rip currents, while the latter can increase or decrease velocities of the wave driven longshore current.

- Since sediment characteristics are not uniform in space, (e.g. coarser material is normally found over steep beach slopes and sand bar crests) simulations of sediment transport that include a realistic sediment size distribution in space will provide more detailed information of how net longshore transport is affected by the existence of different beach states.

- Improving the accuracy of the existent models will allow identification of smaller variations in the transport rates such as the ones expected amongst the created LBT simulation bathymetries.

6 References

Aagaard, T., Greenwood, B. & Nielsen, J., 1997. Mean currents and sediment transport in a rip channel. *Marine Geology,* 140(1-2), pp. 25-45.

Bayram, A., Larson, M., Miller, H. C. & Kraus, N. C., 2001. Cross-shore distribution of longshore sediment transport: comparisson between predictive formulas and field measurements. *Coastal Engineering,* Volumen 44, pp. 79-99.

Bosboom, J. & Stive , M. J. F., 2013. *Coastal Dynamics I.* Delft: VSSD.

Bruneau, N. y otros, 2009. Field observations of an evolving rip current on a meso-macrotidal well-developed inner bar and rip morphology. *Continental Shelf Research,* Volumen 29, pp. 1650-1662.

Castelle, B. y otros, 2009. Rip current system over stron alongshore non-uniformities: on the use of HADCP for model validation. *Journal of Coastal Research,* Volumen SI 56, pp. 1745-1750.

de Schipper, M. y otros, 2013. *Alomgshore topographic variability at a nourished beach.* Arcachon, France, Procceedings of the 7th International Conference on Coastal Dynamics.
Deigaard, R., Fredsøe, J. & Hedegaard, I. B., 1986. Mathematical model for littoral drift. *Journal of Waterway, Port, Coastal and Ocean Engineering,* 112(3), pp. 351-369.

Deltares, 2009. *DELFT3D-WAVE: Simulation of short crested waves with SWAN. User Manual. Version 3.04,* Delft: Deltares.

Deltares, 2014. *DELFT3D-FLOW: Simulation of multi-dimensional hydrodynamic flows and transport phenomena, including sediments. User Manual Version:3.15.34158,* Delft: Deltares.
Deltares, 2015. *Tool-Wave transformation table.* [En línea] Available at: https://publicwiki.deltares.nl/display/BWN1/Tool+-+Wave+Transformation+Table [Último acceso: 20 06 2015].

Houser, C., Arnott, R., Ulzhofer, S. & Barret, G., 2013. Nearshore circulation over transverse bar and rip morphology with oblique wave forcing. *Earth surface processes and landforms,* Volumen 38, pp. 1269-1279.

Kaji, A. O., 2013. *Assesment of the variables influencing sediment transport at the San Motor. (Msc. Thesis),* s.l.: TUDelft.

Kustvisie Zuid-Holland, 2015. *Kustvisie Zuid-Holland.* [En línea] Available at: http://www.kustvisiezuidholland.nl/ [Último acceso: 01 06 2015].

Lippman, T. C. & Holman, R. A., 1995. The spatial and and temporal variability of sand bar morphology. *Jorunal of Geophysical Research,* pp. 11575-11590.

Longuet-Higgins, M. S. & Stewart, R. W., 1964. Radiation stresses in water waves: a physical discurssion with applications. *Deep-Sea Research,* Volumen 11, pp. 529-562.

MacMahan, J. H., Thornton, E. B., Stanton, T. P. & Reniers, A. J., 2005. RIPEX: Observations of a rip current system. *Marine Geology,* Volumen 218, pp. 113-134.

Ministry of Transport, Public Works & Water Management, 1995. Dynamic preservation of the coastline in the Netherlands. *Journal of Coastal Conservation,* Volumen 1, pp. 17-28.

Province of Zuid-Holland, 2014. *The Sand Motor.* [Online] Available at: http://www.dezandmotor.nl/ [Accessed 22 February 2015].

Ranasinghe, R., Symonds, G., Black, K. & Holman, R., 2004. Morphodynamics of intermediate beaches: A video imaging and numerical modelling study. *Coastal Engineering,* pp. 629-655.

Reniers, A. J. H. M., Roelvink, J. A. & Thornton, E. B., 2004. Morphodynamic modelling of an embayed beach under wave group forcing.. *Journal of Geophysical Research: Oceans,* 109(C1), pp. 1978-2012.

Ruessink , B. G. y otros, 2001. Modelling the alongshore current on barred beaches. *Journal of geophysical research,* 106(C10), pp. 22,451-22,463.

Short, A. D., 2006. Australian Beach Systems: Nature and Distribution. *Journal of Coastal Research ,* pp. 11-27.

Smit, M. W. J., Reniers, A. J. H. M. & Stive, M. J. F., 2012. Role of morphological variability in the evolution of nearshore bars. *Coastal Engineering,* Volumen 69, pp. 19-28.

Svendsen, I. A., 1984. Mass flux and Undertow in a surf zone. *Coastal Engineering,* Volumen 8, pp. 347-365.

Tan, Y. C., 2014. *Assesment of beach states at the Sand Motor on the Basis of alongshore variability in bathymetry data. (Msc Thesis),* s.l.: TUDelft.

US Army Corps of Engineers, 1984. *Shore Protection Manual. Volume I.* Fouth Edition ed. Vicksburg, United States: Army Engineer Waterways Experiment Station.

van Rijn , L. C., Walstra, D. & van Ormondt, M., 2004. *Description of TRANSPOR2004 and implementation in DELFT3D-ONLINE. Tech Rep,* Delft, The Netherlands: Delft Hydraulics.

Winter, G., van Dongeren , A. R., de Schipper, M. A. & van Thiel de Vries, J. S. m., 2014. Rip currents under obnliquely incident wind waves and tidal longshore currents. *Coastal Engineering,* Volumen 89, pp. 106-119.

Wright, L. D. & Short, A. D., 1984. Morphodynamic variability of surf zones and beaches: A synthesis. *Marine Geology,* pp. 93-118.

Wright, L. D., Short, A. D. & Green, M. O., 1985. Short Term Changes in the Morphodynamic States of Beaches and Surf Zones: An Empirical Predictive Model. *Marine Geology,* pp. 339-364.

Yu, J. & Slinn, D. N., 2003. Effects of wave-current interaction on rip currents. *Journal of Geophysical Research. Oceans,,* 108(C3), p. 2156:2202.

Appendix A. Velocity and sediment transport maps

Figure A.1 Depth averaged velocity for LBT1 (a), LBT2 (b), TBR2(c) and TBR1 (d) for test "referece-a"

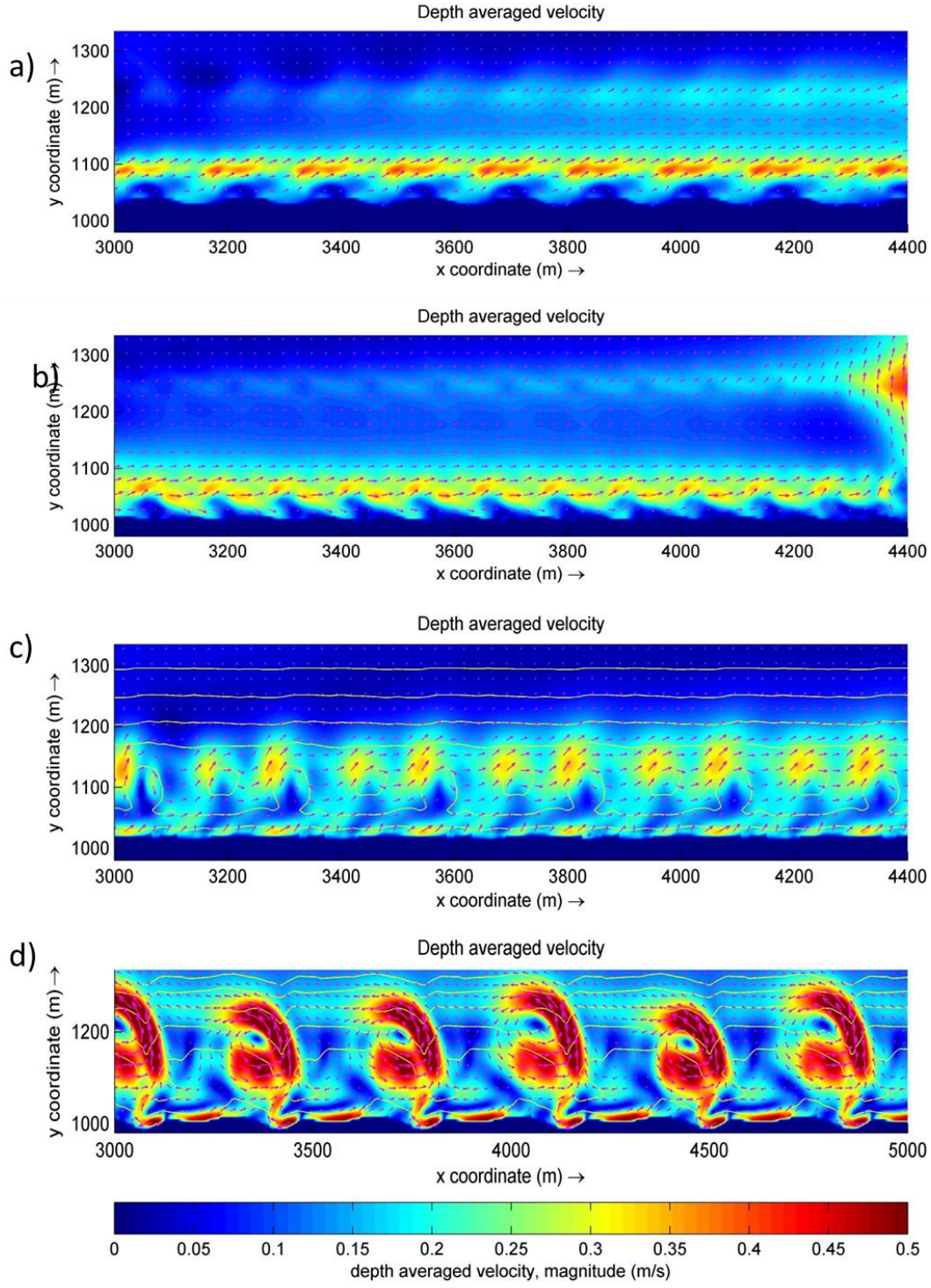

Figure A.2 Longshore sediment transport for LBT1 (a), LBT2 (b), TBR2(c) and TBR1 (d) for test "reference-a"

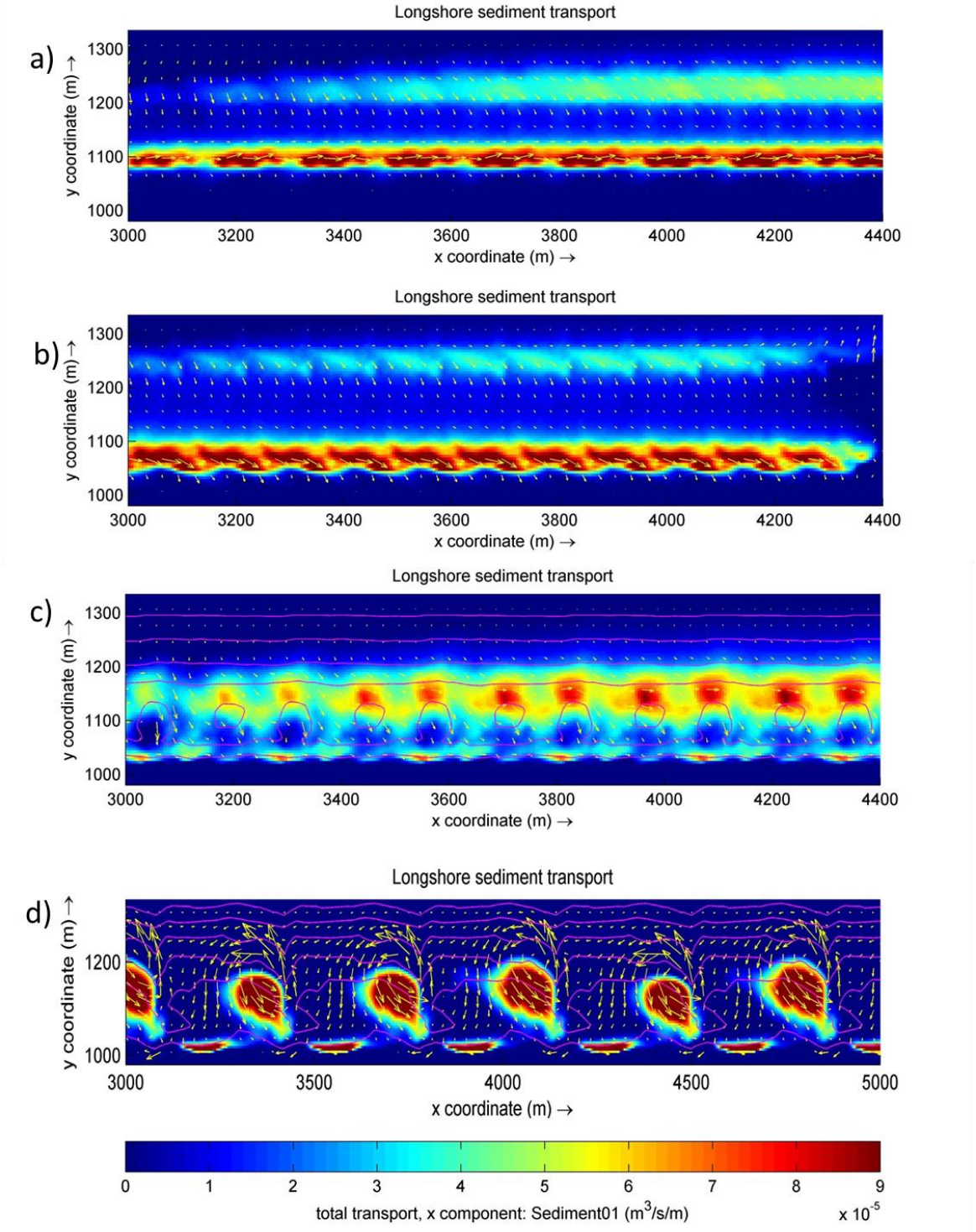

Figure A.3 Depth averaged velocity for LBT1 (a), LBT2 (b), TBR2(c) and TBR1 (d) for test 1-a

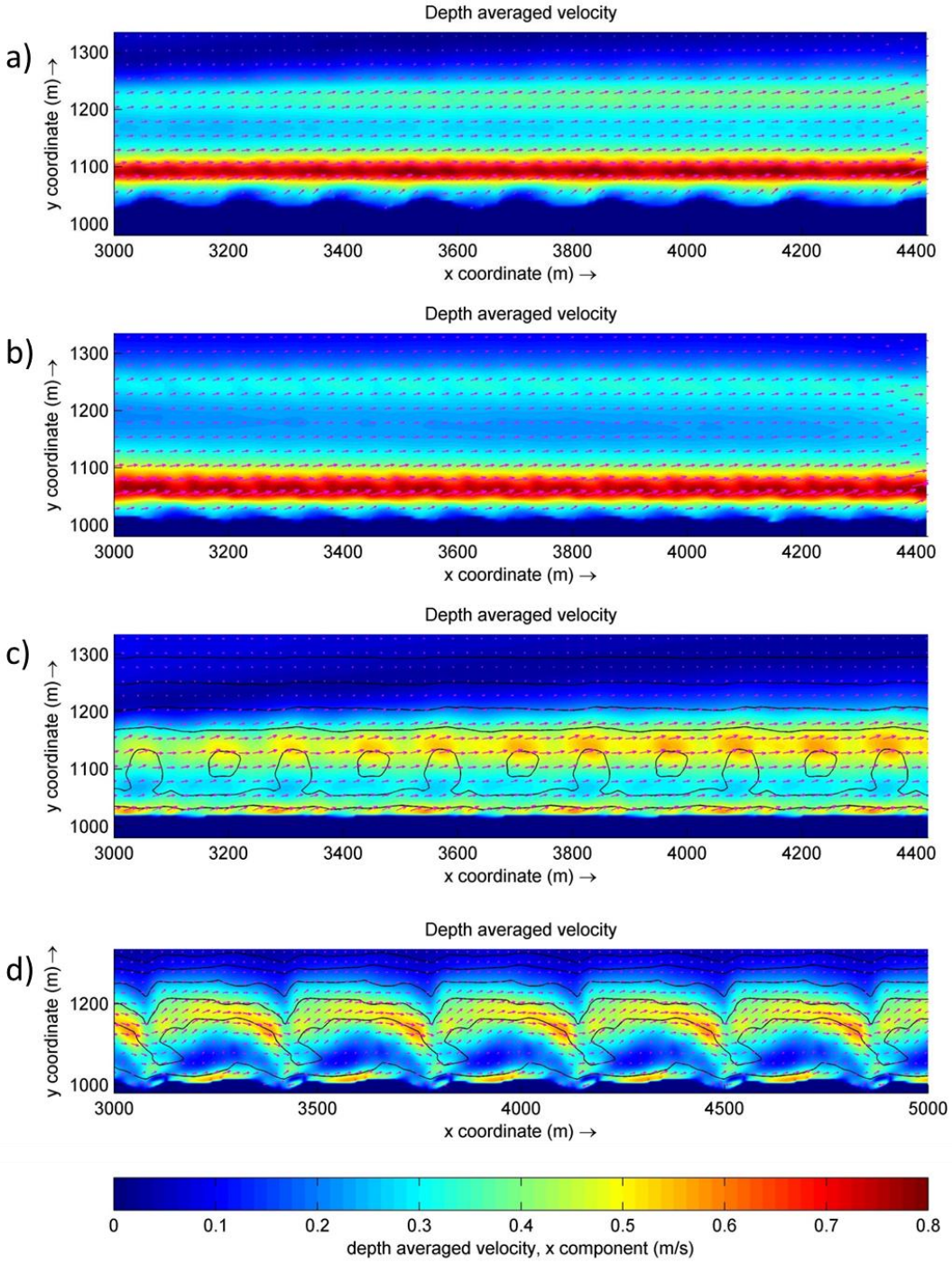

Figure A.4 Longshore sediment transport for LBT1 (a), LBT2 (b), TBR2(c) and TBR1 (d) for test 1-a

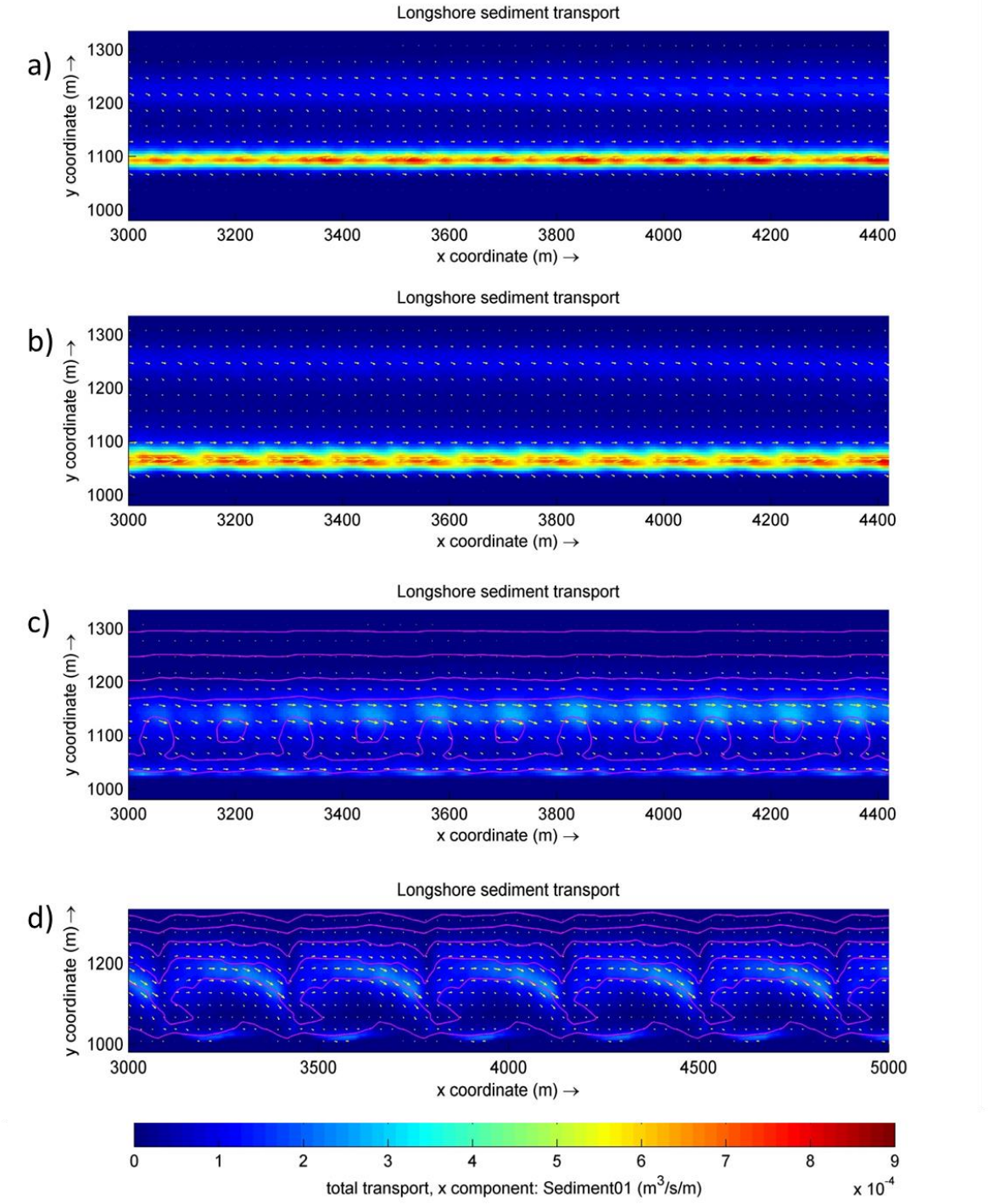

Figure A.5 Depth averaged velocity for LBT1 (a), LBT2 (b), TBR2(c) and TBR1 (d) for test 2-a

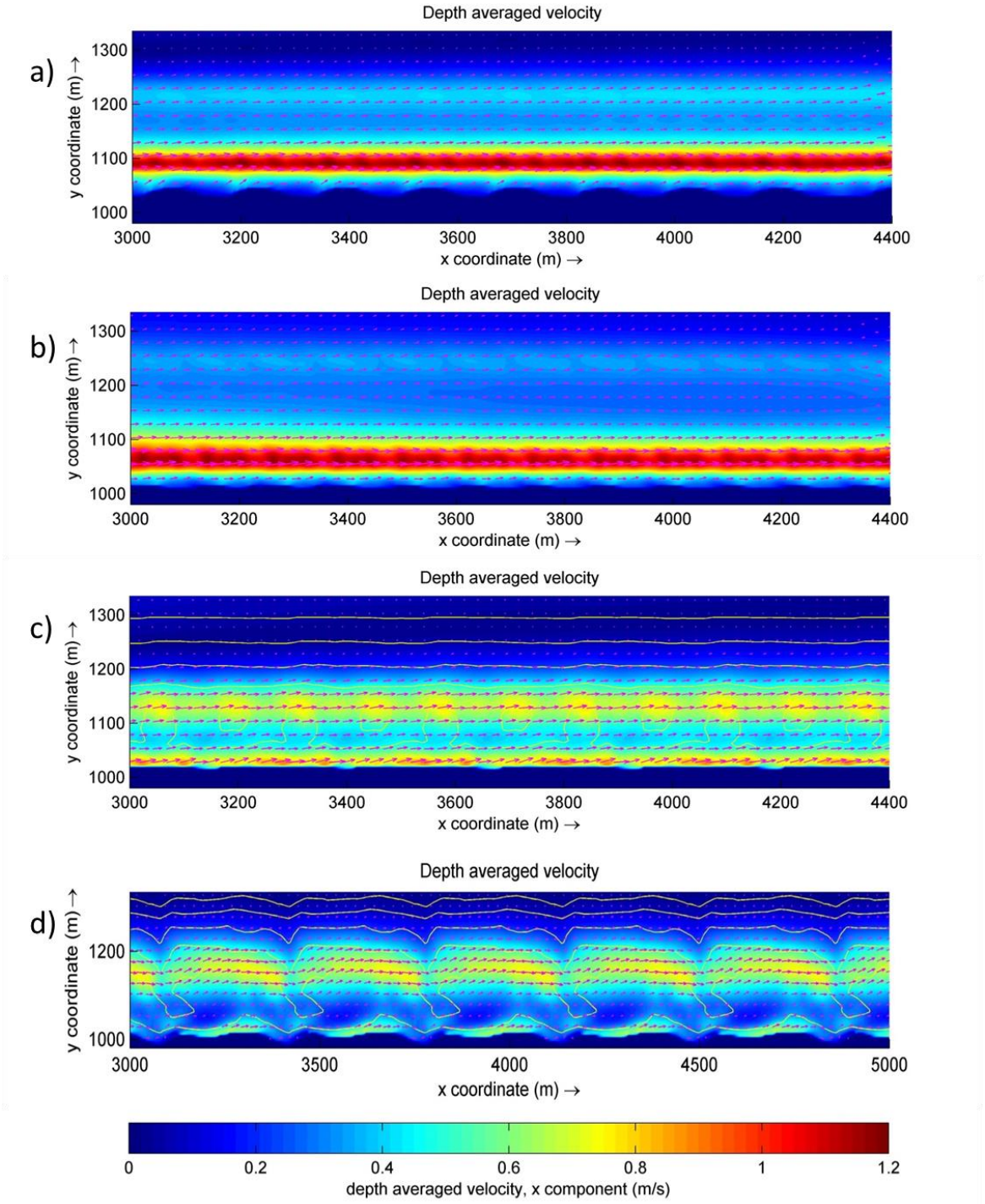

Figure A.6 Longshore sediment transport for LBT1 (a), LBT2 (b), TBR2(c) and TBR1 (d) for test 2-b

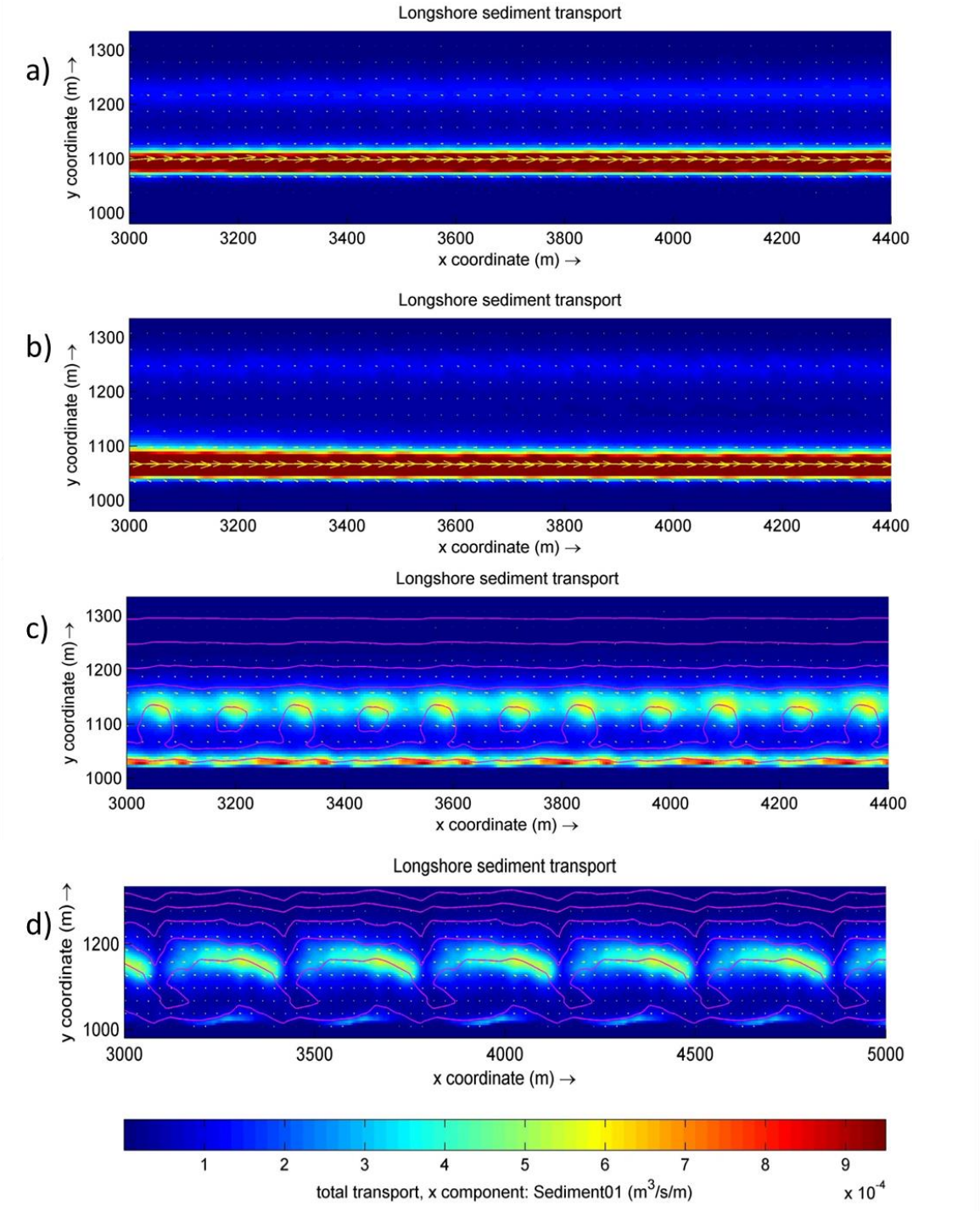

Figure A.7 Depth averaged velocity for LBT1 (a), LBT2 (b), TBR2(c) and TBR1 (d) for test 3-a

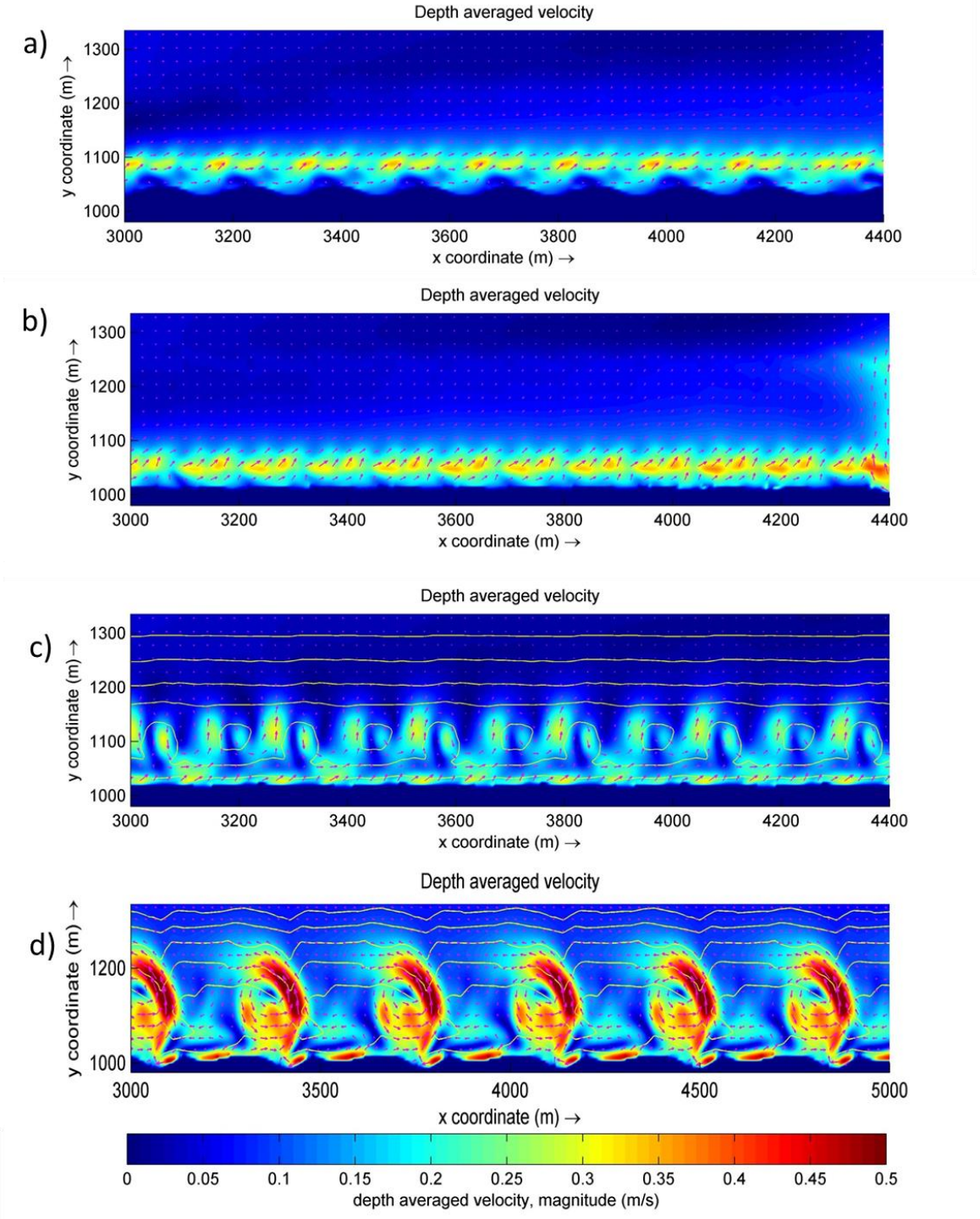

Figure A.8 Longshore sediment transport for LBT1 (a), LBT2 (b), TBR2(c) and TBR1 (d) for test 3-a

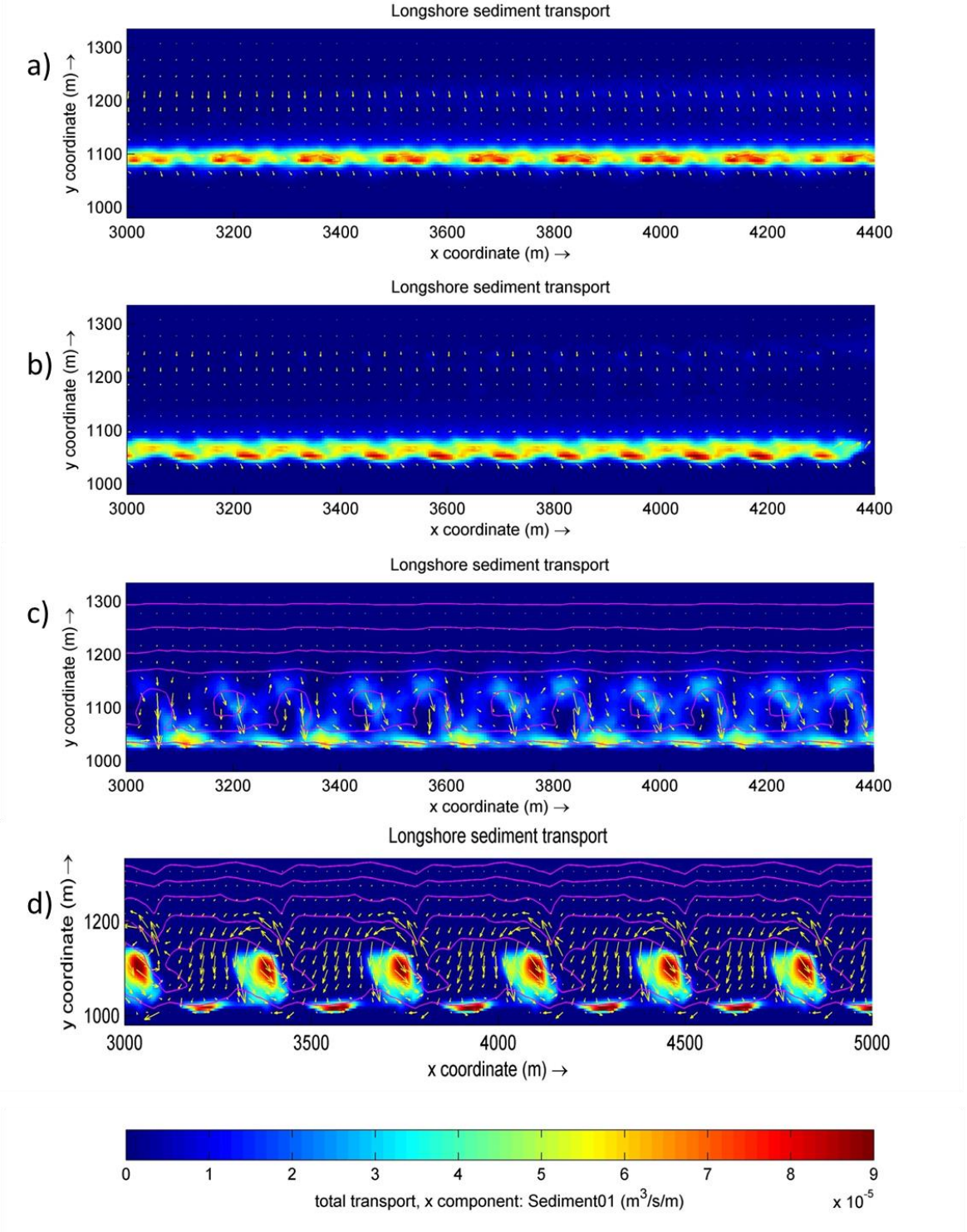

Figure A.9 Depth averaged velocity for LBT1 (a), LBT2 (b), TBR2(c) and TBR1 (d) for test 4-a

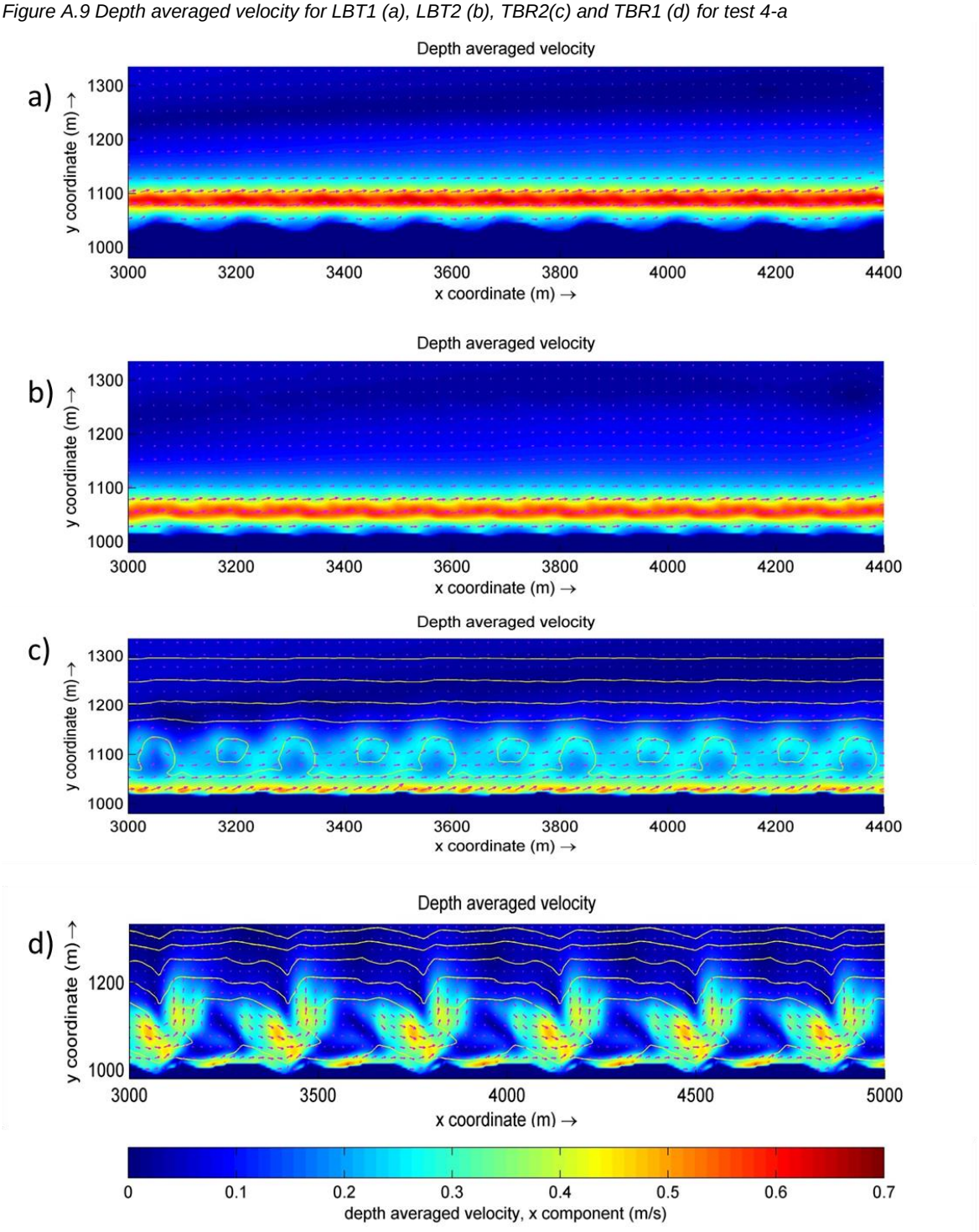

Figure A.10 Longshore sediment transport for LBT1 (a), LBT2 (b), TBR2(c) and TBR1 (d) for test 4-a

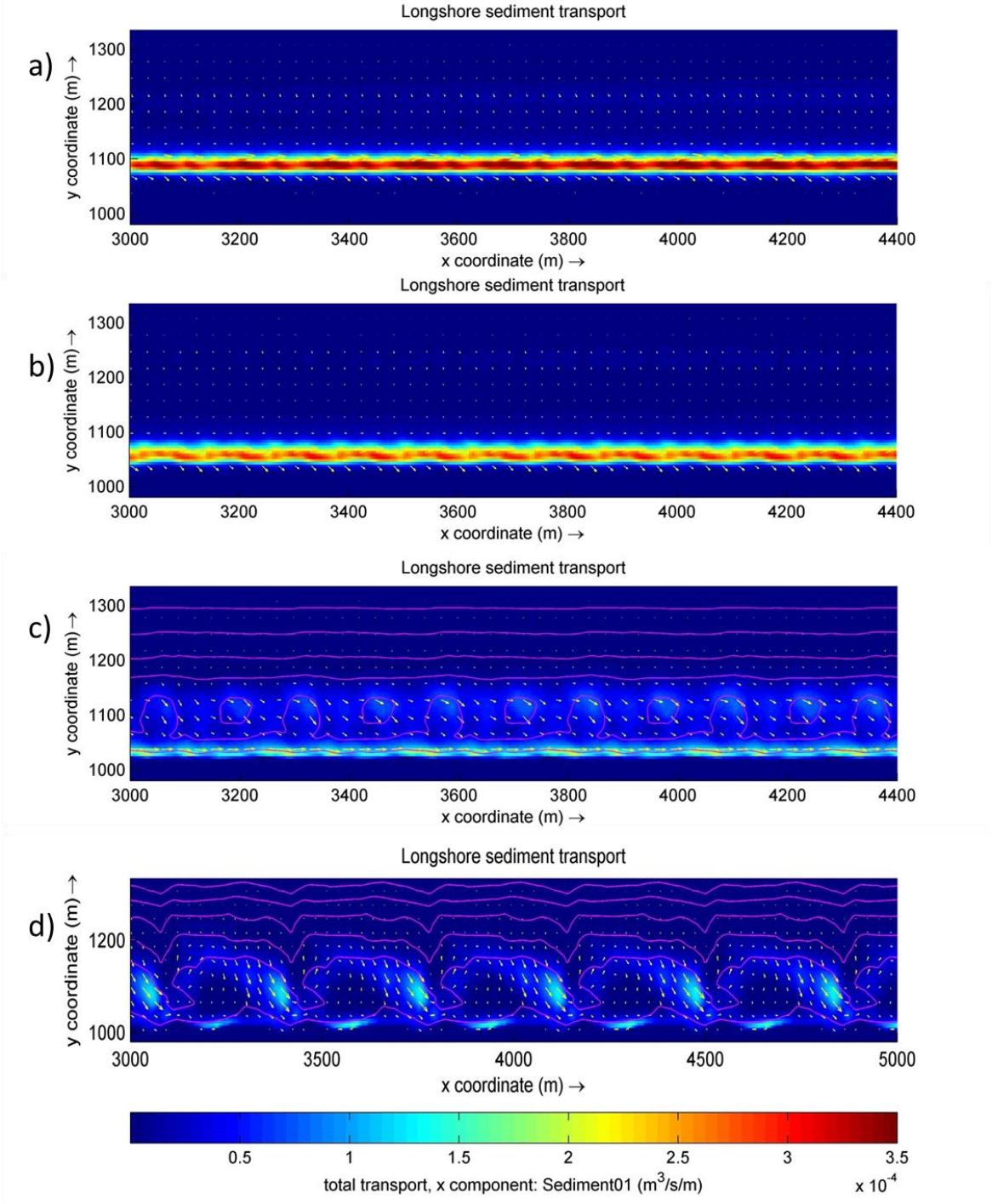

Figure A.11 Depth averaged velocity for LBT1 (a), LBT2 (b), TBR2(c) and TBR1 (d) for test 5-a

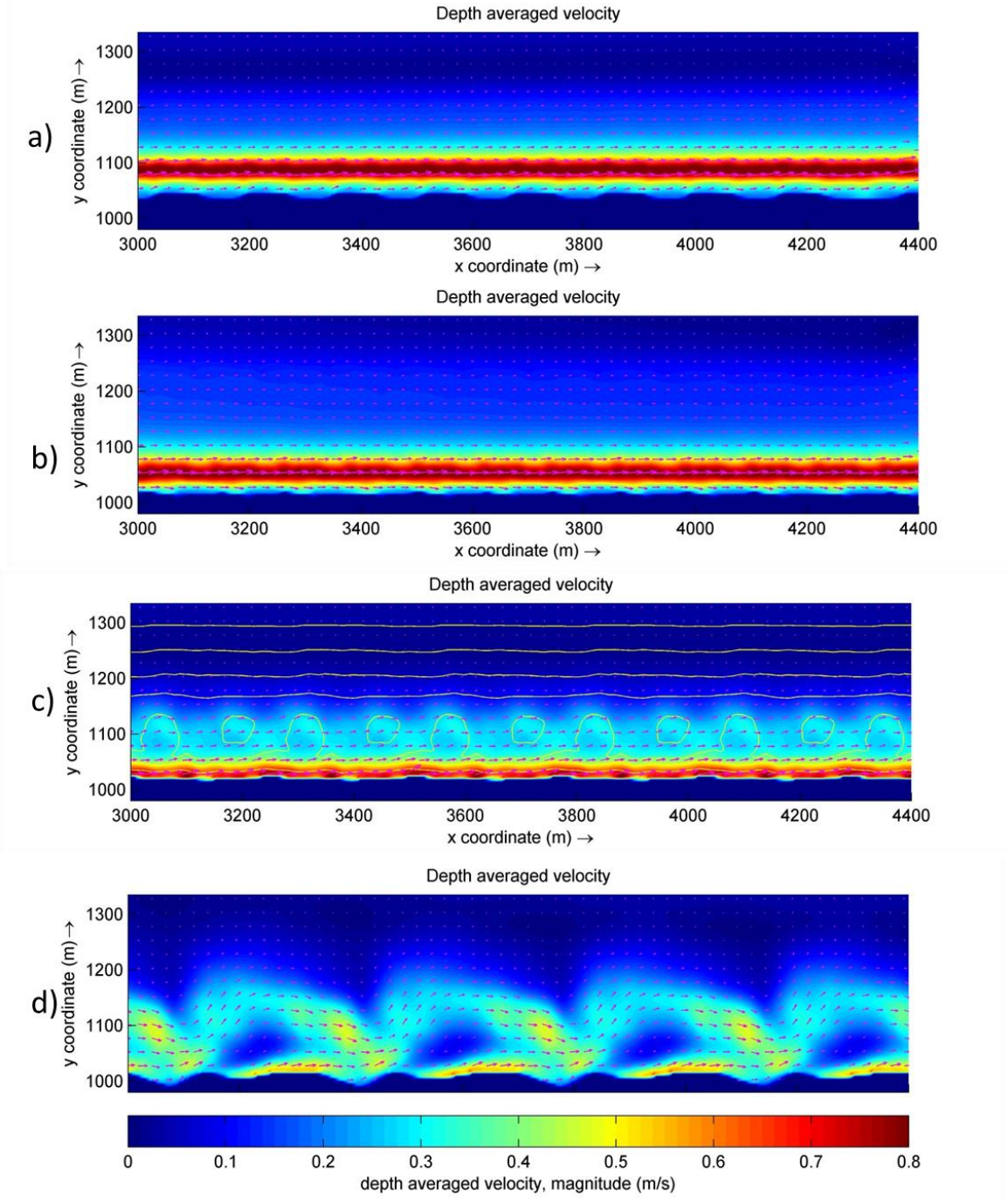

Figure A.12 Longshore sediment transport for LBT1 (a), LBT2 (b), TBR2(c) and TBR1 (d) for test 5-a

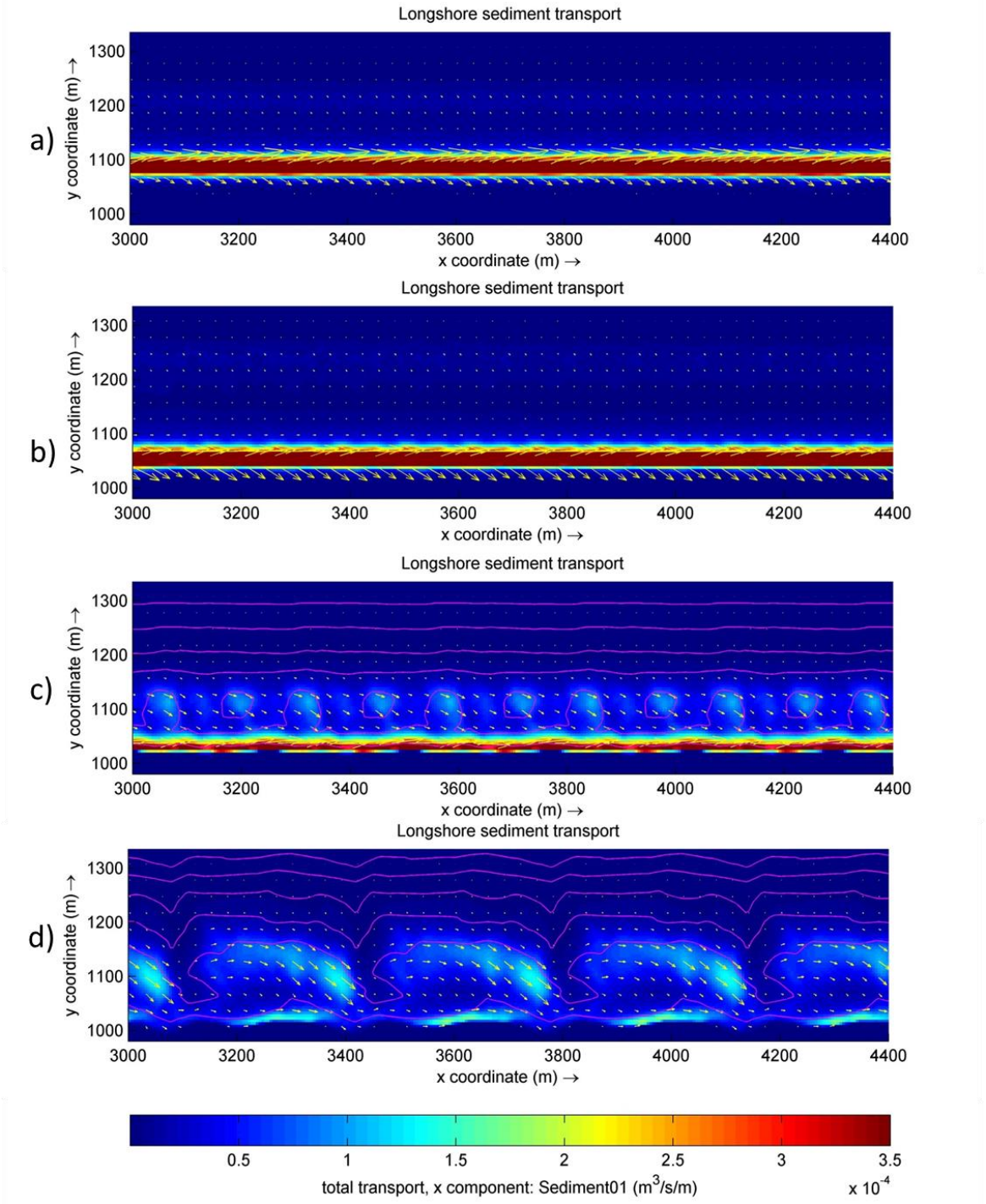

Figure A.13 Depth averaged velocity for LBT1 (a), LBT2 (b), TBR2(c) and TBR1 (d) for test "reference-b"

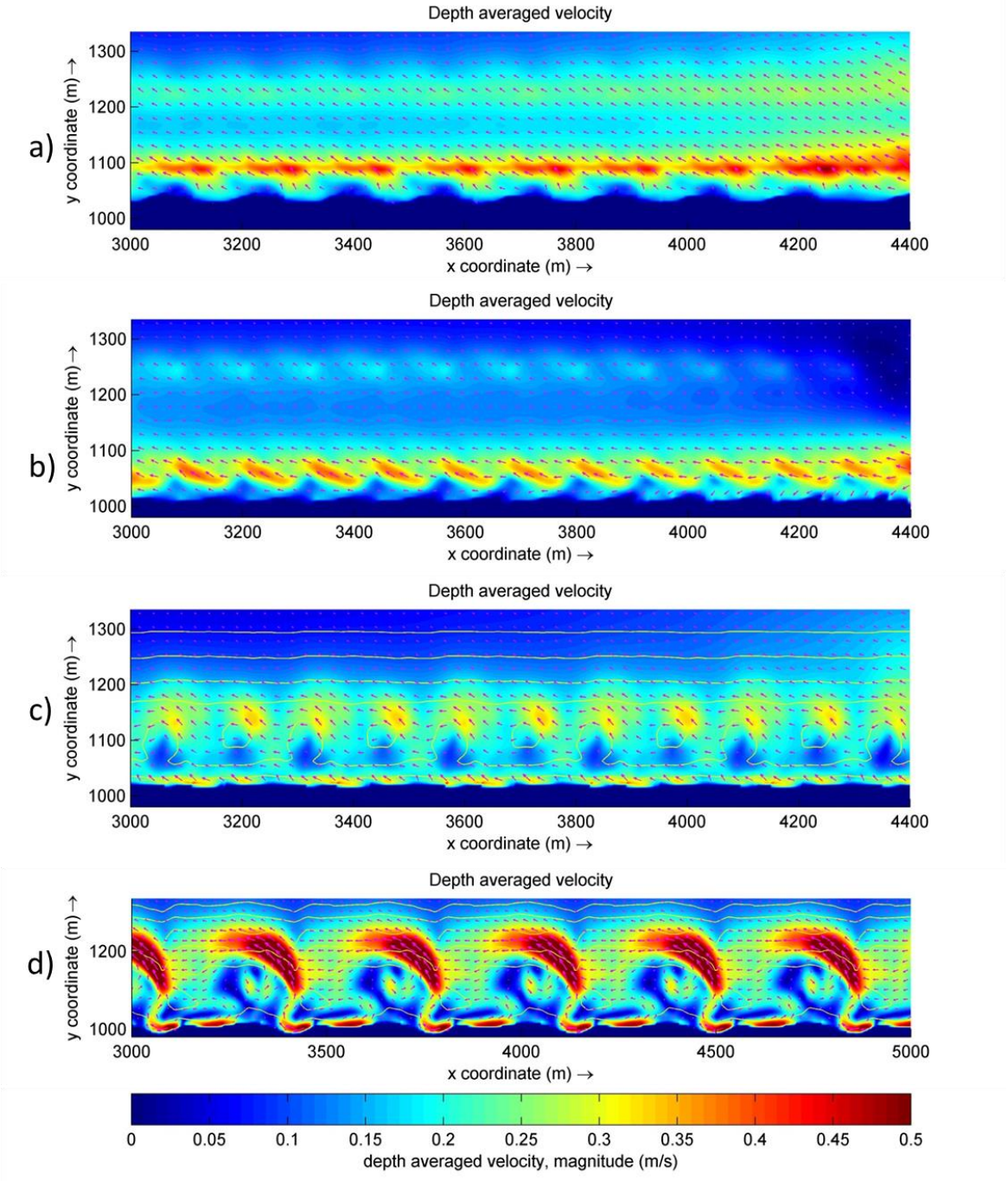

Figure A.14 Longshore sediment transport for LBT1 (a), LBT2 (b), TBR2(c) and TBR1 (d) for test "reference-b"

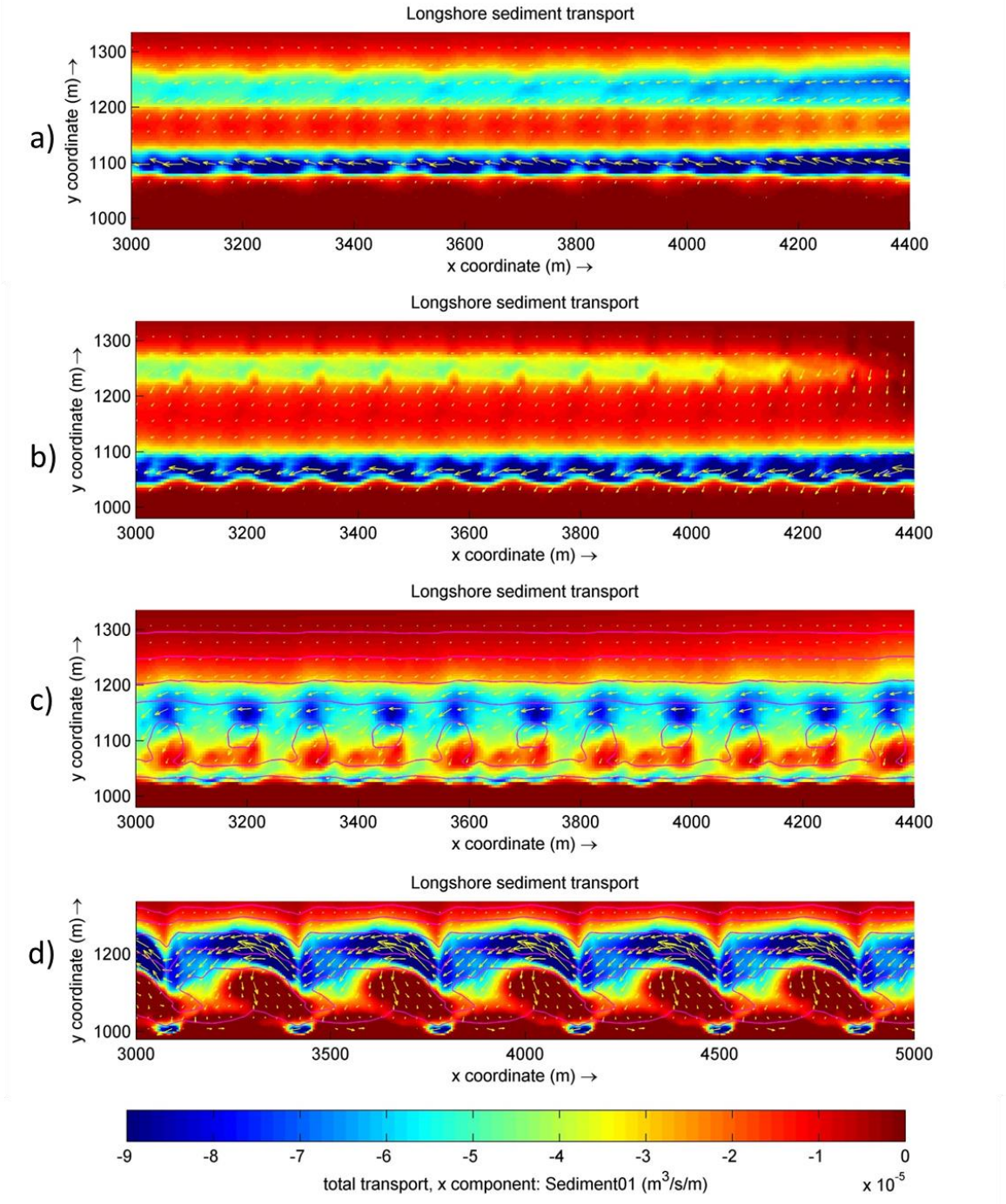

Figure A.15 Depth averaged velocity for LBT1 (a), LBT2 (b), TBR2(c) and TBR1 (d) for test 1-b

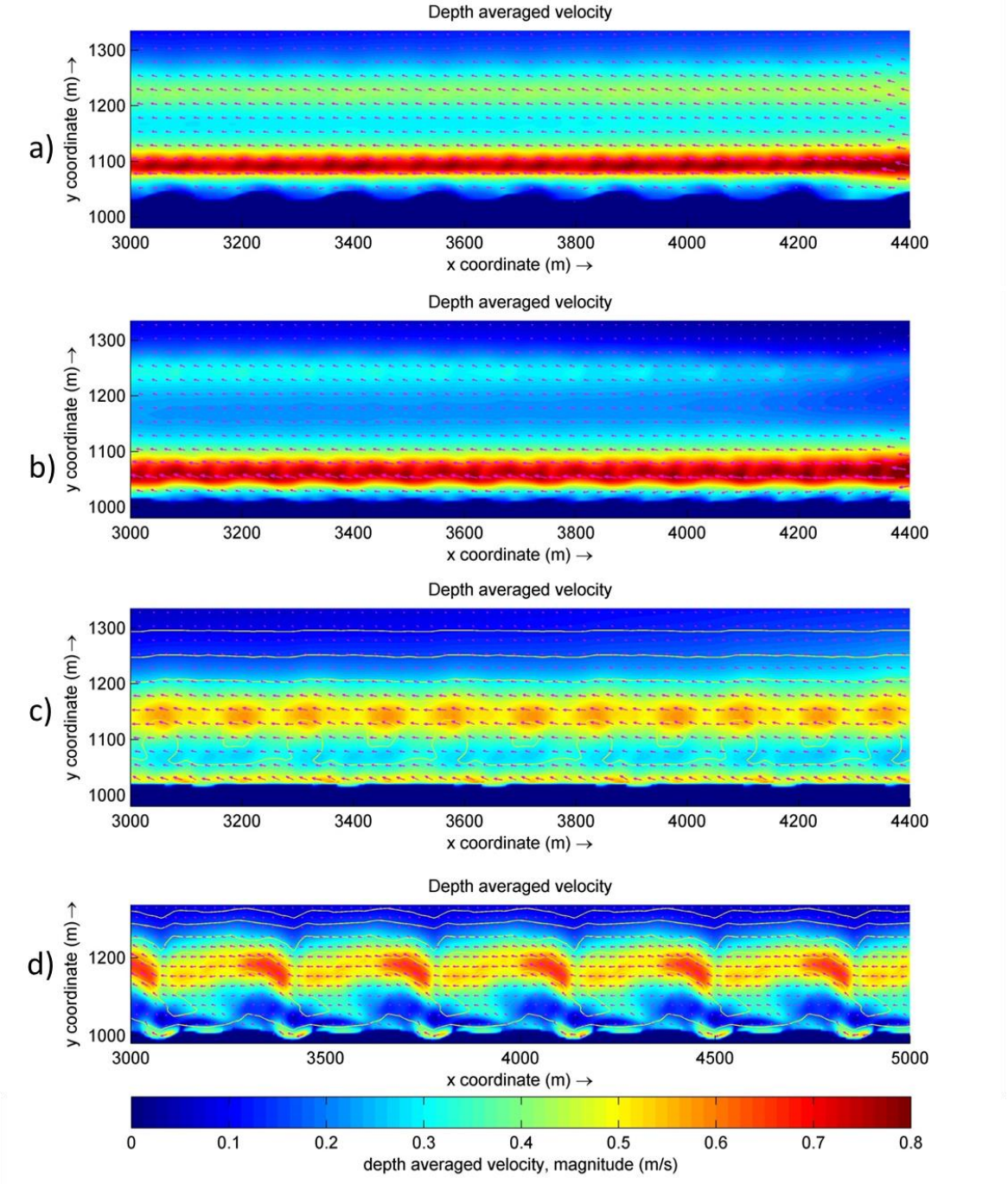

Figure A.16 Longshore sediment transport for LBT1 (a), LBT2 (b), TBR2(c) and TBR1 (d) for test 1-b

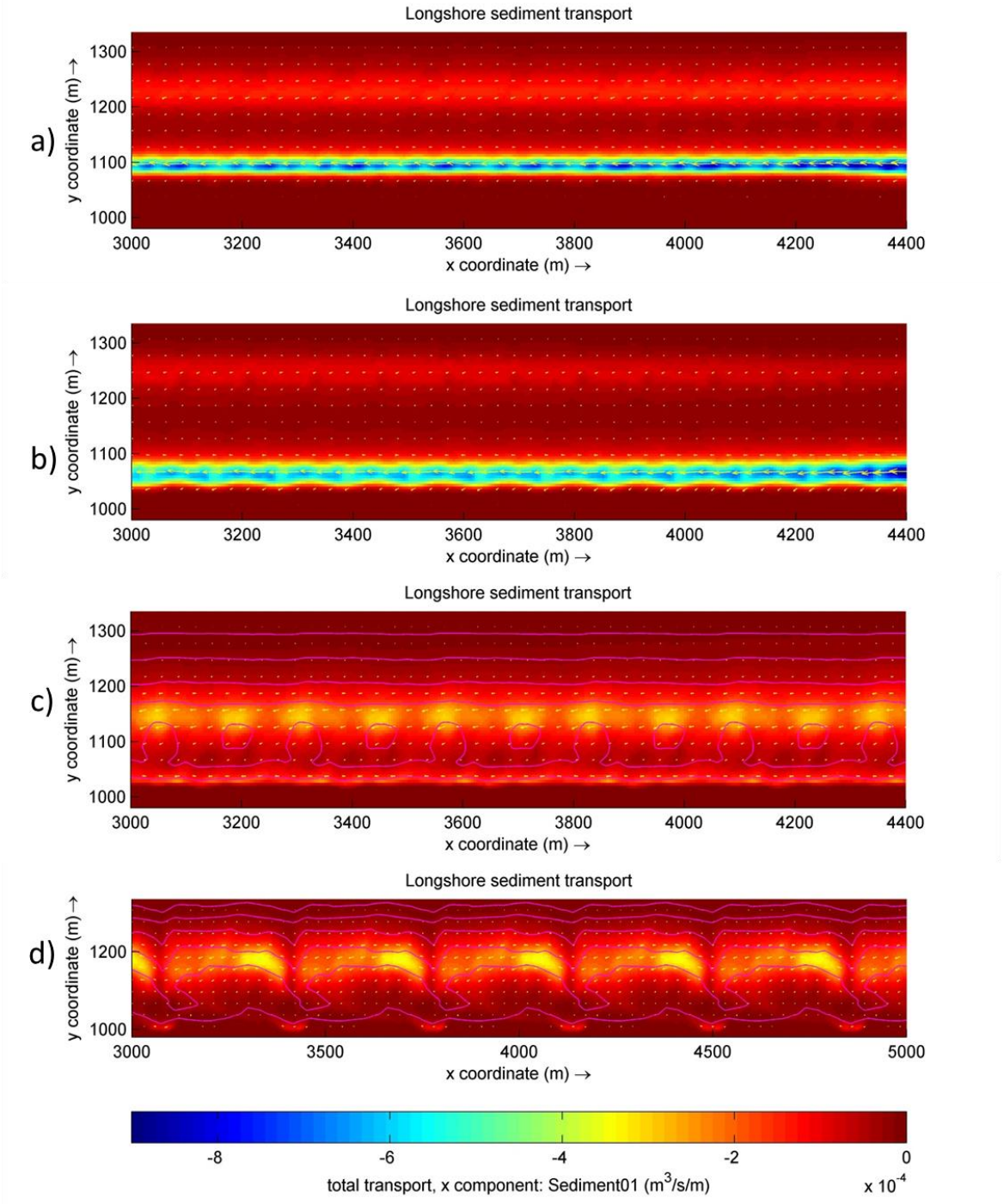

Figure A.17 Depth averaged velocity for LBT1 (a), LBT2 (b), TBR2(c) and TBR1 (d) for test 2-b

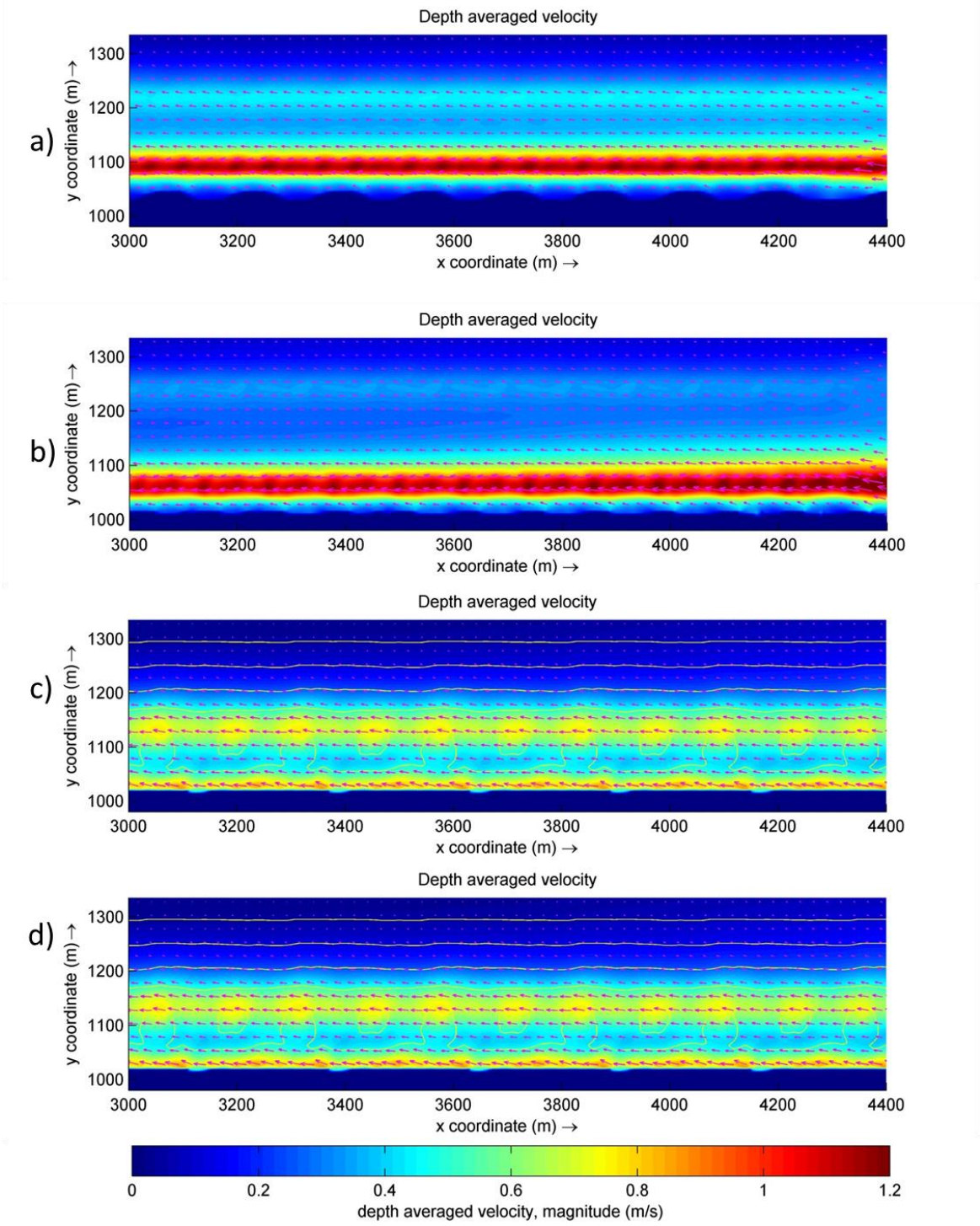

Figure A.18 Longshore sediment transport for LBT1 (a), LBT2 (b), TBR2(c) and TBR1 (d) for test 2-b

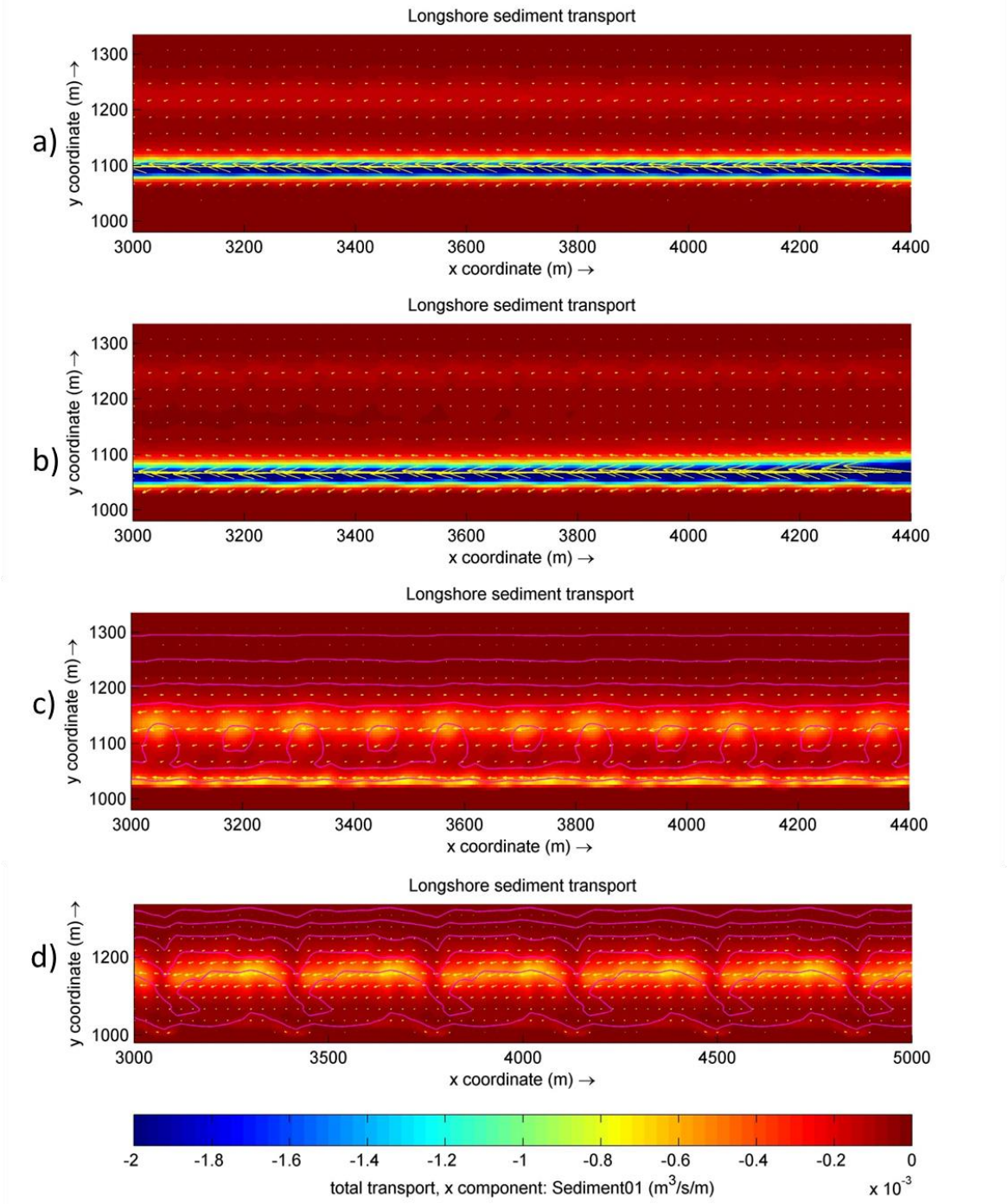

Figure A.19 Depth averaged velocity for LBT1 (a), LBT2 (b), TBR2(c) and TBR1 (d) for test 3-b

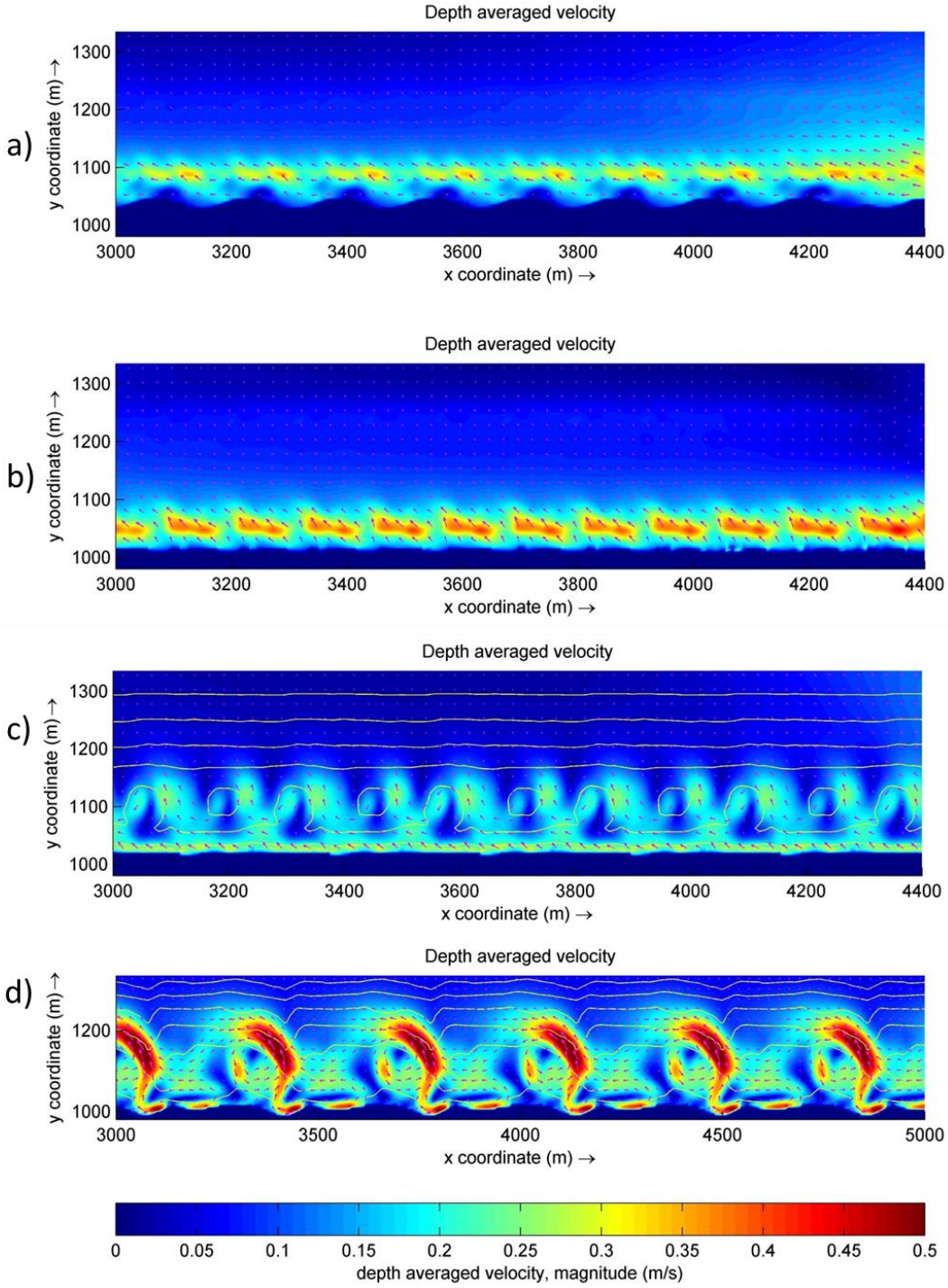

Figure A.20 Longshore sediment transport for LBT1 (a), LBT2 (b), TBR2(c) and TBR1 (d) for test 3-b

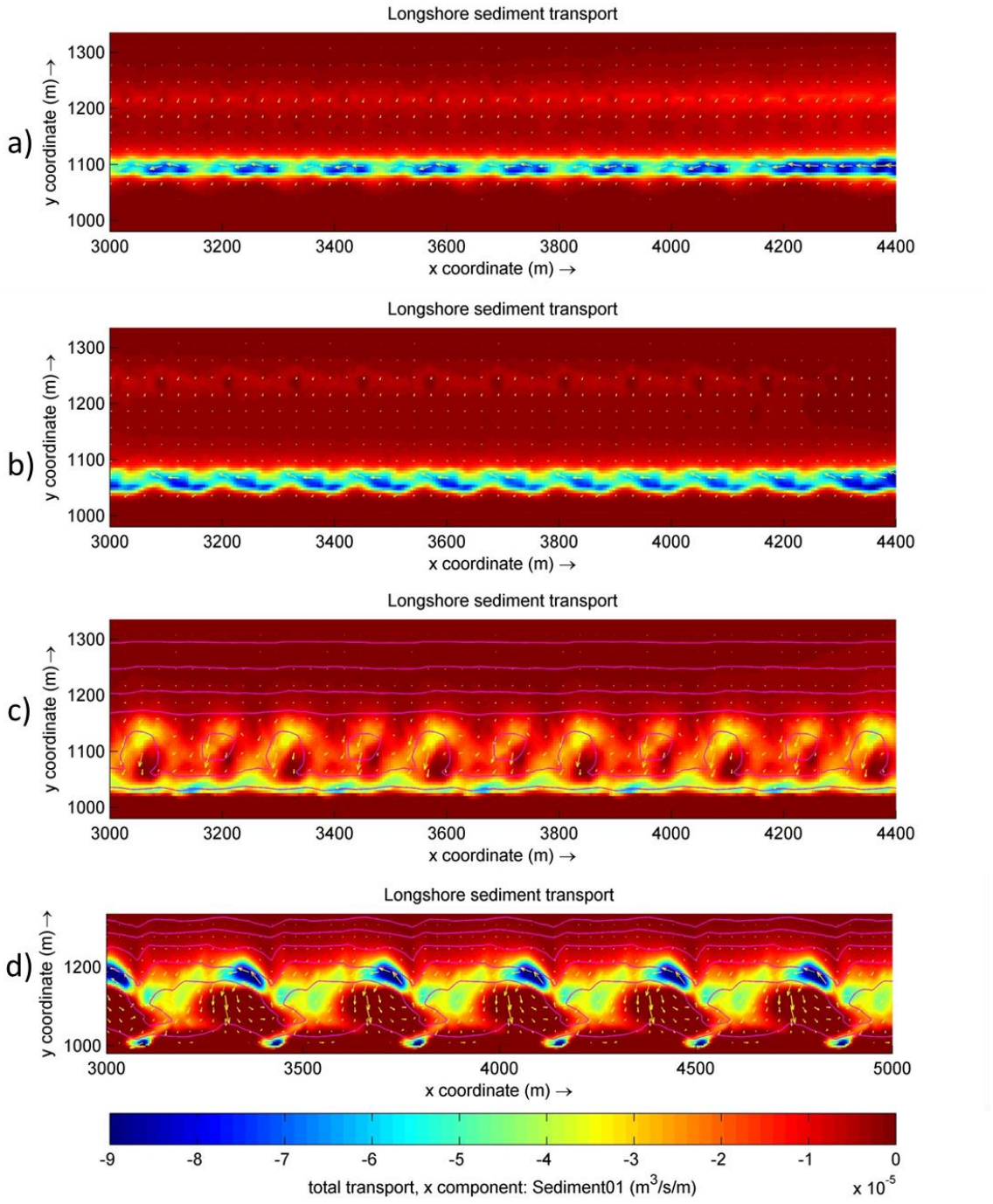

Figure A.21 Depth averaged velocity for LBT1 (a), LBT2 (b), TBR2(c) and TBR1 (d) for test 4-b

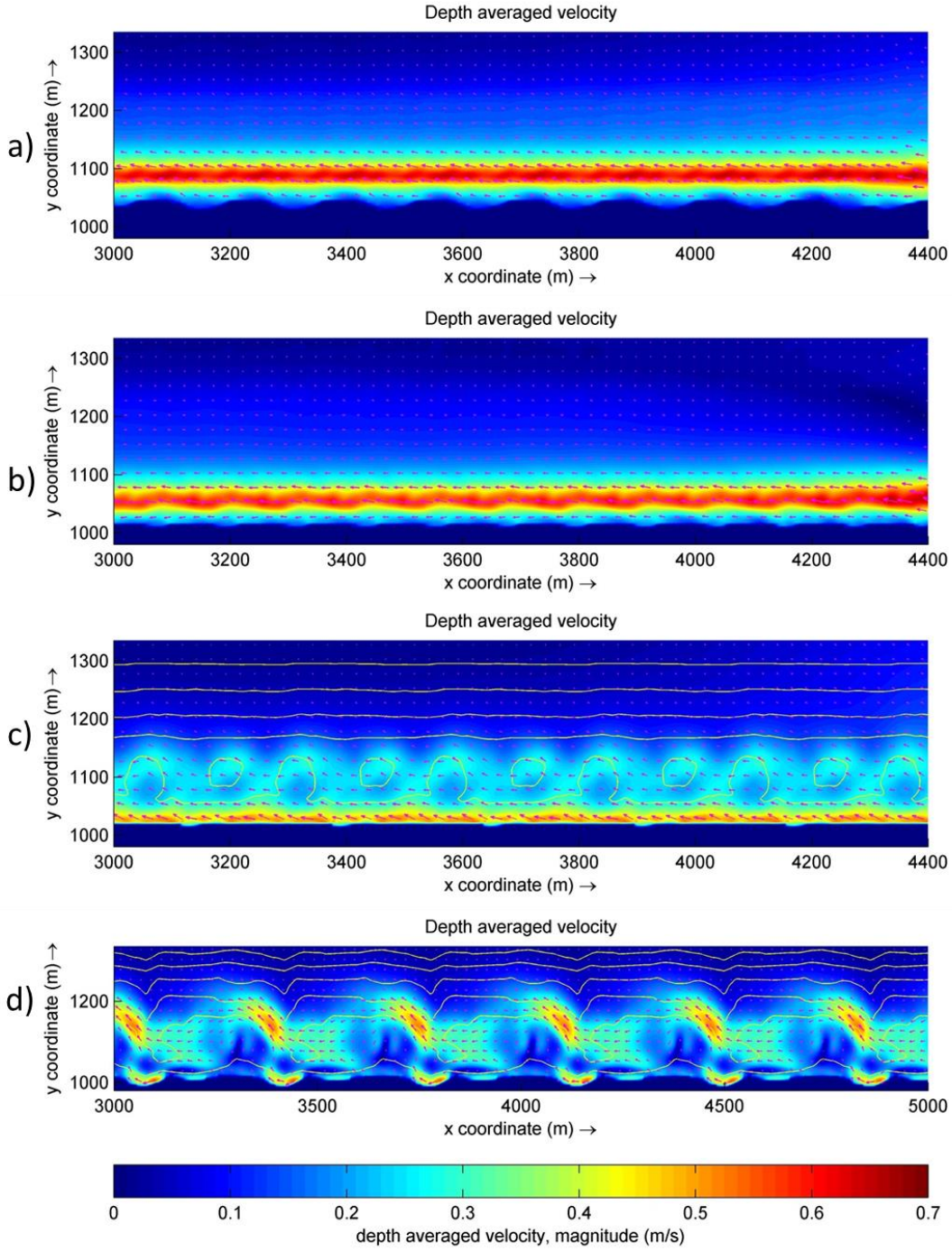

Figure A.22 Longshore sediment transport for LBT1 (a), LBT2 (b), TBR2(c) and TBR1 (d) for test 4-b

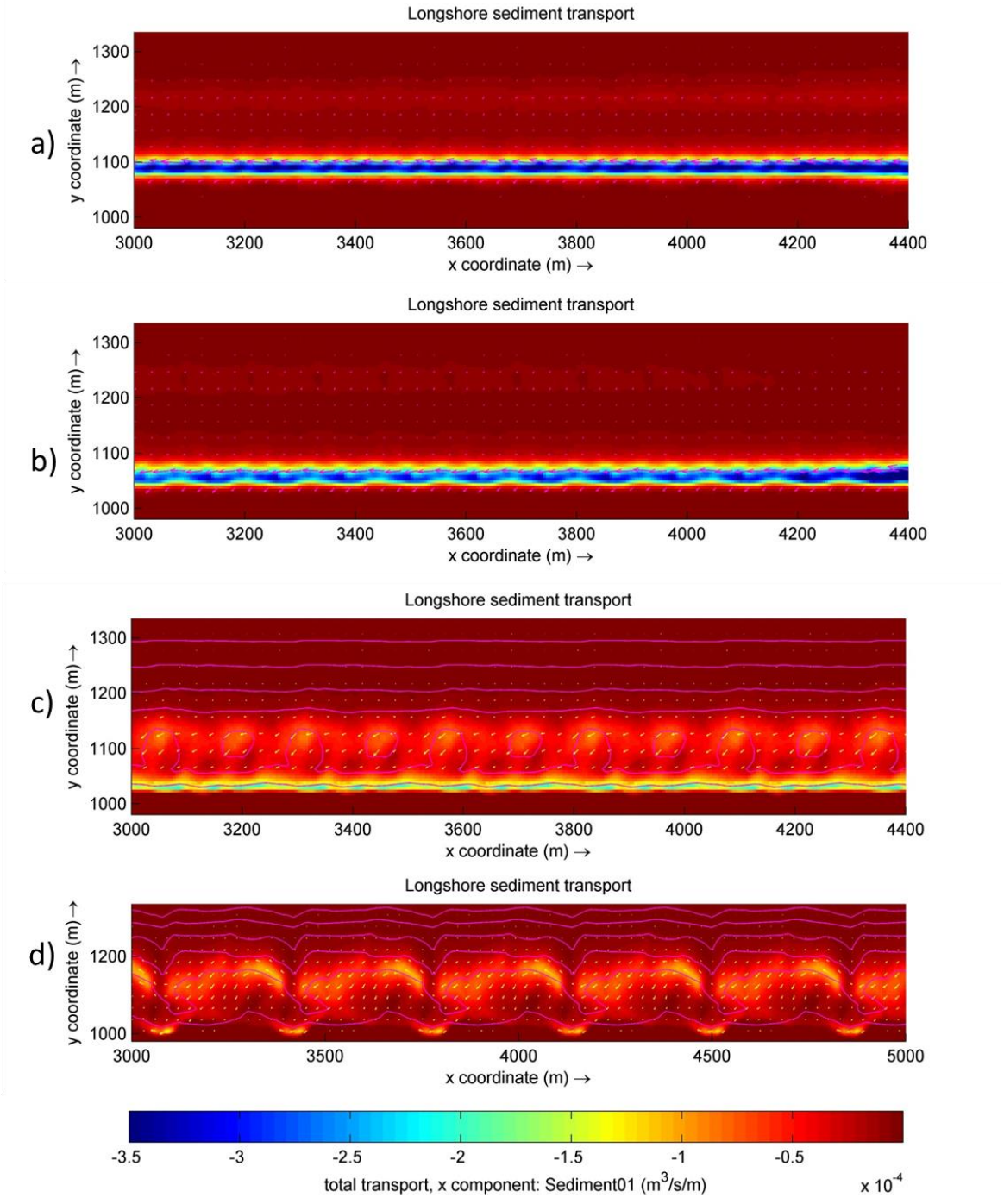

Figure A.23 Depth averaged velocity for LBT1 (a), LBT2 (b), TBR2(c) and TBR1 (d) for test 5-b

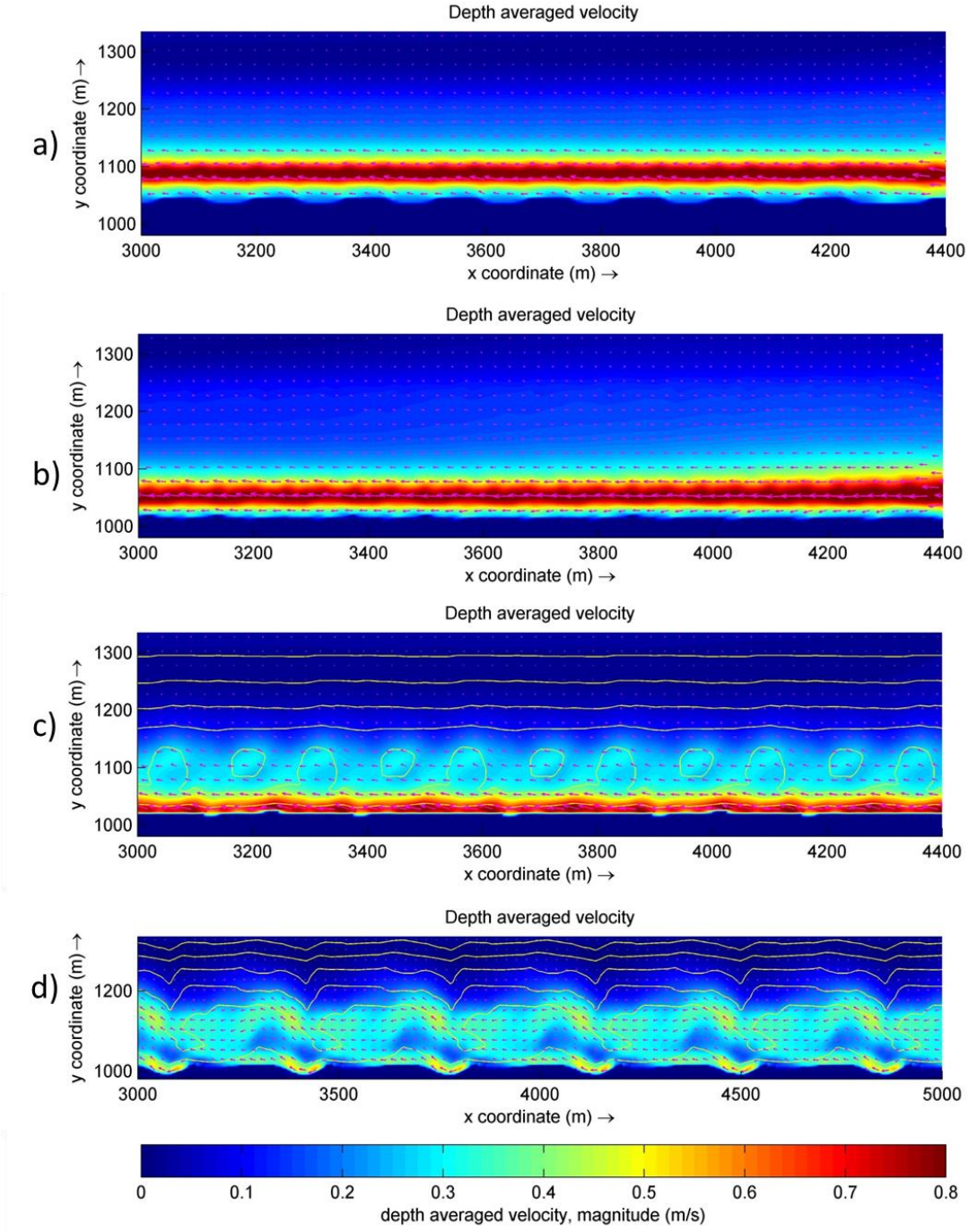

Figure A.24 Longshore sediment transport for LBT1 (a), LBT2 (b), TBR2(c) and TBR1 (d) for test 5-c

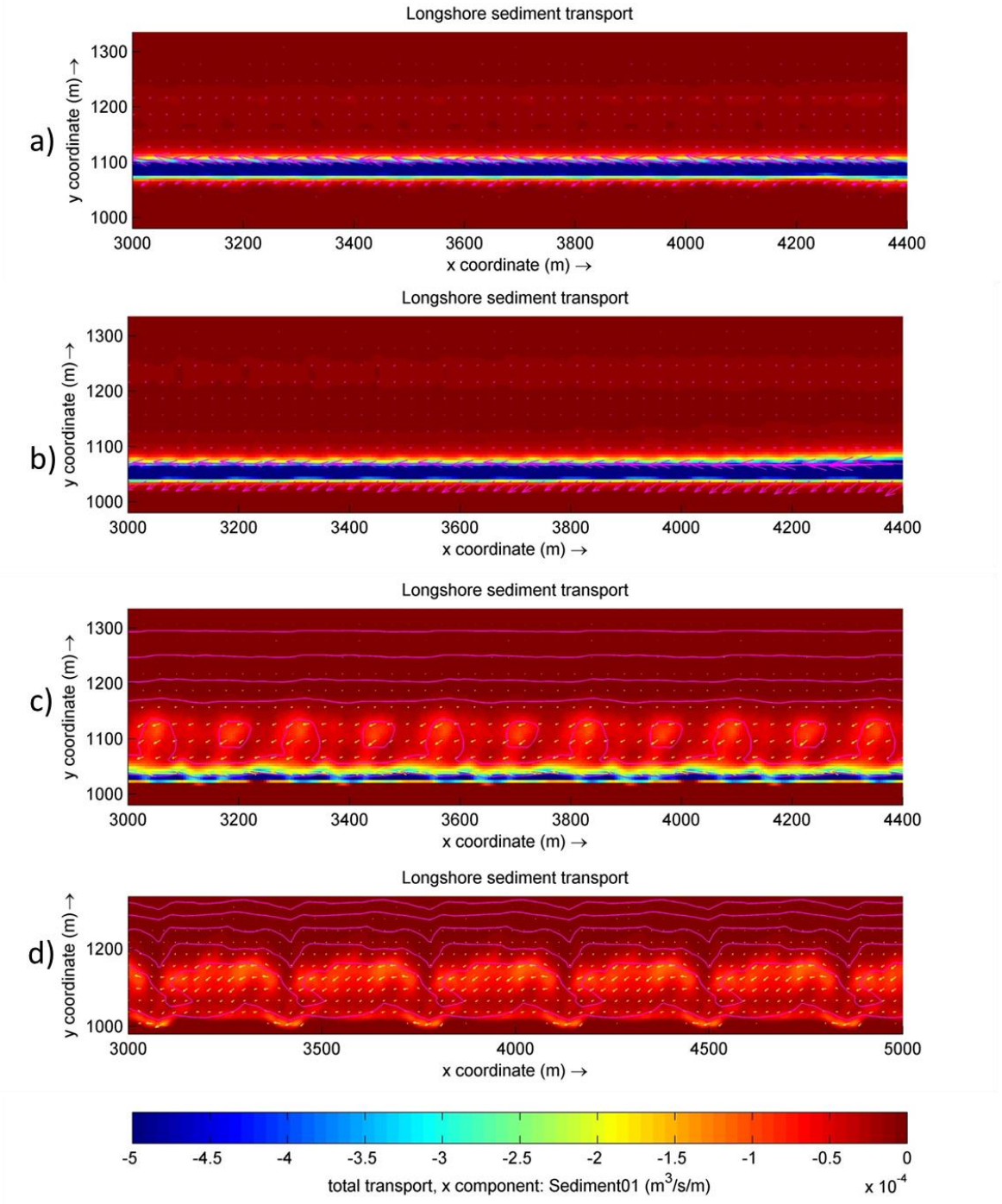

Appendix B. Net longshore sediment transport rates

Table B.1 Net longshore sediment transport rates (in m^3/yr) in the alongshore variable bathymetries simulations for tests-a (negative wave angle)

	LBT1	LBT2	TBR2	TBR1
$Q\ [m^3/yr]$ **Reference test: High waves, low angle**	2.47E+05	2.47E+05	2.67E+05	-6.50E+04
$Q\ [m^3/yr]$ **Test 1 High waves, medium angle**	1.05E+06	1.11E+06	7.79E+05	7.00E+05
$Q\ [m^3/yr]$ **Test 2 High waves, high angle**	2.50E+06	2.68E+06	1.50E+06	1.18E+06
$Q\ [m^3/yr]$ **Test 3 Low waves, low angle**	8.72E+04	8.61E+04	7.89E+04	-3.26E+04
$Q\ [m^3/yr]$ **Test 4 Low waves, medium angle**	3.59E+05	3.13E+05	2.62E+05	1.73E+05
$Q\ [m^3/yr]$ **Test 6 Low waves, high angle**	7.76E+05	6.90E+05	4.56E+05	2.97E+05

Table B.2 Net longshore sediment transport rates (in m^3/yr) in the alongshore variable bathymetries for simulations in tests-b (positive wave angle)

	LBT1	LBT2	TBR2	TBR1
$Q\ [m^3/yr]$ **Reference test: High waves, low angle**	-2.93E+05	-2.82E+05	-3.04E+05	-4.07E+05
$Q\ [m^3/yr]$ **Test 1 High waves, medium angle**	-1.08E+06	-1.06E+06	-8.69E+05	-8.76E+05
$Q\ [m^3/yr]$ **Test 2 High waves, high angle**	-2.58E+06	-2.74E+06	-1.54E+06	-1.49E+06
$Q\ [m^3/yr]$ **Test 3 Low waves, low angle**	-9.11E+04	-9.03E+04	-9.43E+04	-1.16E+05
$Q\ [m^3/yr]$ **Test 4 Low waves, medium angle**	-3.57E+05	-3.26E+05	-2.86E+05	-2.42E+05
$Q\ [m^3/yr]$ **Test 6 Low waves, high angle**	-7.81E+05	-7.19E+05	-4.94E+05	-3.16E+05

Table B.3 Net longshore sediment transport rates (in m^3/yr) in the alongshore uniform bathymetries for simulations in tests-a (negative wave angle)

	$LBT1_{uni}$	**$LBT2_{uni}$**	**$TBR2_{uni}$**	**$TBR1_{uni}$**
$Q\ [m^3/yr]$ Reference test: High waves, low angle	2.84E+05	2.64E+05	3.07E+05	3.09E+05
$Q\ [m^3/yr]$ Test 1 High waves, medium angle	1.05E+06	1.07E+06	8.60E+05	7.96E+05
$Q\ [m^3/yr]$ Test 2 High waves, high angle	2.63E+06	2.61E+06	1.69E+06	1.34E+06
$Q\ [m^3/yr]$ Test 3 Low waves, low angle	9.97E+04	8.97E+04	1.10E+05	1.09E+05
$Q\ [m^3/yr]$ Test 4 Low waves, medium angle	3.50E+05	3.36E+05	3.09E+05	2.70E+05
$Q\ [m^3/yr]$ Test 6 Low waves, high angle	8.11E+05	7.52E+05	6.29E+05	3.87E+05

Table B.4Net longshore sediment transport rates (in m^3/yr) in the alongshore uniform bathymetries for simulations in tests-b (positive wave angle)

	$LBT1_{uni}$	**$LBT2_{uni}$**	**$TBR2_{uni}$**	**$TBR1_{uni}$**
$Q\ [m^3/yr]$ Reference test: High waves, low angle	-2.78E+05	-2.93E+05	-3.07E+05	-3.11E+05
$Q\ [m^3/yr]$ Test 1 High waves, medium angle	-1.08E+06	-1.15E+06	-8.76E+05	-8.12E+05
$Q\ [m^3/yr]$ Test 2 High waves, high angle	-2.63E+06	-2.66E+06	-1.67E+06	-1.35E+06
$Q\ [m^3/yr]$ Test 3 Low waves, low angle	-8.84E+04	-9.32E+04	-1.12E+05	-1.10E+05
$Q\ [m^3/yr]$ Test 4 Low waves, medium angle	-3.86E+05	-3.36E+05	-3.12E+05	-2.71E+05
$Q\ [m^3/yr]$ Test 6 Low waves, high angle	-8.23E+05	-7.26E+05	-6.20E+05	-3.78E+05

Table B.5 Average of the estimated transport rates in the alongshore uniform bathymetries after simulations under a negative and positive wave angle (absolute value in the case of negative transport rates are taken into account).

	LBT1$_{uni}$	**LBT2$_{uni}$**	**TBR2$_{uni}$**	**TBR1$_{uni}$**
$Q\ [m^3/yr]$ Reference test: High waves, low angle	2.81E+05	2.79E+05	3.07E+05	3.10E+05
$Q\ [m^3/yr]$ Test 1 High waves, medium angle	1.06E+06	1.11E+06	8.68E+05	8.04E+05
$Q\ [m^3/yr]$ Test 2 High waves, high angle	2.63E+06	2.63E+06	1.68E+06	1.34E+06
$Q\ [m^3/yr]$ Test 3 Low waves, low angle	9.41E+04	9.14E+04	1.11E+05	1.09E+05
$Q\ [m^3/yr]$ Test 4 Low waves, medium angle	3.68E+05	3.36E+05	3.10E+05	2.70E+05
$Q\ [m^3/yr]$ Test 6 Low waves, high angle	8.17E+05	7.39E+05	6.24E+05	3.82E+05